UNIVERSITY OF CALIFORNIA SAN DIEGO

The Vascular Glycocalyx and Heparan Sulfate in *Staphylococcus aureus* Sepsis

A dissertation submitted in partial satisfaction of the
requirements for the degree Doctor of Philosophy

in

Biomedical Sciences

by

Gregory James Golden

Committee in charge:

Professor Jeffrey Esko, Chair
Professor Victor Nizet, Co-Chair
Professor Richard Gallo
Professor Manuela Raffatellu
Professor Sanford Shattil

2020

The Dissertation of Gregory James Golden is approved, and it is acceptable in quality and form for publication on microfilm and electronically

_____

_____

_____

_____
Co-Chair

_____
Chair

University of California San Diego

2020

DEDICATION

To my wife and love of my life Brandi

To my family, particularly my parents Philip and Patricia

To all those who have passed away from infectious disease and sepsis

EPIGRAPH

For so it had come about, as indeed I and many men might have foreseen had not terror and disaster blinded our minds. These germs of disease have taken toll of humanity since the beginning of things--taken toll of our prehuman ancestors since life began here. But by virtue of this natural selection of our kind we have developed resisting power; to no germs do we succumb without a struggle, and to many--those that cause putrefaction in dead matter, for instance--our living frames are altogether immune. But there are no bacteria in Mars, and directly these invaders arrived, directly they drank and fed, our microscopic allies began to work their overthrow. Already when I watched them they were irrevocably doomed, dying and rotting even as they went to and fro. It was inevitable. By the toll of a billion deaths man has bought his birthright of the earth, and it is his against all comers; it would still be his were the Martians ten times as mighty as they are. For neither do men live nor die in vain.

- H.G. Wells, *War of the Worlds*

TABLE OF CONTENTS

LIST OF FIGURES

Chapter 2

Chapter 3

Chapter 4

Chapter 5

LIST OF TABLES

Chapter 3

LIST OF SUPPLEMENTAL VIDEOS

Chapter 4

Supplemental Videos 1-4

golden_01_first_20_min
golden_02_neutrophil_phagocytosing_MRSA
golden_03_sepsis
golden_04_sterile

ACKNOWLEDGEMENTS

This research was made possible by my support system throughout graduate school. Thank you to Dr. Jeffrey Esko, who allowed me to join his lab, guided me throughout my development as a scientist, and supported me financially throughout graduate school. Additionally, his support of a healthy lab environment and mentor-student relationship was instrumental to my productivity. I will always use his example to mentor developing scientists I will work with in the future. Thank you to Dr. Victor Nizet, who mentored me and included me as a member of his own lab. Without Dr. Nizet, my development as an infectious disease scientist would not have been possible and the projects would not be nearly as productive or innovative. Thank you to my other committee members, Dr. Richard Gallo, Dr. Manuela Raffatellu, and Dr. Sanford Shattil, for providing guidance on constructing my thesis. Thank you to Nora Cadiz, an inspiring AP Biology teacher who opened my eyes to how great biology is. Thank you to Dr. Rachel Muir, the first scientist who taught me how to do research at the bench while I was an intern at DuPont Industrial Biosciences. Thank you to Dr. Robert Gunsalus at UCLA for guiding me on my foundational scientific development as an undergraduate researcher in his lab. Thank you to Dr. Deborah Gordon at Stanford for her mentorship in my gap year between undergraduate and graduate school, where I learned the complex relationships in the *Pogonomyrmex barbatus* colony that apply to a myriad of biological systems.

Thank you to members of the Esko and Nizet labs for not only being helpful scientifically but also for being great friends who made the difficulties of lab work a bit more enjoyable. Thank you to my graduate school friends who understood the struggles of graduate school and were great friends outside of lab. Thank you to my friends not directly tied to science in the San Diego area, who were a huge reason why I enjoyed my time in San Diego. Thank you to my friends from

home, who have greatly influenced me throughout the years. Special thanks to my family. I would like the thank my cousin Phil Sockolov, who was the only family in the area and supported my physical and mental fitness during the COVID-19 pandemic with the J&T lifestyle. Thank you to Daniel Riddle, who transitioned from being one of my best friends to being my stepbrother and one of the people that understands my humor more than just about anyone. Thank you to my brother John, who was the benchmark for my studies through high school and college, and who is always curious about what I do and is someone I have an intellectual connection with that is difficult to describe. Thank you to my mother Patricia, who has been one of the most supportive people throughout my life and was a great example of how to be positive and enjoy life. Thank you to my father Philip, who taught me the values of hard work, use of my intellect to follow my passions, and fostering my love of nature that is a large reason why I study biology today. To all the other family members that I do not have the space to mention, thank you for supporting me over the years and helping me grow as a person.

Lastly and most importantly, thank you to my wife and love of my life Brandi, who has been my best friend and life partner ever since our UCLA days. We have both mirrored each other throughout our professional schools, with her starting and graduating from medical school while I was a graduate student. She has been an incredible support system when I need to confide in her during stressful graduate school times, and she is always motivating me to continue pursuing my goals when there are roadblocks. She is inspirational, as she has defied the odds from getting into medical school to becoming a surgeon, all because of her incredible work ethic, intellect, and dedication to her passions. She taught me what is possible when times are tough and how to always move forward when life sends you backwards. This especially important as we have navigated our professional schools while in a long distance relationship for the last 4+ years. Most importantly,

she is my best friend who I absolutely enjoy sharing my life experiences with. My development into the dedicated scientist I am today would not have been possible without her.

Chapter 1, in part, is being formulated into a manuscript for publication of the material. GJ Golden, CD Painter, JD Esko, 2022. The dissertation author was the primary investigator and author of this material. For Chapter 1, thank you to supportive funding from the National Institute of Health (P01- HL131474) and the UCSD Microbiome Center for Innovation (Microbial Sciences Graduate Research Fellowship Award 1-F17GG and 1-F18GG).

Chapter 2 was published as a manuscript in *Nature Communications* (2019) 10:4656. A Gómez Toledo, GJ Golden, A Rosa Campos, H Cuello, J Sorrentino, N Lewis, N Varki, V Nizet, JW Smith & JD Esko. The dissertation author was a primary investigator and author of this material. For Chapter 2, proteomics analysis was done at the Proteomics Core Facility, Sanford-Burnham-Prebys Medical Discovery Institute, La Jolla, CA, USA. A.G.T. and J.D.E. conceived the study and designed it together with G.G. and J.W.S.; A.G.T., G.G., A.R.C. and H.C. performed all the experiments. A.G.T., G.G., J.S., V.N., N.L. and J.D.E. interpreted the data. N.V. performed the histopathological analysis. A.G.T. and J.D.E. wrote the paper with significant input from all the coauthors. For Chapter 2, the work was supported by grant P01HL131474 to J.D.E. and J.W.S. N.L. and J.S. also acknowledge support from NIGMS R35 GM119850. J.W.S. was supported by R01 GM107523. G.G. was supported by Microbial Sciences Graduate Research Fellowship Awards 1-F17GG and 1-F18GG.

The studies in Chapter 3 are not being formulated for publication. The dissertation author is the primary author of this material. For Chapter 3, thank you to Joshua Olson for assistance with culture and mouse sepsis methods, and Satoshi Uchiyama and Joshua Sun for cell killing assay assistance. The dissertation author is the primary investigator and author of this material. The

studies were supported by the National Institute of Health (P01- HL131474) and the UCSD Microbiome Center for Innovation (Microbial Sciences Graduate Research Fellowship Award 1-F17GG and 1-F18GG).

Chapter 4, in part, is being formulated into a manuscript for publication of the material. GJ Golden, A Gomez Toledo, A Marki, C Morris, RJ Riley, Q Chen, I Cornax, N Varki, D Le, K Ley, V Nizet, and JD Esko. The dissertation author is the primary investigator and author of this material. For Chapter 4, special thanks to the UCSD Mouse Phenotyping Core, especially Michelle Abueg for hematology and Sandra Bretton for histology. Thank you to the La Jolla Institute of Immunology Microscopy and Histology Core, in particular Zbigniew Mikulski and Sara McArdle for intravital microscopy insight and Angela Denn for histology. Thank you to the UCSD Microscopy Core, especially Jennifer Santini and Marcy Erb, for their assistance with immunofluorescence. Additional thanks to James Sorrentino for discussing statistical analyses, and to all the Jeffrey Esko and Victor Nizet lab members for their insight into developing this research. Funding sources include: NHLBI P01 HL131474 to J.D.E., UCSD Microbial Sciences Graduate Research Initiative 1-F17GG and 1-F18GG to G.J.G., and NINDS P30 NS047101 to UCSD Microscopy.

Chapter 5, in part, is being formulated into a manuscript for publication of the material. GJ Golden, A Gomez Toledo, C Morris, V Nizet, and JD Esko. The dissertation author is the primary investigator and author of this material. For Chapter 5, thank you to Joshua Olson for assistance with culture and mouse sepsis methods. Thank you to Juliane Bubeck-Wardenburg for providing recombinant Hla and Hla $H_{35}L$. Special thanks to Alejandro Gomez Toledo for mass spectrometry analysis and assistance with mouse infections. Thank you to the Sanford Burnham Prebys Proteomics Core for mass spectrometry analysis. Thank you to Claire Morris for assistance with

animal husbandry, animal infections, and for working on the Adam10 activity assay. Thank you to Chelsea Painter for assistance with the ion exchange chromatography and Daniel Sandoval for assistance with ion exchange chromatography and protein modeling. For Chapter 5, the studies were supported by the National Institute of Health (P01- HL131474) and the UCSD Microbiome Center for Innovation (Microbial Sciences Graduate Research Fellowship Award 1-F17GG and 1-F18GG).

For Chapter 6, the dissertation author was the author of this material. Thank you to supportive funding from the National Institute of Health (P01- HL131474) and the UCSD Microbiome Center for Innovation (Microbial Sciences Graduate Research Fellowship Award 1-F17GG and 1-F18GG).

VITA

2014	Bachelor of Science, University of California, Los Angeles
2020	Doctor of Philosophy, University of California San Diego

Field of Study

2012 – 2014	Microbiology: characterization of the surface layer proteins of archaea extremophiles
2014 – 2015	Entomology: Exploring the heritage and neurophysiology of collective behavior in the red harvester ant *Pogonomyrmex barbatus*
2015 – 2020	Immunology, Glycobiology, and Microbiology: The vascular glycocalyx and heparan sulfate in *Staphylococcus aureus* sepsis

Publications

B Ramms, S Patel, C Nora, AR Pessentheiner, MW Chang, CR Green, GJ Golden, P Secrest, RM Krauss, CM Metallo, C Benner, VJ Alexander, JL Witztum, S Tsimikas, JD Esko, PLSM Gordts. ApoC-III ASO Promotes Tissue LPL Activity in Absence of ApoE-Mediated TRL Clearance. *Journal of Lipid Research*, 2019. 60, 1379-1395.

A Gómez Toledo*, GJ Golden*, AR Campos, H Cuello, J Sorrentino, N Lewis, N Varki, V Nizet, JW Smith, JD Esko. Proteomic atlas of organ vasculopathies triggered by Staphylococcus aureus sepsis. *Nature Communications*, 2019. 10 (4656) *Authors contributed equally

TM Clausen, DR Sandoval, CB Spliid, J Pihl, CD Painter, BE Thacker, CA Glass, A Narayanan, SA Majowicz, Y Zhang, JL Torres, GJ Golden, R Porell, AF Garretson, L Laubach, J Feldman, X Yin, Y Pu, B Hauser, TM Caradonna, BP Kellman, C Martino, PLSM Gordts, SL Leibel, SK Chanda, AG Schmidt, K Godula, J Jose, KD Corbett, AB Ward, AF Carlin, JD Esko. SARS-CoV-2 Infection Depends on Cellular Heparan Sulfate and ACE2. *Cell*, 2020. 183 (4), 1043 - 1057

A Marki, K Buscher, C Lorenzini, M Meyer, R Saigusa, Z Fan, YT Yeh, N Hartmann, JM Dan, WB Kyosses, GJ Golden, R Ganesan, H Winkels, M Orecchioni, S McArdle, Z Mikulski, Y Altman, J Bui, M Kronenberg, S Chien, JD Esko, V Nizet, D Smalley, J Roth, and Kl Ley. Elongated Neutrophil-Derived Structures (ENDS) are novel blood borne microparticles formed by rolling neutrophils during sepsis. *Journal of Experimental Medicine*, 2021. 218(3)

Honors and Awards

2017-2019	Microbial Sciences Initiative Graduate Research Fellowship
2018	Best Poster, Gordon Research Conference: Proteoglycans
2014	Honors, Microbiology, Immunology, and Molecular Genetics
2014	Cum Laude, Microbiology, Immunology, and Molecular Genetics
2011-2014	Dean’s Honor List, UCA

ABSTRACT OF THE DISSERTATION

The Vascular Glycocalyx and Heparan Sulfate in *Staphylococcus aureus* Sepsis

by

Gregory James Golden

Doctor of Philosophy in Biomedical Sciences

University of California San Diego, 2020

Professor Jeffrey Esko, Chair
Professor Victor Nizet, Co-Chair

Sepsis, a life-threatening organ dysfunction caused by a dysregulated host response to infection, poses a serious threat to human health. Many sepsis pathologies are tied to vascular dysregulation. The vascular glycocalyx (VGC), the collection of proteins and glycans exposed to vascular flow, is critical to vascular function and is dramatically remodeled in sepsis. Little is known about VGC composition in health or in sepsis. This dissertation consists of 6 chapters covering VGC remodeling during infection, detailed characterization of VGC composition using

novel methodologies, and the impacts of specific alteration of the major VGC component heparan sulfate (HS) during sepsis. Chapter 1 is a summary of VGC composition, the VGC role in vascular function, VGC remodeling factors, and how VGC composition changes during infection. Chapter 2 describes a novel technique to characterize VGC protein composition and how it changes in sepsis. By using a perfusion technique to tag proteins exposed to vascular flow, VGC proteins from major organs were purified, identified, and quantified by novel proteomics methods. In healthy vasculatures, there are both shared and unique VGC components across organs. In *Staphylococcus aureus* sepsis, dramatic compositional changes occur in an organotypic fashion that reflect the inflammatory environment. Chapter 3 details studies that use genetic alteration of vascular HS (*Ndst1$^{f/f}$Tie2Cre+*) to stratify sepsis and tissue infection models across a diverse range of sepsis-causing bacterial agents. *Ndst1$^{f/f}$Tie2Cre+* mice exhibit hypersensitivity only to *S. aureus*. Chapter 4 consists of studies showing endothelial HS mediates neutrophil infiltration and hepatic damage induced by *S. aureus* sepsis. Importantly, altering endothelial HS reduces neutrophil trafficking in both sterile and non-sterile hepatic inflammation, the first VGC component characterized to do so. Studies in Chapter 5 further characterize *Ndst1$^{f/f}$Tie2Cre+* mouse hypersensitivity to *S. aureus*. *Ndst1$^{f/f}$Tie2Cre+* mice exhibited a unique heart VGC during sepsis that lacked proteins characteristic of heart-protection, indicating *S. aureus* may induce improper cardiac vascular responses in *Ndst1$^{f/f}$Tie2Cre+* mice. Hypersensitivity was dependent upon *S. aureus* alpha-toxin. Alpha-toxin bound to heparin, and heparan sulfate inhibited the activity of the alpha-toxin receptor Adam10. The studies of thesis uniquely examine the VGC in sepsis from the “omics” to the molecular level.

Chapter 1: Vascular glycocalyx remodeling and infection

1.1 Description of the vascular glycocalyx

1.1.1 Introduction

In 1940, James Danielli first described a thin protein layer on the lumenal surface of blood vessels formed by adsorption of circulating protein that helped filter small particles [1]. Subsequent study of this protein layer utilized perfused albumin-binding Evans blue dye and revealed "thin strands and sheets of a faintly colored blue, translucent material" sloughing off the inner surface of the capillary [2]. In 1979, Bruce Klitzman and Brian Duling led a study describing a "plasma layer" on the inner surface of vessels that affects hematocrit and postulated that capillaries have a thicker plasma layer than larger vessels [3]. Other lines of study described the lumenal layer of vessels. In 1960, Kiyoshi Hama observed a thick "cuticle layer" on the lumenal surface of earthworm blood vessels that excluded large hemoglobin particles and showed a strong periodate-Schiff reaction characteristic of polysaccharides [4]. Considering this study and numerous others showing polysaccharides coating most cells types across divergent eukaryotic and prokaryotic lineages, H. Stanley Bennet described this extracellular polysaccharide layer as the "glycocalyx" in 1963 [5]. The nascent studies of the plasma layer and the endothelial glycocalyx merged over the years to become a rapidly advancing and exciting field of study focused on the lumenal glycocalyx and its many roles in vascular biology. Further, the remodeling of this layer is a critical aspect of diseases associated with the vasculature, including infection and sepsis.

1.1.2 Vascular glycocalyx definition

The glycocalyx exposed to vascular flow is termed the vascular glycocalyx (VGC). The VGC is composed of glycans, proteins, glycoproteins, and glycolipids that form a gel like matrix layer that covers endothelial cells and other cells exposed to vascular flow, including cells adhered to the apical surface of the endothelium. Further, if endothelial barriers are disrupted resulting in

exposure of inter-endothelial cell surfaces, basement membranes, and parenchymal cells, the glycocalyces of these surfaces would interact with circulating factors and would be functionally included in the VGC.

1.1.3 Baseline composition of the vascular glycocalyx

Glycosaminoglycans (GAGs) and proteoglycans (PGs) form the main VGC scaffold [6]. GAGs are linear, anionic polysaccharides composed of alternating uronic acid and hexosamine residues [7]. GAG classes in the VGC are composed of heparan sulfate (HS), chondroitin sulfate (CS), and hyaluronan (HA). HS and CS are biosynthesized in the Golgi and are covalently linked to a limited number of proteins, forming HSPGs and CSPGs. HS chains tend to be 20-100 kDa in size [7]. In contrast, HA is not attached to a core proteins and biosynthesis occurs at the plasma membrane, where it is extruded as long chains that range from 100 – 1000 kDa in size [8]. HSPGs and HA have been studied more than CSPGs in the context of the VGC. Most of the HSPGs characterized as VGC components are membrane associated either through a transmembrane domain (Syndecans 1-4) or a GPI anchor (Glypicans 1-6), whereas HSPGs such as agrin, perlecan, or collagen XVIII are secreted into the extracellular matrix. Glypican-1 and Syndecan-1 (Sdc1) are the most studied HSPGs in the VGC [9], although their true abundance in the VGC relative to other HSPGs is not understood and probably varies across different vascular beds. Quantitative studies into the relative amounts of GAGs and PGs in the VGC are needed to accurately determine their composition.

Glycoproteins containing covalently linked *N*- and *O*- glycans form a substantial portion of the VGC as well. Intravital staining with the lectin wheat germ agglutinin, which targets glycoconjugates containing sialic acid and β1-4 linked *N*-acetylglucosamine, showed strong staining on the VGC in subcutaneous vessels [10]. Additionally, ConA, a lectin that targets *N*-

glycans, binds to the endothelial cell plasma membrane and is enriched near cell-cell junctions [11]. Although it is generally acknowledged that a majority of secreted and transmembrane proteins contain glycosylation sites, there has yet to be a global study of glycosylation of this protein set in endothelial cells or the vasculature. Studies targeting the effects of glycosylation on individual endothelial proteins demonstrate their importance in endothelial function. The most detailed characterization of glycosylated endothelial proteins are cell adhesion molecules from the selectin family and the immunoglobulin superfamily [9], which are discussed in detail below. Importantly, the role of glycosylation in a litany of VGC proteins warrants further study.

Numerous secreted proteins are intercalated in lumenal glycans. Albumin, the most abundant plasma protein, is highly integrated in the VGC and is critical to controlling vascular permeability [12]. Fibrinogen, a critical coagulation factor, is found within the VGC [13]. There are many signaling factors that bind to HS *in vitro* [7], such as growth factors, chemokines, complement factors, and coagulation factors, yet many of these interactions have yet been demonstrated to be present in the VGC *in vivo*. Chemokines are an exception, where studies have demonstrated they form gradients in the VGC by binding to endothelial HS [14,15]. Although it is generally understood that there are many secreted host factors that bind to VGC components, evidence of these interactions in an intact VGC is lacking. Further, it is not clear how much of the VGC is made of secreted versus membrane-anchored factors, highlighting the need for a comprehensive analysis of VGC proteins, glycans, and glycoproteins.

1.2 Remodeling and the function of vascular glycocalyx

1.2.1 Remodeling definition

We define VGC remodeling as the structural or compositional alteration of the vascular glycocalyx. The VGC can be remodeled by changing composition via addition or subtraction of

proteins, glycans, and glycoproteins. There are several strategies to experimentally induce VGC remodeling, including activation of endothelial cells, enzymatically removing VGC components, or genetically manipulating VGC proteins and glycosylation biosynthesis enzymes. VGC remodeling occurs naturally in numerous ways, including "shedding" of VGC elements via enzymatic removal with proteases and glycosidases or by endocytosis into endothelial cells. VGC components are added to the system by *de novo* synthesis and exocytosis. The lumenal glycocalyx has unique functions that are critical to the vascular barrier, vascular tone, and interaction between circulating cells and endothelium. In this section, we describe how VGC remodeling affects these functions.

1.2.2 Remodeling and the endothelial barrier

One of the most fundamental actions of the endothelium is to act as a selective barrier to lumenal molecules and cells crossing into the interstitium. The structure of the VGC is critical to controlling this selective permeability. Due to the anionic nature of the glycan-rich glycocalyx, amphipathic albumin saturates the VGC and promotes the formation of the glycocalyx into a protein rich lattice-like structure with a net-negative charge [12], which likely explains the "plasma layer" observed in the 1940s to 1970s [2]. The fiber matrix forms a molecular sieve, blocking negatively charged and/or large molecules and cells from transvascular flow [13,16]. Additionally, the protein rich layer controls fluid flux across the endothelium along the colloid osmotic pressure gradient, as described by the revised Starling Equation [17]. GAG remodeling appears to affect both VGC macrostructure and permeability. Digestion of VGC HS via perfusion guinea pig heart with *Flavobacterium heparinum* heparinase increased fluid efflux from the lumen without affecting colloid efflux. Further, inhibiting HS digestion by genetic deletion of heparanase inhibits lung fluid exudate with endotoxemia challenge [18], highlighting how fluid filtration may depend on certain

VGC components [19]. Degrading VGC components also affects particle infiltration into the endothelial barrier. *In vivo* digestion of lumenal HA using intravenous *Streptomyces* hyaluronidase allowed for penetration of ≤145 kDa FITC-dextran particles into the cremaster VGC, yet larger FITC-dextran particles and red blood cells were still excluded from the glycocalyx space. Infusion of HA and CS mixture back into the digested vasculature restored VGC selectivity [20]. Digesting specific GAG classes appears to have varying effects on VGC permeability and structure. Systemic infusion with heparinase, chondroitinase, and hyaluronidase decreased post-capillary venule VGC thickness by 43%, 34%, and 12%, respectively, with all 3 enzymes infused together decreasing VGC thickness by 89% [6]. In short, GAGs are required to maintain VGC permeability and macrostructure, but remodeling each GAG uniquely alters these parameters.

1.2.3 Remodeling, vascular tone, and mechanotransduction

Endothelial cells sense both lumenal shear stress and vasoactive factors to relay information to smooth muscle cells, which ultimately control vascular tone by mediating vasodilation or vasocontraction [21]. The VGC plays a critical role in mechanotransduction of shear force to the cytosol of the endothelium. Transmembrane VGC components such as Glypican-1 sense shear stress and transmit the signal to intracellular signaling cascades, allowing for integration of hemodynamic and vasoactive factor signaling [22]. Remodeling of the VGC has profound effects on endothelial shear stress responses. Enzymatic removal of HS or HA ablates endothelial production of the vasodilator nitrous oxide (NO) in shear force. After HS and HA removal, NO synthase agonists still induce NO synthesis, indicating that the VGC amplifies shear force signals that mediate vasoactive factor production [23–25]. Lumenal shear flow also regulates the localization and abundance of VGC components on the apical membrane of the endothelium. Endothelial HA production is boosted under shear stress, while HS abundance is unaffected [26].

Under shear stress, most of the cell surface HS colocalizes to cell-cell junctions, as did Glypican-1 and associated lipid rafts [25,27]. However, Sdc1 and CS localization did not re-organize in this context [27]. Shear stress appears to depend on and specifically affect the localization of certain VGC components, implying that certain VGC components are more involved in shear flow mechanotransduction than others.

Downstream of mechanotransduction, the cell undergoes a myriad of signaling responses in response to shear stress. Apical transmembrane ion channels and their glycosylation status are critical to responding to shear forces after mechanotransduction [21]. Epithelial Na^+ channel (ENaC) in endothelial cells mediates vascular responsiveness to blood pressure. Removal of ENaC N-glycosylation via enzymatic removal with PNGase or by individually replacing asparagines with alanines ablated ENaC control of blood pressure. Interestingly, remodeling ENaC glycosylation does not affect its abundance or the ability of the channel to transport ions [28]. How glycosylation remodeling affects ENaC activity, and the signaling ability of other vaso-sensatory ion channels, has yet to be elucidated.

1.2.4 Remodeling and endothelial cell-circulating cell interactions

The location of the VGC allows it to influence how circulating cells in the lumen interact with the apical endothelial surface. The VGC is involved in several aspects of cell-cell interactions, including maintaining laminar flow, containing ligands and receptors for circulating cell adhesion, and concentrating signaling proteins that promote cell adhesion to the endothelium [9]. VGC remodeling greatly changes how cells interact with the apical endothelial surface. Before remodeling, the physical thickness of the VGC varies greatly depending upon the tissue, with thinner non-fixed glycocalyces such as the cremasteric microvessels measuring around 670 nm [18]. P-selectin, a major adhesion molecule present on the apical surfaces of activated endothelial cells,

protrudes only 50 nm from the endothelial plasma membrane [29]. Thus, adhesion molecules are likely buried under the VGC until remodeling of the VGC occurs. Enzymatic degradation of the VGC with heparinase, chondroitinase, or hyalurondase, or induction of degradation with pro-inflammatory cytokines or angiopoetin-2 (Ang2), decreases VGC thickness by 50-70% [18,30,31]. After VGC thinning, white blood cells (WBCs) more readily adhere to the endothelial surface in a selectin-dependent manner [18,32,33]. Thus, during inflammatory conditions when the VGC undergoes extensive remodeling and thinning, WBC adhere to activated endothelium proximal to areas of inflammation after possible uncovering of adhesion molecules.

The VGC also holds chemoattractant signaling molecules that recruit WBCs. Chemokines are held near the endothelial surface by engaging electronegative HS with their highly electropositive domains, creating gradients that attract leukocytes [34]. Modulating HS greatly affects chemotactic abilities of chemokines. Altering endothelial HS by either reducing its sulfation, inhibiting its biosynthesis, or overexpressing endogenous heparanase inhibits leukocyte chemotaxis [14,15,35,36]. Reducing HS sulfation also decreases chemokine transcytosis across the endothelium and chemokine presentation on the endothelial apical surface [35]. Conversely, increasing HS sulfation promotes chemokine binding to endothelial HS [36]. Modulating HS structure provides a mechanism for controlling engagement of endothelial cells to chemokines and thus chemotaxis of WBCs.

Upon inflammatory insult, endothelial cells express ligands and receptors in the VGC that engage circulating neutrophils and monocytes, leading to a process of WBC rolling, firm adhesion, and diapedesis through the endothelium, in a process known as extravasation [37]. Both the endothelium and circulating WBCs express pro-adhesive molecules that are utilized in different stages of this process. Selectins, including P-selectin, E-selectin, and L-selectin, are VGC

glycoproteins that mediate initial adherence and rolling stages of extravasation, allowing for engaging of chemokines and further WBC activation. Subsequent firm adhesion and diapedesis of the WBC is largely mediated by glycoprotein receptors in the immunoglobulin superfamily, namely ICAM-1, ICAM-2, VCAM-1, and PECAM-1 [37]. The variation in abundance and glycosylation of these receptors, and their respective ligands, greatly influences their functionality.

Endothelial P-selectin is contained within vesicle Weibel-Palade bodies (WPBs). Upon endothelial cell activation, WPB fusion to the plasma membrane rapidly distributes P-selectin to the endothelial surface [38]. E-selectin is not expressed in endothelial cells until induction by pro-inflammatory cytokines or other endothelial activating stimuli [39,40]. L-selectin, which is constitutively expressed on circulating leukocytes, engages multiple glycan ligands on the endothelial surface [37,41]. The tetrasaccharide Sialyl Lewis X (sLe^x) is the minimal structural determinant for luminal L-selectin ligands in the VGC [42], and structural modification of sLe^x greatly impacts its function. Removal of sialic acid with sialidase abrogates L-selectin mediated binding of leukocytes to high endothelial venules [43]. The majority of sLe^x is located on O-glycans decorating protein backbones as Core-1 or Core-2 O-glycans [41]. However, mice lacking both Core-1 extension and Core-2 branching enzymes had increased lymphocyte rolling velocities yet still had robust lymphocyte homing due to *N*-glycans containing sLe^x [44]. sLe^x can be modified with the addition of a sulfate ester on C6 of GlcNAc, which occurs on core-1 O-glycans, or C-6 on galactose of Core-2 O-glycans. GlcNAc 6-sulfo sLe^x is the dominant L-selectin ligand expressed in high endothelial venules and chronically inflamed microvessels [45,46]. Deletion of both *N*-acetylglucosamine-6-*O*-sulfotransferases completely abolished 6-sulfo sLe^x. Interestingly, this sLe^x remodeling resulted in a 75% reduction in lymphocyte homing to lymph nodes, indicating other L-selectin ligands are used in this process [45]. L-selectin also engages endothelial HS in a

sulfation-dependent manner. Remodeling endothelial HS by decreasing HS sulfation increases L-selectin mediated rolling velocity, while increasing endothelial HS sulfation decreases L-selectin mediated rolling velocity [35,36]. Considering the redundancy of L-selectin ligands and how remodeling L-selectin ligands modulates leukocyte engagement to endothelial cells, it is enticing to study how unique inflammatory stimuli may differentially affect L-selectin ligand structures and downstream leukocyte trafficking.

Transcellular adhesion receptors in the immunoglobulin superfamily such as ICAM-1, VCAM-1, and PECAM-1 are VGC components that bind leukocyte integrins to mediate leukocyte tight adhesion and diapedesis during extravasation. The expression of these glycoproteins increases in endothelial cells during inflammation [37]. Further, they are enriched in the VGC during pro-inflammatory responses such as infection [37,47], which potentiates leukocyte trans-endothelial migration. The cellular adhesion receptors in the immunoglobulin superfamily are heavily glycosylated and their glycosylation status affects their function. The extracellular domain of ICAM-1 contains up to 9 *N*-glycosylation sites. In TNF-α activated endothelial cells there is an enrichment of high-mannose or complex type *N*-glycans with a α-2,6 sialic cap [48,49]. Pharmacological inhibition of complex *N*-glycan synthesis increases monocyte and neutrophil adherence to endothelial cells in an ICAM-1 dependent manner [49,50]. Interestingly, enzymatic removal of sialic acid from ICAM-1 slightly increased its resistance to elastase cleavage that is common in inflammation [51]. Modulation of PECAM-1 glycosylation also changes its function. Genetic ablation of *N*-glycan α-2,6 sialic acid biosynthesis or mutagenesis of the asparagine-25 *N*-glycosylation site interferes with homophilic interactions that are critical to its function [52,53]. Clearly, glycosylation remodeling can greatly influence immunoglobulin superfamily cell adhesion receptor function, and further work characterizing how endothelial activation induces

this remodeling would provide critical knowledge on fine-tuning receptor function in leukocyte extravasation.

1.3 Host remodeling factors and their regulation

1.3.1 Overview of Remodeling Factors

A litany of host factors remodel specific VGC components. Proteases degrade VGC proteins while glycosidases degrade glycans attach to lumenal glycoconjugates, with both enzymatic classes possessing the ability to drastically alter VGC structure. Further, host cells can add or withdraw new VGC components from the lumen. Regulation of these remodeling factors is critical to controlling VGC structure and responding to vascular perturbations. In this section, the critical host VGC remodeling factors and their regulation will be summarized.

1.3.2 Proteolytic Remodeling

Matrix metalloproteinases (MMPs) and the adamalysins, including a disintegrin and metalloproteinases (ADAMs) and ADAMs with thrombospondin motifs (ADAMTSs), are two major classes of zinc and calcium dependent endopeptidases [54]. The MMPs and adamalysins have long been implicated in ECM remodeling, with well characterized roles in tissue development, immunity, angiogenesis, and homeostasis [54]. MMPs and adamlysins are also critical factors in VGC remodeling. Chelation of divalent cations or small molecule inhibition of MMPs increases circulating lectin and WBC binding to the venular vascular glycocalyx over time, suggesting MMP-mediated VGC turnover occurs in baseline conditions [55,56]. MMPs have been shown to cleave specific targets in the VGC. Inhibition of MMP2 and MMP9 decreases the release of soluble ICAM1 from the apical surface of cultured endothelial cells [57]. Deletion of MMP9 increases age-related release of endothelial markers VCAM1 and von Willebrand factor (vWF), indicating a compensatory increase in proteolytic activity on endothelial VGC components [58]. Inhibition of

MMPs, ADAM10, or ADAM17 limits TNF-α-induced shedding of cell-surface endomucin, a heavily O-glycosylated transmembrane protein important for leukocyte interaction with quiescent endothelium [59]. ADAM15 mediates apical glycocalyx loss and cleavage of endothelial CD44 [60]. Oligomerized vWF, a potent ligand of platelets and circulating WBCs, is bound to the apical surface of activated endothelium and is digested by endothelium-bound ADAMTS13, thus inhibiting cell adhesion to vWF [61,62]. VE-cadherin, a cornerstone of endothelial tight junctions that are commonly proximal to the apical surface [63], is shed from endothelium by activated endothelial ADAM10 [64,65]. MMP2 and MMP9 mediate Sdc1 and Sdc4 shedding from endothelial cells, with MMP2 and MMP9 activity correlated with glomerular vascular permeability [66–70]. Pan-MMP inhibition limits oxidative stress induced shedding of Sdc1 from endothelial cells [70]. Vasodilation is also modulated by MMP activity, with MMP2 cleaving Big Endothelin-1and converting it into a potent vasoconstrictor [71]. While many of these studies detail MMP and adamalysin editing of apical glycocalyx *in vitro*, more research into their editing of VGC *in vivo* is needed.

MMP and adamalysins are regulated through a complex network of transcriptional controls, trafficking networks, and endogenous inhibitors, as extensively reviewed elsewhere [54]. Examples of MMP and adamlysin regulation in the context of VGC remodeling will be discussed here. MMPs and adamalysins are inhibited by endogenously encoded inhibitors. There are four tissue inhibitors of metalloproteinases (TIMPs), endogenous metalloproteinase inhibitors that wedge into the active site of metalloproteinases [54]. TIMP3 binds to sulfated GAGs [72], but there is no evidence of TIMP interaction with GAG in the VGC. TIMP3 directly inhibits ADAM10, ADAM17, ADAMTS4, and ADAMTS5 [73–75]. TIMP2 and TIMP3 block membrane-type 1 MMP-meditated cleavage of ICAM1 during monocyte transmigration across the endothelium [76]. TIMP3 inhibits Sdc1 and Sdc4 endothelial shedding [66], while TIMP2 blocks MMP2-mediated generation

of vasoactive Big Endothelin-1 [71]. Another endogenous factor, sphingosine-1-phosphate (S1P), stabilizes the VGC and Sdc1 from shedding by suppressing MMP activity through an unknown mechanism [67]. Host signaling also controls MMP and adamalysin expression. Expression of MMPs is partly mediated through the PKC-ERK-MAP Kinase pathway [77]. Cytokine signaling through TNF-α, TGFβ, and IL-8 increases expression of MMPs though activation of NF-κB mediated transcriptional systems [68,78–80]. TNF-α also induces expression of endothelial ADAM17[81]. NO also increases the activity and translation of endothelial MMP13 [82]. Shear stress on HUVECs increases ADAM15 and ADAM19 expression while suppressing ADAM23 expression. Shear stress does not affect expression of any other ADAM, indicating that shear stress activates pathways that control selective ADAM expression [83]. Although research into MMP and adamalysin regulation is abundant, additional focus of these processes in endothelial cells, and their impact on the VGC, is needed.

1.3.3 Glycosidase-mediated extracellular remodeling

GAG degradation and remodeling on the cell surface has a dramatic impact on VGC integrity [18,30,31,84]. GAGs are shed from cell surfaces and detected in circulation, as reviewed extensively elsewhere [85]. However, the origin of shed GAGs is not precisely known, although it is hypothesized to come from the VGC. There are limited studies detailing VGC remodeling by endogenous glycosidases in culture or *in vivo*. Although there are up to 8 potential hyaluronidases in the human genome [86,87], endogenous hyaluronidase activity has been mostly studied in 4 endogenous hyaluronidases: hyaluronidase-1 (Hyal1), Hyal2, TMEM2, and Kiaa1199 [86–89]. Large HA chains are degraded into smaller HA fragments by Hyal2 and TMEM2, which are then internalized in a CD44-dependent mechanism and further degraded in the lysosome by Hyal1 [87,89,90]. Hyal2 is widely expressed on the lumenal surfaces of endothelial cells and loss of Hyal2

leads to VGC HA accumulation [91]. Human umbilical vein endothelial cells (HUVECs) under low shear stress conditions express Hyal2 that degrades glycocalyx HA [92], and during models of inflammatory bowel disease platelet Hyal2 degrades intestinal endothelial HA and increases inflammation [93]. However, it is unclear if this corresponds to apical or basal HA. Endothelial TMEM2-mediated HA degradation is required for angiogenesis [87], but TMEM2 has not been observed to remodel the VGC in stable blood vessels.

Extracellular HS chains can be degraded by Heparanase (HPSE), a single gene that encodes an endo-β-glucuronidase enzyme that is created as a precursor protein and is cleaved to a more active form [94]. Endothelial HPSE expression is upregulated in certain contexts, including pro-inflammatory cytokine signaling, exposure to low-density lipoproteins, inhibition of NO synthase, or ligand engagement of receptor for advanced glycation end products (RAGE) [94–96]. Post-translational regulation of HPSE provides insight into its endogenous role. HPSE is most active at pH 6.0 and has only 25% activity at physiological pH [97,98]. Further, HPSE acts as an non-enzymatic adhesion molecule and is stabilized by HS chains at physiological pH, while lowering the pH converts HS-bound HPSE back to an enzymatic form [97,98]. However, HPSE is critical to VGC remodeling in pathological conditions. In endotoxemia and cecal ligation and puncture sepsis models, *Hpse*$^{-/-}$ animals do not undergo VGC degradation and have reduced adherence of pro-inflammatory neutrophils to the pulmonary endothelium, leading to protection from lethality [18]. It was shown that adoptively transferred *Hpse*$^{+/+}$ neutrophils do not adhere to *Hpse*$^{-/-}$ pulmonary endothelium *in vivo*, indicative that neutrophil HPSE may not be responsible for endothelial HS remodeling [18]. However, it is unknown which tissue or cell type produces VGC-degrading HPSE. Additionally, it is not clear if HPSE either directly degrades the VGC or assists a cell type or another host enzyme in VGC remodeling through its HS-binding functionality. It has been shown

that HPSE from activated platelets or platelet lysate can cleave endothelial HS but only in acidic conditions that may be found in inflammatory contexts [98]. Further study into the cellular origin, enzymology, and HS-binding activity of endogenous HPSE in the context of infection is needed.

Although *N*- and *O*- glycan structures are common on glycoproteins in the VGC, there is limited work observing extracellular degradation of these structures by endogenous enzymes. α-glycosidic linked sialic acids cap many of these structures and are cleaved by endogenous neuraminidase activity. However, the four neuraminidase genes (*Neu1-4*) have maximal activity at lysosomal or early-lysosomal pH, with surface activity mostly occurring during cell activation or stress where lysosomal fusion occurs with the plasma membrane [99]. Neu1 and Neu3 are expressed in human endothelial cells where Neu1 can de-sialylate PECAM1, although it is unclear if this occurs on the cell surface or in the lysosome [100]. Neutrophil neuraminidase activation can lead to loss of surface endothelial sialic acid and increased neutrophil adherence [101]. Treatment of human pulmonary endothelial cells with dengue virus non-structural protein-1 can activate loss of surface sialic acids, leading to an increase in trans-endothelial permeability [102]. Although other exo-glycosidases cleave de-sialylated terminal residues from *N*- and *O*- glycans, evidence of this occurring in the VGC is lacking. Further studies detailing the extracellular versus lysosomal degradation of *N*- and *O*- glycans are needed.

1.3.4 De novo synthesis

As inflammation increases VGC shedding and degradation, there is evidence that biosynthesis increases simultaneously. HA synthesis increases in human endothelial cells upon stimulation with pro-inflammatory signals including TNF-α, IL-1β, and IL-15, which promotes NF-κB signaling and CD44-dependent adherence of leukocytes to the endothelium [103–105]. Surface HA increased alongside Hyaluronan Synthase 2 (Has2) expression [105], which extrudes HA from

the plasma membrane directly into the vascular glycocalyx. Interestingly, IFN-γ and TGF-β do not induce HA content increase on the cell surface or Has2 expression, indicating selective control of HA biosynthesis [105]. Stimulation of human microvascular endothelial cells with TNF-α and IL-1β increases HS sulfation, HS biosynthesis enzyme *N*-deacetylase-*N*-sulfotransferase 1 (*Ndst1*) expression, and HS-dependent CCL5 binding 16 hours after treatment [106]. Expression of Exostosin-1 (*Ext1*), a critical HS biosynthesis enzyme that forms part of the HS-extending co-polymerase, increases upon activation of fibroblast growth factor receptor 1 (FGFR1) [30]. S1P signaling also greatly increases HS, CS, and Sdc1 biosynthesis after endothelial cell starvation [107]. Non-GAG glycans also increase in expression with pro-inflammatory signals, where N-glycan expression rises 4 hours after stimulation of HUVECs with TNF-α and stimulates monocyte adhesion [11]. More studies detailing VGC turnover through simultaneous degradation and *de novo* biosynthesis are needed, as most studies focus on one aspect of VGC turnover.

1.3.5 Endocytosis

Most glycoconjugates are degraded within the lysosome after endocytosis from the plasma membrane. There is also evidence that VGC components are endocytosed from the endothelial surface. Negatively charged particle tracers injected intra-venously associate with the VGC and coat both caveolae and clatherin-coated pits on endothelial cells [108]. HA binding proteins are also associated with endocytic vesicles and mediate HA uptake for degredation. HA receptor for endocytosis (HARE) uptakes HA via clatherin-coated pits [109], while Kiaa1199 and CD44 independently bind to HA to process it through caveolae [88,110]. Glycoproteins are also internalized on clatherin-coated pits and caveolae [111,112]. Approaches studying global effects of endocytic-mediated VGC remodeling would give greater insight into glycan and glycoprotein removal from the cell surface through lysosomal degradation.

1.4 Infection-induced vascular glycocalyx remodeling

1.4.1 Overview of VGC remodeling during infection

During infection, the endothelium and other vascular cells receive signals that facilitate pathogen clearance and host tolerance and recovery. Both host and pathogen factors manipulate these responses that determine the balance of the immune response, and in cases of severe infection leads to immune imbalance and dysregulation. Sepsis, a life threatening organ dysfunction caused by a dysregulated host response to infection [113], may even develop in cases of infection-induced host-wide vascular dysregulation and subsequent organ failure. Because the VGC is critical to vascular function, how host and pathogen factors influence VGC status during infection is critical to disease outcome. Additionally, infection promotes endothelial-associated glycocalyx changes, host immune cell attachment to the endothelium, and opening of sub-endothelial glycocalyx to vascular flow, all of which involve changes in composition and function of the VGC. In this section, VGC remodeling that occurs in infection and sepsis, and how it affects the host immune response, will be summarized.

1.4.2 Pathogen induction of host remodeling

Pathogen associated molecular patterns (PAMPs) are often used to substitute true infection. Although PAMPs do not represent the complexity of true infections, valuable information can be gathered by studying how PAMPs affect the VGC. Lipopolysaccharide (LPS), a lipopolysaccharide PAMP found on the outer membrane of gram-negative pathogens, promotes potent inflammation that leads to ~50% reduction in VGC thickness in a TNF-α dependent manner [18,84]. LPS promotes VGC turnover via induction of remodeling factors and synthesis of new VGC components. For example, LPS induces MMP1, ADAM15, and ADAM17 to cleave and shed glycocalyx components, leading to increased vascular leakage and leukocyte adhesion to the

endothelium [60,114,115]. LPS also induces HPSE activity and HS loss in endothelial cells [116]. Simultaneously, endotoxin induces *de novo* synthesis of endothelial HA, Sdc4, and cell adhesion glycoproteins on the endothelial surface [103,117,118], thus increasing VGC turnover.

Although endotoxin induces VGC remodeling, it is a common antigen on both pathogenic and non-pathogenic gram-negative bacteria. Pathogens have non-PAMP factors that upregulate or activate VGC remodeling components to disrupt the immune response. *Staphylococcus aureus* induces VGC remodeling via secretion of α-hemolysin, also known as α-toxin, that activates host ADAM10 to cleave endothelial junction glycoproteins, promote pro-inflammatory neutrophil and platelet activation in the vasculature, and drive vascular leakage [64,119]. Further, *S. aureus* sepsis induces dramatic pro-inflammatory changes in the VGC, with enrichment of acute phase proteins, adhesion receptors, complement components, coagulation factors, and proteoglycans [47]. Although both *Neisseria meningitidis* and dengue virus infection induced endothelial barrier breakdown in an MMP-dependent manner [120,121], it is unclear if MMP activity directly acts upon the VGC. The sublingual vasculature in sepsis patients has a thinner glycocalyx than other critically ill patients, but it is unknown if certain pathogens promote more VGC loss than others [122]. Pathogens commonly express proteases and glycosidases to modulate host responses, but it is largely unknown how or if these pathogen enzymes affect VGC structure, composition, or function in an *in vivo* setting. More studies with live infection models are needed to understand how pathogens induce VGC remodeling.

1.4.3 Weibel-Palade bodies and angiopoietins in VGC remodeling

Endothelial cells can rapidly respond to inflammatory insult common to infection and induce multiple processes that lead to VGC remodeling. Central to this rapid response are Weibel-Palade Bodies (WBPs), secretory bodies that rapidly fuse to the lumenal plasma membrane upon

endothelial stimulation by TLR2, coagulation and complement factors, host signaling molecules, cytokines such as TNF-α, and other agonists [123–125]. The contents of WBPs impact many aspects of endothelial inflammation and directly change VGC composition. WBPs are highly enriched in the glycoprotein vWF and other coagulation factors, which can attach to the vessel wall and promote coagulation. WBPs also contain P-selectin to initiate leukocyte rolling and anchor vWF to the cell surface within minutes of endothelial activation [123,126]. Importantly, WBPs contain and release angiopoietin-2 (Ang2) [127], a critical regulator of endothelial permeability and host inflammation during infection. Serum Ang2 abundance increases greatly during severe sepsis and correlates strongly with cytokines such as TNF-α [128]. Ang2 sensitizes endothelial cells to TNF-α and is required for TNF-α-induced ICAM1 and VCAM1 expression in endothelial cells [129]. Ang2 contextually can act as an agonist or antagonist of endothelial Tie2, where antagonism destabilizes endothelial junctions [130]. Interestingly, some anti-Ang2 monoclonal antibodies induce Ang2 agonism of Tie2, which preserves the VGC, reduces glomerular endothelial HPSE expression, and protects HS associated pulmonary vasculature during cecal ligation and puncture sepsis [131]. Further, Ang2 mediates HPSE-dependent VGC degradation and edema after LPS exposure [31], indicating that Ang2 can either promote or exacerbate VGC remodeling depending upon context. Further studies are needed to fully understand the connection between Ang2-Tie2 activity and VGC status.

1.4.4 Coagulation and complement

Coagulation and complement are critical aspects of vascular immunity that modulate infection outcome and can drive vasculopathy with imbalanced homeostasis [132]. During infection, VGC composition in major organs becomes enriched with both complement and coagulation factors [47], and studies have observed thrombosis occurring during bacterial infection associated

with glycoprotein shedding and major VGC remodeling [47,133]. Multiple studies have shown coagulation factors can directly act upon the VGC and how these factors change VGC composition. Thrombin activity leads to a 40-50% reduction in VGC thickness and stiffness [84]. Upon endothelial activation and WBP exocytosis, vWF forms large multimer fibers on the endothelial surface that forms anchor points for platelets and pro-thrombotic neutrophil extracellular traps (NETs) [61,134]. Further, vWF anchoring to the endothelial surface depends upon VGC HS [135]. Platelet and neutrophil attachment to the VGC induces immunothrombosis in microvessels, generating an intra-vascular scaffold that facilitates the recognition, containment, and destruction of pathogens [132]. During *Escherichia coli* and *S. aureus* intravascular infection, platelets bundle bacteria in the sinusoids and associate with neutrophils and NETs [136]. In *S. aureus* sepsis models, platelet-neutrophil aggregates can exacerbate thrombosis and intravascular NET formation in the liver that leads to severe hepatic damage [47,119,137]. These thrombotic events have a clear impact on VGC composition, as neutrophil NETs components, platelet degranulation factors, and coagulation factors increase in the liver VGC during *S. aureus* sepsis [47]. As the VGC forms the surface where thrombotic events occur, further studies detailing how the VGC interacts with coagulopathy and complement deposition would give further insight into the VGC's influence on these systems.

1.4.5 Leukocyte adhesion and VGC remodeling

During infection and sepsis, inflammation increases cell adhesion glycoproteins on the endothelial surface. After LPS injection, cell adhesion molecules including VCAM-1, P-selectin, and E-selectin increase in expression and VGC abundance [118,138,139], which promotes neutrophil adherence to the pulmonary endothelium and subsequent lung pathology [18]. Remodeling of certain VGC glycans may be critical to leukocyte adherence and infiltration during infection. In the liver

VGC, HA plays on important role in neutrophil recruitment and inflammation. VGC HA is abundant in the liver at baseline conditions, and during endotoxemia neutrophils adhere to sinusoidal-HA in a CD44 manner [118,137]. In *S. aureus* sepsis, HA binding and remodeling proteins are enriched in the liver VGC and circulating HA also increases [47], perhaps indicating that HA remodeling and turnover occurs in the sinusoids during infection. As highlighted in the previous section, neutrophils adhered to the endothelium can promote immunothrombosis or, in cases of sepsis, liver pathology. Remodeling sulfated GAGs impacts host cell attachment to the VGC and subsequent trafficking during infection. Overexpression of HPSE interferes with chemokine gradients that attract leukocytes to cites of inflammation and decreases the ability to clear *S. aureus* subcutaneous infection [140]. HPSE activity is required for LPS-induced neutrophil adherence and inflammation in the pulmonary vasculature [18]. Reducing endothelial HS sulfation reduces neutrophil transmigration across the endothelium toward LPS in an air pouch model [35], while increasing overall HS sulfation has the opposite affect [36]. Although modulating the VGC can impact leukocyte interactions with the endothelium, recruited leukocytes also bring factors that change VGC composition. As highlighted in the previous section, neutrophil and platelet driven immunothrombosis changes VGC composition and can drive pathology. During sepsis, the VGC becomes enriched with leukocyte factors [47], underscoring how the VGC can modulate leukocyte adherence and thus allowing recruited leukocytes to change VGC composition.

1.4.6 Vascular glycocalyx protection and recovery

During infection and sepsis, there is evidence of dysregulation in the mechanisms that promote VGC reconstitution and protection. S1P, which has been shown to preserve normal glycocalyx and increase synthesis of VGC components [107], has decreased levels in the serum of sepsis patients and is negatively correlated with sepsis severity [141]. In non-septic VGC degradation,

HS fragments and FGF2 can activate HS biosynthesis enzyme expression. However, in septic conditions FGFR1 activation is inhibited and prevents downstream activation of HS biosynthesis which correlates to a decrease in VGC thickness [30]. As previously described, the endothelial junction regulator Ang2 is released from endothelial cell WBPs in sepsis and mediates HPSE-mediated VGC degradation [31]. Ang1-Tie2 signaling, which stabilizes endothelial junctions, can be antagonized by Ang2 and can promote endothelial destabilization in certain contexts [130]. Use of Ang2 inhibitor, Tie2 agonist, or recombinant Ang1 treatment protects the VGC from degradation after LPS treatment [131,142], and treatment of vessels with Ang1 increases VGC thickness and decreases vessel permeability after proteolytic injury [143]. Despite disruption of VGC recovery during sepsis, there is evidence that the altered VGC can blunt subsequent inflammatory insult. After CLP sepsis, VGC HS was resistant to heparinase-III digestion, which targets under-sulfated regions of HS, indicating that HS remodeling may have occurred in sepsis [144]. Interestingly, expression of sulfatase-1 (Sulf-1), a cell-surface enzyme that removes 6-*O*-sulfation from HS chains, is decreased after CLP sepsis, which correlated to an enrichment of 6-*O*-sulfated HS in plasma. Endothelial *Sulf1* deletion recapitulated post-septic VGC resistance to Heparinase-III. In post-CLP animals, intravenous injection of Sulf-1 increased pulmonary leukocyte infiltration after intratracheal LPS compared to vehicle control animals, indicating that vascular Sulf-1 activity can potentiate post-septic inflammatory insult [144]. Considering this study, it would be valuable to investigate how the multitude of VGC remodeling factors affect VGC recovery. Protection of the VGC, or how it recovers from infection and sepsis, may impact host recovery from the disease. Sepsis survivors often have chronic health issues [145], highlighting the importance of promoting proper sepsis recovery, with the VGC being an interesting therapeutic target.

1.4.7 Global compositional changes

Attempts have been made to characterize pan-endothelial VGC remodeling during sepsis by measuring shed VGC components in circulation. For example, proteoglycan shedding is a commonly used measure of VGC degradation in sepsis, as reviewed extensively by Uchimido, et al [85]. However, this type of analysis makes the assumption that the circulating analytes are derived from the endothelium. Hypothetically, parenchymal cells may secrete or shed VGC components that end up in circulation. More target analyses of the VGC have the potential to specifically observe changes on the vascular surface. A common strategy is to isolate one endothelial bed and study VGC remodeling after inflammatory insult. However, there are multiple reports of endothelial cells undergo major phenotyping drift in culture [138,146,147], highlighting the importance of micro-environmental cues in maintaining endothelial heterogeneity.

In vivo sepsis studies focusing on omics-level changes in the vasculature demonstrate that not only are there shared pan-endothelial changes but individual vascular beds exhibit unique changes [47,138]. During endotoxemia, the pan-endothelial translatome was enriched for adhesion receptors required for leukocyte recruitment and de-enriched for genes involved in barrier maintenance, while individual vascular beds showed distinctive translational responses [138]. Specifically targeting the VGC by vascular proteome enrichment during *S. aureus* sepsis shows a distinct enrichment compared to the LPS translatome, albeit with some overlap [47]. Pan endothelial changes include acute phase proteins, coagulation factors, complement components, and ECM-remodeling factors. Importantly, the VGC underwent organotypic changes in *S. aureus* sepsis. The liver VGC was enriched with neutrophil degranulation factors such as MPO, which coincides with intravascular NETs driving thrombosis during *S. aureus* infection [137]. Further, the liver was enriched with leukocyte adhesion, integrin signaling, and GAG metabolism factors, especially those associated with HA turnover [47]. Kidney VGC was enriched with renal adhesion proteins and

renal epithelial morphogenesis factors, while the heart VGC was enriched for muscle contraction and hypertrophic cardiomyopathy proteins. White adipose tissue and the brain VGC showed few unique changes. While this study highlights the heterogeneity of VGC remodeling across each organ during *S. aureus* sepsis, other sepsis-causing agents may have unique signatures. Additionally, this study focused on one timepoint, while the dynamic nature of sepsis may only be addressed across multiple timepoints.

1.5 Diagnostics and therapeutics

1.5.1 Diagnostics, therapeutics, and the VGC

With the VGC forming a dynamic and fundamental aspect of vascular biology, it would be advantageous to use the VGC as a therapeutic and diagnostic tool during infection and sepsis. Diagnostics that detect VGC remodeling as a proxy for sepsis severity have been developed and show promise. Additionally, manipulation of host remodeling factor activity or VGC composition have been explored as therapeutic options. In this section, diagnostics and therapeutics centered around VGC remodeling, and their medical benefit during infection and sepsis, will be summarized.

1.5.2 Diagnostics

Detection of shed VGC components in patient plasma or serum is a leading VGC-based diagnostic in severe trauma and sepsis, as reviewed extensively in Uchimido, et al 2019 [85]. In short, diagnostics based upon VGC remodeling or shedding fall into two categories: bedside intravital microscopy and detection of shed GAGs and proteoglycans. Bedside intravital microscopy techniques measure the perfusable diameter of vessels, which is inversely correlated with VGC thickness. One study demonstrated that the perusable diameter of vessels was increased in septic ICU patients versus non-septic ICU patients. However, there is considerable variation among

patients and the perfusable vessel diameter did not correlate with sepsis score severity or other measures [122]. Although this is an attractive and non-invasive measurement, more studies are needed to understand if intravital microscopy has efficacy as an accurate diagnostic. Detection of VGC shedding components in circulation, mainly GAGs and proteoglycans. Is another potential diagnostic [85]. Both HA and HS circulating levels are elevated in sepsis patients over controls. Additionally, several studies have shown that circulating Sdc1 levels are elevated in sepsis patients and correlate with sepsis severity [85]. However, it is crucial to note that although these parameters are useful tools in determining sepsis prognostics, their origin as VGC or parenchymal components is unknown. Analysis of verified VGC components may be a useful diagnostic parameter of VGC shedding and health, particularly in individual organs or vascular beds [47]. Further, studying novel organotypic changes in VGC composition may reveal new therapeutic windows to protect the VGC and promote vascular health.

1.5.3 Therapeutics

The use of glycans or glycan mimetics to inhibit VGC remodeling factors has been explored as a strategy to protect the VGC during sepsis. Heparin, a form of short chain and highly sulfated HS, is a widely used anticoagulant that has been shown to inhibit VGC degradation. Unfractionated heparin, which consists of a large diversity of anticoagulant HS chains, has been shown to protect canines from endotoxemia and mice from CLP sepsis [18,148]. In mouse endotoxemia, heparin was shown to inhibit VGC degradation, neutrophil adherence, and neutrophil activation in pulmonary vessels while reducing shed Sdc1 levels in circulation. Further, these VGC-protective effects are not dependent upon heparin anti-coagulant activity, as non-anticoagulant *N*-desulfated/re-*N*-acetylated heparin (NAH) recapitulates these phenotypes [18,149]. Although it is suggested that heparin and NAH may exert these protective effects by inhibit

heparanase activity, other means of inhibiting inflammation may account for these phenotypes. Therapeutically, using heparin as a VGC-protective agent is complicated by its anticoagulant effects, which may not be advantageous to patients undergoing hypovolemic shock or thrombocytopenia. Further testing of NAH or more small molecule inhibitors of heparanase in the context of infection and sepsis is a promising alternative to heparin.

Other VGC degradation inhibition strategies have targeted proteases and steroid hormone pathways. Antithrombin, an important regulator of coagulation, inhibits TNF-α induced VGC degradation and shedding [150], although use of antithrombin as a sepsis therapeutic is not recommended due to a lack of benefit to patients and increased bleeding risk [151]. Inhibition of MMPs is a promising strategy to blunt VGC remodeling but has not been explored extensively therapeutically in the context of infection or sepsis. Use of MMP inhibitor GM6001, also known as Ilomistat, has been shown to inhibit VGC shedding induced by fMLP and TNF-α [55], and specific MMP inhibitors have shown protective effects in experimental sepsis [152]. Inhibition of proteases ADAM10 and ADAM17 reduces TNF-α induced shedding of endothelial cell surface endomucin [59]. Steroid hormones have also been explored as therapeutics that support the VGC. After perfusion of guinuea pig hearts with TNF-α, hydrocortisone treatment greatly reduced VGC component shedding and protected overall VGC structure [153], although the mechanism for this protective effect is unclear.

Supporting VGC superstructure during remodeling has been attempted with both resuscitation and reconstruction. Because proteins like albumin have been shown to be important in maintaining a lattice-like structure in the VGC [12], it has been suggested that replenishing protein lost during remodeling can support the VGC. In a rat model of hemorrhagic shock, reperfusion of animals with fresh frozen plasma greatly reduced VGC loss compared to lactated electrolyte

solution commonly used to treat patients with low blood pressure [154]. Indeed, the choice of fluids and volume of fluid resuscitation can have impacts of VGC shedding during vascular stress [85]. An alternative strategy of supporting VGC structure is the addition of VGC-mimetic constructs that coat activated endothelium and reduce inflammation. An injectable construct consisting of a dermatan sulfate backbone and multiple selectin-binding peptides (EC-SEAL) was able to coat activated endothelial cells expressing selectins and block platelet activation on the cell surface. Further, in an mouse model of DVT, EC-SEAL blocked thrombosis to the same extent as heparin [155]. VGC mimetics or treatments that support VGC superstructure need to be studied more to understand their benefit in the context of infection and sepsis.

1.6 Opportunities and challenges

Knowledge about the VGC has rapidly expanded with the discovery and characterization of VGC components. However, several barriers have barred detailed global characterization of VGC composition until recently. First, it is technically challenging to isolate and purify enough VGC material for composition analysis. As phenotypic drift changes *ex vivo* cultured endothelial transcriptomes and proteomes [138,146,147], *in vivo* analysis of the VGC composition provides a more accurate, albeit more challenging, experimental window. New studies are using *in vivo* endothelial translatomics and proteomics to characterize how different vascular beds have shared and unique baseline profiles that undergo distinctive remodeling trajectories during sepsis [47,138]. However, most mass spectrometry techniques used in proteomics are limited by a relatively small dynamic range in protein detection that may exclude low abundance proteins that are critical to vascular biology. New mass spectrometry techniques such as data-independent acquisition show promise for an expanded dynamic range of protein detection and characterization [156]. A second barrier to VGC characterization is identification of the source of VGC components. Many studies have

shown VGC remodeling concomitant with increases in VGC component circulation during sepsis and trauma, implying they are abundant in the VGC [85]. However, several VGC components, such as albumin and coagulation factors, are manufactured in the distal cell populations and are deposited in the VGC. Determining the cell population that manufactures a certain VGC component can be achieved with cell-specific genetic deletion and subsequent loss from the VGC. A third barrier to studying VGC composition is characterizing the relative contributions of glycan species. Several GAGs have been shown to be essential to the macrostructure of the VGC [9,20]. However, *N*- and *O*- glycans are also extremely common on membrane bound and secreted proteins. To date, there has not been a comprehensive analysis of VGC glycan composition across all the various glycan classes. Global VGC glycan composition is possible with glycomics or glycoproteomics, although using these analyses *in vivo* may prove challenging.

Current infection models used to study VGC remodeling do not account for the diversity of infectious agents. Many of these studies have used LPS as a surrogate for infection, although LPS does not recapitulate the complex nature of bacterial infections or represent viral or parasitic infection. Use of common sepsis causing agents is critical to understanding the complex nature of VGC remodeling during sepsis. Further, most infection models are based around bacterial sepsis, although many severe infections are caused by viruses and parasites. SARS-Cov2, the viral agent that causes COVID-19, has been shown to induce coagulopathies tied to VGC remodeling [157], and circulating VGC components are more abundant in COVID-19 patients [158]. Malaria, one of the leading causes of sepsis worldwide [159], and other parasitic diseases that cause systemic infection are greatly understudied in the context of VGC remodeling. Important insight into VGC remodeling regulation can be gathered by using a diversity of pathogens to identify both shared and unique remodeling signatures across infection types. [47]

Shed glycoproteins in circulation are a long-standing marker for VGC remodeling activity and sepsis severity [85], although the cellular origin of these species is not exactly known. Detection of circulating analytes known to come from the VGC would be valuable not only as a diagnostic but as a theragnostic. For example, the VGC can be used as a proxy for vascular health recovery after the start of therapy. Suspected sepsis patients are rapidly placed on broad-spectrum antibiotics [151], even though the causative agent is unknown at the time and in most cases is never identified [160]. Using a theragnostic to gauge if the patient's vasculature is stabilizing or continuing to deteriorate would be a tool to determine if the administered antibiotic is effective. Detection of circulating VGC components could also be useful for identifying which vascular beds are undergoing extensive remodeling. Due to recent developments in characterizing organotypic VGC profiles [47], detection of certain VGC species is a possible avenue for detecting if a certain VGC component is coming from a certain organ's vasculature, thus giving insight into the organ's health. Future development of methods to further characterize the VGC and its remodeling during infection and sepsis provides exciting avenues for therapeutic, diagnostic, and theragnostic development.

1.7 Acknowledgments

Chapter 1, in part, is being formulated into a manuscript for publication of the material. GJ Golden, CD Painter, JD Esko, 2022. The dissertation author was the primary investigator and author of this material. Thank you to supportive funding from the National Institute of Health (P01- HL131474) and the UCSD Microbiome Center for Innovation (Microbial Sciences Graduate Research Fellowship Award 1-F17GG and 1-F18GG).

1.8 References

1. Danielli, J. F. Capillary permeability and oedema in the perfused frog. *J. Physiol.* **98,** 109–129 (1940).

2. Chambers, R. & Zweifach, B. W. Intercellular Cement and Capillary Permeability. *Physiol. Rev.* **27,** 436–463 (1947).

3. Klitzman, B. & Duling, B. R. Microvascular hematocrit and red cell flow in resting and contracting striated muscle. *Am. J. Physiol.* **237,** H481–H490 (1979).

4. Hama, K. The fine structure of some blood vessels of the earthworm, Eisenia foetida. *J. Biophys. Biochem. Cytol.* **7,** 717–724 (1960).

5. Bennett, H. S. Morphological aspects of extracellular polysaccharides. *J. Histochem. Cytochem.* **11,** 14–22 (1963).

6. Gao, L. & Lipowsky, H. H. Composition of the endothelial glycocalyx and its relation to its thickness and diffusion of small solutes. *Microvasc. Res.* **80,** 394–401 (2010).

7. Xu, D. & Esko, J. D. Demystifying heparan sulfate-protein interactions. *Annu. Rev. Biochem.* **83,** 129–157 (2014).

8. Kamhi, E., Joo, E. J., Dordick, J. S. & Linhardt, R. J. Glycosaminoglycans in infectious disease. *Biol. Rev.* **88,** 928–943 (2013).

9. Gaudette, S., Hughes, D. & Boller, M. The endothelial glycocalyx: Structure and function in health and critical illness. *J. Vet. Emerg. Crit. Care* **30,** 117–134 (2020).

10. Kataoka, H., Ushiyama, A., Kawakami, H., Akimoto, Y., Matsubara, S. & Iijima, T. Fluorescent imaging of endothelial glycocalyx layer with wheat germ agglutinin using intravital microscopy. *Microsc. Res. Tech.* **79,** 31–37 (2016).

11. Chacko, B. K., Scott, D. W., Chandler, R. T. & Patel, R. P. Endothelial Surface N - Glycans Mediate Monocyte Adhesion and Are Targets for Anti-inflammatory Effects of Peroxisome Proliferator-activated Receptor Ligands *. *J. Biol. Chem.* **286,** 38738–38747 (2011).

12. Jacob, M., Bruegger, D., Rehm, M., Stoeckelhuber, M., Welsch, U., Conzen, P. & Becker, B. F. The endothelial glycocalyx affords compatibility of Starling's principle and high cardiac interstitial albumin levels. *Cardiovasc. Res.* **73,** 575–586 (2007).

13. Vink, H. & Duling, B. R. Capillary endothelial surface layer selectively reduces plasma solute distribution volume. *Am. J. Hear. Circ. Physiol.* **278,** H285–H289 (2000).

14. Tsuboi, K., Hirakawa, J., Seki, E., Imai, Y., Yamaguchi, Y., Fukuda, M. & Kawashima, H. Role of high endothelial venule-expressed heparan sulfate in chemokine presentation and lymphocyte homing. *J Immunol* **191,** 448–455 (2013).

15. Massena, S., Christoffersson, G., Hjertström, E., Zcharia, E., Vlodavsky, I., Ausmees, N., Rolny, C., Li, J. P. & Phillipson, M. A chemotactic gradient sequestered on endothelial heparan sulfate induces directional intraluminal crawling of neutrophils. *Blood* **116,** 1924–1931 (2010).

16. Van Haaren, P. M. A., VanBavel, E., Vink, H. & Spaan, J. A. E. Localization of the permeability barrier to solutes in isolated arteries by confocal microscopy. *Am. J. Physiol. - Hear. Circ. Physiol.* **285,** 2848–2856 (2003).

17. Levick, J. R. & Michel, C. C. Microvascular fluid exchange and the revised Starling principle. *Cardiovasc. Res.* **87,** 198–210 (2010).

18. Schmidt, E. P., Yang, Y., Janssen, W. J., Gandjeva, A., Perez, M. J., Barthel, L., Zemans, R. L., Bowman, J. C., Koyanagi, D. E., Yunt, Z. X., Smith, L. P., Cheng, S. S., Overdier, K. H., Thompson, K. R., Geraci, M. W., Douglas, I. S., Pearse, D. B. & Tuder, R. M. The pulmonary endothelial glycocalyx regulates neutrophil adhesion and lung injury during experimental sepsis. *Nat Med* **18,** 1217–1223 (2012).

19. Rehm, M., Zahler, S., Lötsch, M., Welsch, U., Conzen, P., Jacob, M. & Becker, B. F. Endothelial Glycocalyx as an Additional Barrier Determining Extravasation of 6% Hydroxyethyl Starch or 5% Albumin Solutions in the Coronary Vascular Bed. *Anesthesiology* **100,** 1211–1223 (2004).

20. Henry, C. B. S. & Duling, B. R. Permeation of the luminal capillary glycocalyx is determined by hyaluronan. *Am. J. Physiol. - Hear. Circ. Physiol.* **277,** (1999).

21. Sandoo, A., Veldhuijzen van Zanten, J. J. C. ., Metsios, G. S., Carroll, D. & Kitas, G. D. The Endothelium and Its Role in Regulating Vascular Tone. *Open Cardiovasc. Med. J.* **4,** 302–312 (2015).

22. Zeng, Y. Endothelial glycocalyx as a critical signalling platform integrating the extracellular haemodynamic forces and chemical signalling. *J. Cell. Mol. Med.* **21,** 1457–1462 (2017).

23. Florian, J. A., Kosky, J. R., Ainslie, K., Pang, Z., Dull, R. O. & Tarbell, J. M. Heparan sulfate proteoglycan is a mechanosensor on endothelial cells. *Circ. Res.* **93,** (2003).

24. Mochizuki, S., Vink, H., Hiramatsu, O., Kajita, T., Shigeto, F., Spaan, J. A. E. & Kajiya, F. Role of hyaluronic acid glycosaminoglycans in shear-induced endothelium-derived nitric oxide release. *Am. J. Physiol. - Hear. Circ. Physiol.* **285,** 722–726 (2003).

25. Yao, Y., Rabodzey, A. & Dewey, C. F. Glycocalyx modulates the motility and proliferative response of vascular endothelium to fluid shear stress. *Am. J. Physiol. - Hear. Circ. Physiol.* **293,** 1023–1030 (2007).

26. Gouverneur, M., Spaan, J. A. E., Pannekoek, H., Fontijn, R. D. & Vink, H. Fluid shear stress stimulates incorporation of hyaluronan into endothelial cell glycocalyx. *Am. J. Physiol. - Hear. Circ. Physiol.* **290,** 458–462 (2006).

27. Zeng, Y., Waters, M., Andrews, A., Honarmandi, P., Ebong, E. E., Rizzo, V. & Tarbell, J. M. Fluid shear stress induces the clustering of heparan sulfate via mobility of glypican-1 in lipid rafts. *Am. J. Physiol. - Hear. Circ. Physiol.* **305,** 811–820 (2013).

28. Knoepp, F., Ashley, Z., Barth, D., Baldin, J. P., Jennings, M., Kazantseva, M., Saw, E. L., Katare, R., de la Rosa, D. A., Weissmann, N. & Fronius, M. Shear force sensing of epithelial Na+ channel (ENaC) relies on N-glycosylated asparagines in the palm and knuckle domains of αENaC. *Proc. Natl. Acad. Sci. U. S. A.* **117,** 717–726 (2020).

29. Erlandsen, S. L., Bittermann, A. G., White, J., Leith, A. & Marko, M. High-resolution CryoFESEM of individual cell adhesion molecules (CAMs) in the glycocalyx of human platelets: Detection of P-selectin (CD62P), GPI-IX complex (CD42a/CD42bα,bβ), and integrin GPIIbIIIa (CD41/CD61) by immunogold labeling and stereo imaging. *J. Histochem. Cytochem.* **49,** 809–819 (2001).

30. Yang, Y., Haeger, S. M., Suflita, M. A., Zhang, F., Dailey, K. L., Colbert, J. F., Ford, J. A., Picon, M. A., Stearman, R. S., Lin, L., Liu, X., Han, X., Linhardt, R. J. & Schmidt, E. P. Fibroblast growth factor signaling mediates pulmonary endothelial glycocalyx reconstitution. *Am. J. Respir. Cell Mol. Biol.* **56,** 727–737 (2017).

31. Lukasz, A., Hillgruber, C., Oberleithner, H., Kusche-Vihrog, K., Pavenstädt, H., Rovas, A., Hesse, B., Goerge, T. & Kümpers, P. Endothelial glycocalyx breakdown is mediated by angiopoietin-2. *Cardiovasc. Res.* **113,** 671–680 (2017).

32. Dragovich, M. A., Genemaras, K., Dailey, H. L., Jedlicka, S. & Frank Zhang, X. Dual Regulation of L-Selectin-Mediated Leukocyte Adhesion by Endothelial Surface Glycocalyx. *Cell. Mol. Bioeng.* **10,** 102–113 (2017).

33. Iba, T. & Levy, J. H. Derangement of the endothelial glycocalyx in sepsis. *J. Thromb. Haemost.* **17,** 283–294 (2019).

34. Lortat-Jacob, H., Grosdidier, A. & Imberty, A. Structural diversity of heparan sulfate binding domains in chemokines. *Proc. Natl. Acad. Sci. U. S. A.* **99,** 1229–1234 (2002).

35. Wang, L., Fuster, M., Sriramarao, P. & Esko, J. D. Endothelial heparan sulfate deficiency impairs L-selectin- and chemokine-mediated neutrophil trafficking during inflammatory responses. *Nat. Immunol.* **6,** 902–10 (2005).

36. Axelsson, J., Xu, D., Kang, B. N., Nussbacher, J. K., Handel, T. M., Ley, K., Sriramarao, P. & Esko, J. D. Inactivation of heparan sulfate 2- O -sulfotransferase accentuates neutrophil infiltration during acute inflammation in mice. *Blood* **120,** 1742–1751 (2012).

37. Muller, W. A. Getting Leukocytes to the Site of Inflammation. *Vet. Pathol.* **50,** 7–22 (2013).

38. Hattori, R., Hamilton, K. K., Fugate, R. D., McEver, R. P. & Sims, P. J. Stimulated secretion of endothelial von Willebrand factor is accompanied by rapid redistribution to the cell surface of the intracellular granule membrane protein GMP-140. *J. Biol. Chem.*

264, 7768–7771 (1989).

39. Bevilacqua, M. P., Pober, J. S., Mendrick, D. L., Cotran, R. S. & Gimbrone, M. A. Identification of an inducible endothelial-leukocyte adhesion molecule. *Proc. Natl. Acad. Sci. U. S. A.* **84,** 9238–9242 (1987).

40. Vestweber, D. & Blanks, J. E. Mechanisms that regulate the function of the selectins and their ligands. *Physiol. Rev.* **79,** 181–213 (1999).

41. Ivetic, A., Green, H. L. H. & Hart, S. J. L-selectin: A major regulator of leukocyte adhesion, migration and signaling. *Front. Immunol.* **10,** 1–22 (2019).

42. Imai, Y., Singer, M. S., Fennie, C., Lasky, L. A. & Rosen, S. D. Identification of a carbohydrate-based endothelial ligand for a lymphocyte homing receptor. *J. Cell Biol.* **113,** 1213–1221 (1991).

43. Rosen, S. D., Singer, M. S. & Yednock, T. A. Involvment of Sialic Acid on Endothelial Cells in Organ-Specific Lymphocyte Recirculation. *Science (80-.).* **228,** 1005–1007 (1985).

44. Mitoma, J., Bao, X., Petryanik, B., Schaerli, P., Gauguet, J.-M., Yu, S.-Y., Kawashima, H., Saito, H., Ohtsubo, K., Marth, J. D., Khoo, K.-H., Andrian, U. H. von, Lowe, J. B. & Fukuda, M. Critical functions of N-glycans in L-selectin-mediated lymphocyte homing and recruitment. *Nat. Immunol.* **8,** 409–418 (2007).

45. Kawashima, H., Petryniak, B., Hiraoka, N., Mitoma, J., Huckaby, V., Nakayama, J., Uchimura, K., Kadomatsu, K., Muramatsu, T., Lowe, J. B. & Fukuda, M. N-acetylglucosamine-6-O-sulfotransferases 1 and 2 cooperatively control lymphocyte homing through L-selectin ligand biosynthesis in high endothelial venules. *Nat. Immunol.* **6,** 1096–1104 (2005).

46. Uchimura, K., Kadomatsu, K., El-Fasakhany, F. H., Singer, M. S., Izawa, M., Kannagi, R., Takeda, N., Rosen, S. D. & Muramatsu, T. N-acetylglucosamine 6-O-sulfotransferase-1 regulates expression of L-selectin ligands and lymphocyte homing. *J. Biol. Chem.* **279,** 35001–35008 (2004).

47. Gómez Toledo, A., Golden, G., Campos, A. R., Cuello, H., Sorrentino, J., Lewis, N., Varki, N., Nizet, V., Smith, J. W. & Esko, J. D. Proteomic atlas of organ vasculopathies triggered by Staphylococcus aureus sepsis. *Nat. Commun.* **10,** (2019).

48. Otto, V. I., Damoc, E., Cueni, L. N., Schürpf, T., Frei, R., Ali, S., Callewaert, N., Moise, A., Leary, J. A., Folkers, G. & Przybylski, M. N-Glycan structures and N-glycosylation sites of mouse soluble intercellular adhesion molecule-1 revealed by MALDI-TOF and FTICR mass spectrometry. *Glycobiology* **16,** 1033–1044 (2006).

49. Scott, D. W., Dunn, T. S., Ballestas, M. E., Litovsky, S. H. & Patel, R. P. Identification of a high-mannose ICAM-1 glycoform: Effects of ICAM-1 hypoglycosylation on monocyte adhesion and outside in signaling. *Am. J. Physiol. - Cell Physiol.* **305,** 228–237 (2013).

50. Sriramarao, P., Berger, E., Chambers, J. D., Arfors, K. -E & Gehlsen, K. R. High mannose type N-linked oligosaccharides on endothelial cells may influence β2 integrin mediated neutrophil adherence in vitro. *J. Cell. Biochem.* **51,** 360–368 (1993).

51. Champagne, B., Tremblay, P., Cantin, A. & St Pierre, Y. Proteolytic cleavage of ICAM-1 by human neutrophil elastase. *J. Immunol.* **161,** 6398–405 (1998).

52. Lertkiatmongkol, P., Paddock, C., Newman, D. K., Zhu, J., Thomas, M. J. & Newman, P. J. The role of sialylated glycans in human platelet endothelial cell adhesion molecule 1 (PECAM-1)-mediated trans homophilic interactions and endothelial cell barrier function. *J. Biol. Chem.* **291,** 26216–26225 (2016).

53. Kitazume, S., Imamaki, R., Ogawa, K., Komi, Y., Futakawa, S., Kojima, S., Hashimoto, Y., Marth, J. D., Paulson, J. C. & Taniguchi, N. α2,6-sialic acid on Platelet Endothelial Cell Adhesion Molecule (PECAM) regulates its homophilic interactions and downstream antiapoptotic signaling. *J. Biol. Chem.* **285,** 6515–6521 (2010).

54. Khokha, R., Murthy, A. & Weiss, A. Metalloproteinases and their natural inhibitors in inflammation and immunity. *Nat. Rev. Immunol.* **13,** 649–65 (2013).

55. Mulivor, A. W. & Lipowsky, H. H. Inhibition of glycan shedding and leukocyte-endothelial adhesion in postcapillary venules by suppression of matrixmetalloprotease activity with doxycycline. *Microcirculation* **16,** 657–666 (2009).

56. Lipowsky, H. H., Sah, R. & Lescanic, A. Relative roles of doxycycline and cation chelation in endothelial glycan shedding and adhesion of leukocytes. *Am. J. Physiol. - Hear. Circ. Physiol.* **300,** 415–423 (2011).

57. Manthe, R. L. & Muro, S. ICAM-1-targeted nanocarriers attenuate endothelial release of soluble ICAM-1, an inflammatory regulator. *Bioeng. Transl. Med.* **2,** 109–119 (2017).

58. Yabluchanskiy, A., Ma, Y., Chiao, Y. A., Lopez, E. F., Voorhees, A. P., Toba, H., Hall, M. E., Han, H. C., Lindsey, M. L. & Jin, Y. F. Cardiac aging is initiated by matrix metalloproteinase-9-mediated endothelial dysfunction. *Am. J. Physiol. - Hear. Circ. Physiol.* **306,** 1398–1407 (2014).

59. Yang, J., LeBlanc, M. E., Cano, I., Saez-Torres, K. L., Saint-Geniez, M., Ng, Y. S. & D'Amore, P. A. ADAM10 and ADAM17 proteases mediate proinflammatory cytokine-induced and constitutive cleavage of endomucin from the endothelial surface. *J. Biol. Chem.* **295,** 6641–6651 (2020).

60. Yang, X., Meegan, J. E., Jannaway, M., Coleman, D. C. & Yuan, S. Y. A disintegrin and metalloproteinase 15-mediated glycocalyx shedding contributes to vascular leakage during inflammation. *Cardiovasc. Res.* **114,** 1752–1763 (2018).

61. Dong, J. fei, Moake, J. L., Nolasco, L., Bernardo, A., Arceneaux, W., Shrimpton, C. N., Schade, A. J., McIntire, L. V., Fujikawa, K. & López, J. A. ADAMTS-13 rapidly cleaves newly secreted ultralarge von Willebrand factor multimers on the endothelial surface

under flowing conditions. *Blood* **100,** 4033–4039 (2002).

62. Vomund, A. N. & Majerus, E. M. ADAMTS13 bound to endothelial cells exhibits enhanced cleavage of von Willebrand factor. *J. Biol. Chem.* **284,** 30925–30932 (2009).

63. Lampugnani, M. G. Endothelial cell-to-cell junctions: Adhesion and signaling in physiology and pathology. *Cold Spring Harb. Perspect. Med.* **2,** 1–14 (2012).

64. Powers, M. E., Kim, H. K., Wang, Y. & Wardenburg, J. B. ADAM10 mediates vascular injury induced by staphylococcus aureus α-hemolysin. *J. Infect. Dis.* **206,** 352–356 (2012).

65. Flemming, S., Burkard, N., Renschler, M., Vielmuth, F., Meir, M., Schick, M. A., Wunder, C., Germer, C. T., Spindler, V., Waschke, J. & Schlegel, N. Soluble VE-cadherin is involved in endothelial barrier breakdown in systemic inflammation and sepsis. *Cardiovasc. Res.* **107,** 32–44 (2015).

66. Fitzgerald, Marilyn L; Wang, Zihua; Park, Pyong Woo; Murphy, Gillian; Bernfield, M. Shedding of syndecan-1 and -4 ectodommains is regulated by multiple signaling pathways and mediated by a TIMP-3 sensitive metalloproteinase. *J. Cell Biol.* **148,** 811–824 (2000).

67. Zeng, Y., Adamson, R. H., Curry, F. R. E. & Tarbell, J. M. Sphingosine-1-phosphate protects endothelial glycocalyx by inhibiting syndecan-1 shedding. *Am. J. Physiol. - Hear. Circ. Physiol.* **306,** 363–372 (2014).

68. Ramnath, R., Foster, R. R., Qiu, Y., Cope, G., Butler, M. J., Salmon, A. H., Mathieson, P. W., Coward, R. J., Welsh, G. I. & Satchell, S. C. Matrix metalloproteinase 9-mediated shedding of syndecan 4 in response to tumor necrosis factor α: A contributor to endothelial cell glycocalyx dysfunction. *FASEB J.* **28,** 4686–4699 (2014).

69. Ramnath, R. D., Butler, M. J., Newman, G., Desideri, S., Russell, A., Lay, A. C., Neal, C. R., Qiu, Y., Fawaz, S., Onions, K. L., Gamez, M., Crompton, M., Michie, C., Finch, N., Coward, R. J., Welsh, G. I., Foster, R. R. & Satchell, S. C. Blocking matrix metalloproteinase-mediated syndecan-4 shedding restores the endothelial glycocalyx and glomerular filtration barrier function in early diabetic kidney disease. *Kidney Int.* **97,** 951–965 (2020).

70. Ali, M. M., Mahmoud, A. M., Master, E. Le, Levitan, I. & Phillips, S. A. Role of matrix metalloproteinases and histone deacetylase in oxidative stress-induced degradation of the endothelial glycocalyx. *Am. J. Physiol. - Hear. Circ. Physiol.* **316,** H647–H663 (2019).

71. Fernandez-Patron, C., Radomski, M. W. & Davidge, S. T. Vascular matrix metalloproteinase-2 cleaves big endothelin-1 yielding a novel vasoconstrictor. *Circ. Res.* **85,** 906–911 (1999).

72. Yu, W. H., Yu, S. S. C., Meng, Q., Brew, K. & Woessner, J. F. TIMP-3 binds to sulfated glycosaminoglycans of the extracellular matrix. *J. Biol. Chem.* **275,** 31226–31232 (2000).

73. Amour, A., Slocombe, P. M., Webster, A., Butler, M., Knight, C. G., Smith, B. J.,

Stephens, P. E., Shelley, C., Hutton, M., Knäuper, V., Docherty, A. J. p. & Murphy, G. TNF-α converting enzyme (TACE) is inhibited by TIMP-3. *FEBS Lett.* **435,** 39–44 (1998).

74. Amour, A., Knight, C. G., Webster, A., Slocombe, P. M., Stephens, P. E., Knäuper, V., Docherty, A. J. P. & Murphy, G. The in vitro activity of ADAM-10 is inhibited by TIMP-1 and TIMP-3. *FEBS Lett.* **473,** 275–279 (2000).

75. Kashiwagi, M., Tortorella, M., Nagase, H. & Brew, K. TIMP-3 Is a Potent Inhibitor of Aggrecanase 1 (ADAM-TS4) and Aggrecanase 2 (ADAM-TS5). *J. Biol. Chem.* **276,** 12501–12504 (2001).

76. Sithu, S. D., English, W. R., Olson, P., Krubasik, D., Baker, A. H., Murphy, G. & D'Souza, S. E. Membrane-type 1-matrix metalloproteinase regulates intracellular adhesion molecule-1 (ICAM-1)-mediated monocyte transmigration. *J. Biol. Chem.* **282,** 25010–25019 (2007).

77. Genersch, E., Hayeb, K., Neuenfeld, Y. & Haller, H. Sustained ERK phosphorylation is necessary but not sufficient for MMP-9 regulation in endothelial cells: Involvement of Ras-dependent and-independent pathways. *J. Cell Sci.* **113,** 4319–4330 (2000).

78. Behzadian, M. A., Wang, X. L., Windsor, L. J., Ghaly, N. & Caldwell, R. B. TGF-β increases retinal endothelial cell permeability by increasing MMP-9: Possible role of glial cells in endothelial barrier function. *Investig. Ophthalmol. Vis. Sci.* **42,** 853–859 (2001).

79. Li, A., Dubey, S., Varney, M. L., Dave, B. J. & Singh, R. K. IL-8 Directly Enhanced Endothelial Cell Survival, Proliferation, and Matrix Metalloproteinases Production and Regulated Angiogenesis. *J. Immunol.* **170,** 3369–3376 (2003).

80. Sun, H. W., Li, C. J., Chen, H. Q., Lin, H. L., Lv, H. X., Zhang, Y. & Zhang, M. Involvement of integrins, MAPK, and NF-κB in regulation of the shear stress-induced MMP-9 expression in endothelial cells. *Biochem. Biophys. Res. Commun.* **353,** 152–158 (2007).

81. Bzowska, M., Jura, N., Lassak, A., Black, R. A. & Bereta, J. Tumour necrosis factor-α stimulates expression of TNF-α converting enzyme in endothelial cells. *Eur. J. Biochem.* **271,** 2808–2820 (2004).

82. Zaragoza, C., Balbín, M., López-Otín, C. & Lamas, S. Nitric oxide regulates matrix metalloprotease-13 expression and activity in endothelium. *Kidney Int.* **61,** 804–808 (2002).

83. Babendreyer, A., Molls, L., Simons, I. M., Dreymueller, D., Biller, K., Jahr, H., Denecke, B., Boon, R. A., Bette, S., Schnakenberg, U. & Ludwig, A. The metalloproteinase ADAM15 is upregulated by shear stress and promotes survival of endothelial cells. *J. Mol. Cell. Cardiol.* **134,** 51–61 (2019).

84. Wiesinger, A., Peters, W., Chappell, D., Kentrup, D., Reuter, S., Pavenstädt, H.,

Oberleithner, H. & Kümpers, P. Nanomechanics of the endothelial glycocalyx in experimental sepsis. *PLoS One* **8,** 1–14 (2013).

85. Uchimido, R., Schmidt, E. P. & Shapiro, N. I. The glycocalyx: a novel diagnostic and therapeutic target in sepsis. *Crit. Care* **23,** 1–12 (2019).

86. Wang, G., Tiemeier, G. L., van den Berg, B. M. & Rabelink, T. J. Endothelial Glycocalyx Hyaluronan: Regulation and Role in Prevention of Diabetic Complications. *Am. J. Pathol.* **190,** 781–790 (2020).

87. De Angelis, J. E., Lagendijk, A. K., Chen, H., Tromp, A., Bower, N. I., Tunny, K. A., Brooks, A. J., Bakkers, J., Francois, M., Yap, A. S., Simons, C., Wicking, C., Hogan, B. M. & Smith, K. A. Tmem2 Regulates Embryonic Vegf Signaling by Controlling Hyaluronic Acid Turnover. *Dev. Cell* **40,** 123–136 (2017).

88. Yoshida, H., Nagaoka, A., Kusaka-Kikushima, A., Tobiishi, M., Kawabata, K., Sayo, T., Sakai, S., Sugiyama, Y., Enomoto, H., Okada, Y. & Inoue, S. KIAA1199, a deafness gene of unknown function, is a new hyaluronan binding protein involved in hyaluronan depolymerization. *Proc. Natl. Acad. Sci. U. S. A.* **110,** 5612–5617 (2013).

89. Yamamoto, H., Tobisawa, Y., Inubushi, T., Irie, F., Ohyama, C. & Yamaguchi, Y. A mammalian homolog of the zebrafish transmembrane protein 2 (TMEM2) is the long-sought-after cell-surface hyaluronidase. *J. Biol. Chem.* **292,** 7304–7313 (2017).

90. Harada, H. & Takahashi, M. CD44-dependent intracellular and extracellular catabolism of hyaluronic acid by hyaluronidase-1 and -2. *J. Biol. Chem.* **282,** 5597–5607 (2007).

91. Chowdhury, B., Hemming, R., Faiyaz, S. & Triggs-Raine, B. Hyaluronidase 2 (HYAL2) is expressed in endothelial cells, as well as some specialized epithelial cells, and is required for normal hyaluronan catabolism. *Histochem. Cell Biol.* **145,** 53–66 (2016).

92. Kong, X., Chen, L., Ye, P., Wang, Z., Zhang, J., Ye, F. & Chen, S. The role of HYAL2 in LSS-induced glycocalyx impairment and the PKA-mediated decrease in eNOS-Ser-633 phosphorylation and nitric oxide production. *Mol. Biol. Cell* **27,** 3972–3979 (2016).

93. Petrey, A. C., Obery, D. R., Kessler, S. P., Zawerton, A., Flamion, B. & de la Motte, C. A. Platelet hyaluronidase-2 regulates the early stages of inflammatory disease in colitis. *Blood* **134,** 765–775 (2019).

94. Chen, G., Wang, D., Vikramadithyan, R., Yagyu, H., Saxena, U., Pillarisetti, S. & Goldberg, I. J. Inflammatory Cytokines and Fatty Acids Regulate Endothelial Cell Heparanase Expression. *Biochemistry* **43,** 4971–4977 (2004).

95. Garsen, M., Rops, A. L., Li, J., Van Beneden, K., Van Den Branden, C., Berden, J. H. M., Rabelink, T. J. & Van Der Vlag, J. Endothelial nitric oxide synthase prevents heparanase induction and the development of proteinuria. *PLoS One* **11,** 4–11 (2016).

96. An, X. F., Zhou, L., Jiang, P. J., Yan, M., Huang, Y. J., Zhang, S. N., Niu, Y. F., Ten, S.

C. & Yu, J. Y. Advanced glycation end-products induce heparanase expression in endothelial cells by the receptor for advanced glycation end products and through activation of the FOXO4 transcription factor. *Mol. Cell. Biochem.* **354,** 47–55 (2011).

97. Gilat, D., Hershkoviz, R., Goldkorn, I., Cahalon, L., Korner, G., Vlodavsky, I. & Lider, O. Molecular behavior adapts to context: Heparanase functions as an extraceuular matrix-degrading enzyme or as a T cell adhesion molecule, depending on the local pH. *J. Exp. Med.* **181,** 1929–1934 (1995).

98. Ihrcke, N. S., Parker, W., Reissner, K. J. & Platt, J. L. Regulation of platelet heparanase during inflammation: Role of pH and proteinases. *J. Cell. Physiol.* **175,** 255–267 (1998).

99. Miyagi, T. & Yamaguchi, K. Mammalian sialidases : Physiological and pathological roles in cellular functions. *Glycobiology* **22,** 880–896 (2012).

100. Lee, C., Liu, A., Miranda-Ribera, A., Hyun, S. W., Lillehoj, E. P., Cross, A. S., Passaniti, A., Grimm, P. R., Kim, B. Y., Welling, P. A., Madri, J. A., DeLisser, H. M. & Goldblum, S. E. NEU1 sialidase regulates the sialylation state of CD31 and disrupts CD31-driven capillary-like tube formation in human lung microvascular endothelia. *J. Biol. Chem.* **289,** 9121–9135 (2014).

101. Sakarya, S., Rifat, S., Zhou, J., Bannerman, D. D., Stamatos, N. M., Cross, A. S. & Goldblum, S. E. Mobilization of neutrophil sialidase activity desialylates the pulmonary vascular endothelial surface and increases resting neutrophil adhesion to and migration across the endothelium. *Glycobiology* **14,** 481–494 (2004).

102. Puerta-guardo, H., Glasner, D. R. & Harris, E. Dengue Virus NS1 Disrupts the Endothelial Glycocalyx , Leading to Hyperpermeability. *PLoS Pathog.* (2016). doi:10.1371/journal.ppat.1005738

103. Mohamadzadeh, M., DeGrendele, H., Arizpe, H., Estess, P. & Siegelman, M. Proinflammatory stimuli regulate endothelial hyaluronan expression and CD44/HA-dependent primary adhesion. *J. Clin. Invest.* **101,** 97–108 (1998).

104. Estess, B. P., Nandi, A., Mohamadzadeh, M. & Siegelman, M. H. Interleukin 15 Induces Endothelial Hyaluronan Expression through a CD44-dependent Pathway In Vivo. *J. Exp. Med.* **190,** 9–19 (1999).

105. Vigetti, D., Genasetti, A., Karousou, E., Viola, M., Moretto, P., Clerici, M., Deleonibus, S., Luca, G. De, Hascall, V. C. & Passi, A. Proinflammatory Cytokines Induce Hyaluronan Synthesis and Monocyte Adhesion in Human Endothelial Cells through Hyaluronan Synthase 2 (HAS2) and the Nuclear Factor- □ B. *J. Biol. Chem.* **285,** 24639–24645 (2010).

106. Carter, N. M., Ali, S. & Kirby, J. A. Endothelial inflammation: the role of differential expression of N-deacetylase/N-sulphotransferase enzymes in alteration of the immunological properties of heparan sulphate. *J. Cell Sci.* **116,** 3591–3600 (2003).

107. Zeng, Y., Liu, X. H., Tarbell, J. & Fu, B. Sphingosine 1-phosphate induced synthesis of glycocalyx on endothelial cells. *Exp. Cell Res.* **339,** 90–95 (2015).

108. Ghitescu, L. & Fixman, A. Surface charge distribution on the endothelial cell of liver sinusoids. *J. Cell Biol.* **99,** 639–647 (1984).

109. Pandey, M. S., Harris, E. N., Weigel, J. A. & Weigel, P. H. The cytoplasmic domain of the hyaluronan receptor for endocytosis (hare) contains multiple endocytic motifs targeting coated pit-mediated internalization. *J. Biol. Chem.* **283,** 21453–21461 (2008).

110. Bourguignon, L. Y. W., Singleton, P. A., Diedrich, F., Stern, R. & Gilad, E. CD44 interaction with Na+-H+ exchanger (NHE1) creates acidic microenvironments leading to hyaluronidase-2 and cathepsin B activation and breast tumor cell invasion. *J. Biol. Chem.* **279,** 26991–27007 (2004).

111. Setiadi, H. & McEver, R. P. Clustering endothelial E-selectin in clathrin-coated pits and lipid rafts enhances leukocyte adhesion under flow. *Blood* **111,** 1989–1998 (2008).

112. Han, J., Shuvaev, V. V., Davies, P. F., Eckmann, D. M., Muro, S. & Vladimir R. Muzykantov. Flow shear stress differentially regulates endothelial uptake of nanocarriers targeted to distinct epitopes of PECAM-1. *J. Control. Release* **210,** 39–47 (2015).

113. Singer, M., Deutschman, C. S., Seymour, C. W., Shankar-Hari, M., Annane, D., Bauer, M., Bellomo, R., Bernard, G. R., Chiche, J.-D., Coopersmith, C. M., Hotchkiss, R. S., Levy, M. M., Marshall, J. C., Martin, G. S., Opal, S. M., Rubenfeld, G. D., van der Poll, T., Vincent, J. & Angus, D. C. The Third International Consensus Definitions for Sepsis and Septic Shock (Sepsis-3). *JAMA* **315,** 801–10 (2016).

114. Dreymueller, D., Martin, C., Kogel, T., Pruessmeyer, J., Hess, F. M., Horiuchi, K., Uhlig, S. & Ludwig, A. Lung endothelial ADAM17 regulates the acute inflammatory response to lipopolysaccharide. *EMBO Mol. Med.* **4,** 412–423 (2012).

115. Tressel, S. L., Kaneider, N. C., Kasuda, S., Foley, C., Koukos, G., Austin, K., Agarwal, A., Covic, L., Opal, S. M. & Kuliopulos, A. A matrix metalloprotease-PAR1 system regulates vascular integrity, systemic inflammation and death in sepsis. *EMBO Mol. Med.* **3,** 370–384 (2011).

116. Kiyan, Y., Tkachuk, S., Kurselis, K., Shushakova, N., Stahl, K., Dawodu, D., Kiyan, R., Chichkov, B. & Haller, H. Heparanase-2 protects from LPS-mediated endothelial injury by inhibiting TLR4 signalling. *Sci. Rep.* **9,** 1–13 (2019).

117. Ishiguro, K., Kadomatsu, K., Kojima, T., Muramatsu, H., Iwase, M., Yoshikai, Y., Yanada, M., Yamamoto, K., Matsushita, T., Nishimura, M., Kusugami, K., Saito, H. & Muramatsu, T. Syndecan-4 Deficiency Leads to High Mortality of Lipopolysaccharide-injected Mice. *J. Biol. Chem.* **276,** 47483–47488 (2001).

118. Mcdonald, B., Mcavoy, E. F., Lam, F., Gill, V., Motte, C. De, Savani, R. C. & Kubes, P. Interaction of CD44 and hyaluronan is the dominant mechanism for neutrophil

sequestration in inflamed liver sinusoids. *J. Exp. Med.* **205,** 915–927 (2008).

119. Powers, M. E., Becker, R. E. N., Sailer, A., Turner, J. R. & Bubeck Wardenburg, J. Synergistic Action of Staphylococcus aureus α-Toxin on Platelets and Myeloid Lineage Cells Contributes to Lethal Sepsis. *Cell Host Microbe* **17,** 775–787 (2015).

120. Schubert-Unkmeir, A., Konrad, C., Slanina, H., Czapek, F., Hebling, S. & Frosch, M. Neisseria meningitidis induces brain microvascular endothelial cell detachment from the matrix and cleavage of occludin: A role for MMP-8. *PLoS Pathog.* **6,** 1–15 (2010).

121. Luplerdlop, N., Missé, D., Bray, D., Deleuze, V., Gonzalez, J. P., Leardkamolkarn, V., Yssel, H. & Veas, F. Dengue-virus-infected dendritic cells trigger vascular leakage through metalloproteinase overproduction. *EMBO Rep.* **7,** 1176–1181 (2006).

122. Donati, A., Damiani, E., Domizi, R., Romano, R., Adrario, E., Pelaia, P., Ince, C. & Singer, M. Alteration of the sublingual microvascular glycocalyx in critically ill patients. *Microvasc. Res.* **90,** 86–89 (2013).

123. Lowenstein, C. J., Morrell, C. N. & Yamakuchi, M. Regulation of Weibel-Palade body exocytosis. *Trends Cardiovasc. Med.* **15,** 302–308 (2005).

124. Zannettino, A. C. W., Holding, C. A., Diamond, P., Atkins, G. J., Kostakis, P., Farrugia, A., Gamble, J., To, L. B., Findlay, D. M. & Haynes, D. R. Osteoprotegerin (OPG) is localized to the Weibel-Palade bodies of human vascular endothelial cells and is physically associated with von Willebrand factor. *J. Cell. Physiol.* **204,** 714–723 (2005).

125. Into, T., Kanno, Y., Dohkan, J. I., Nakashima, M., Inomata, M., Shibata, K. I., Lowenstein, C. J. & Matsushita, K. Pathogen recognition by toll-like receptor 2 activates Weibel-Palade body exocytosis in human aortic endothelial cells. *J. Biol. Chem.* **282,** 8134–8141 (2007).

126. Padilla, A., Moake, J. L., Bernardo, A., Ball, C., Wang, Y., Arya, M., Nolasco, L., Turner, N., Berndt, M. C., Anvari, B., López, J. A. & Dong, J. F. P-selectin anchors newly released ultralarge von Willebrand factor multimers to the endothelial cell surface. *Blood* **103,** 2150–2156 (2004).

127. Fiedler, U., Scharpfenecker, M., Koidl, S., Hegen, A., Grunow, V., Schmidt, J. M., Kriz, W., Thurston, G. & Augustin, H. G. The Tie-2 ligand Angiopoietin-2 is stored in and rapidly released upon stimulation from endothelial cell Weibel-Palade bodies. *Blood* **103,** 4150–4156 (2004).

128. Orfanos, S. E., Kotanidou, A., Glynos, C., Athanasiou, C., Tsigkos, S., Dimopoulou, I., Sotiropoulou, C., Zakynthinos, S., Armaganidis, A., Papapetropoulos, A. & Roussos, C. Angiopoietin-2 is increased in severe sepsis: Correlation with inflammatory mediators. *Crit. Care Med.* **35,** 199–206 (2007).

129. Fiedler, U., Reiss, Y., Scharpfenecker, M., Grunow, V., Koidl, S., Thurston, G., Gale, N. W., Witzenrath, M., Rosseau, S., Suttorp, N., Sobke, A., Herrmann, M., Preissner, K. T.,

Vajkoczy, P. & Augustin, H. G. Angiopoietin-2 sensitizes endothelial cells to TNF-alpha and has a crucial role in the induction of inflammation. *Nat. Med.* **12,** 235–239 (2006).

130. Augustin, H. G., Young Koh, G., Thurston, G. & Alitalo, K. Control of vascular morphogenesis and homeostasis through the angiopoietin - Tie system. *Nat. Rev. Mol. Cell Biol.* **10,** 165–177 (2009).

131. Han, S., Lee, S.-J., Kim, K. E., Lee, H. S., Oh, N., Park, I., Ko, E., Oh, S. J., Lee, Y.-S., Kim, D., Lee, S.-J., Lee, D. H., Lee, K.-H., Chae, S. Y., Lee, J.-H., Kim, S.-J. H., Kim, H.-C., Kim, S.-J. H., Kim, S.-J. H., Kim, C., Nakaoka, Y., He, Y., Augustin, H. G., Hu, J., Song, P. H., Kim, Y.-I., Kim, P., Kim, I. & Koh, G. Y. Amelioration of sepsis by TIE2 activation-induced vascular protection. *Sci. Transl. Med.* **8,** 335ra55-335ra55 (2016).

132. Engelmann, B. & Massberg, S. Thrombosis as an intravascular effector of innate immunity. *Nat. Rev. Immunol.* **13,** 34–45 (2013).

133. Haynes, A., Ruda, F., Oliver, J., Hamood, A. N., Griswold, J. A., Park, P. W. & Rumbaugh, K. P. Syndecan 1 shedding contributes to Pseudomonas aeruginosa sepsis. *Infect. Immun.* **73,** 7914–7921 (2005).

134. Williams, J. M., Duckworth, C. A., Burkitt, M. D. & Watson, A. J. M. Epithelial Cell Shedding and Barrier Function : A Matter of Life and Death at the Small Intestinal Villus Tip. *Vet. Pathol.* **52,** 445–455 (2015).

135. Kalagara, T., Moutsis, T., Yang, Y., Pappelbaum, K. I., Farken, A., Cladder-Micus, L., Vidal-Y-Sy, S., John, A., Bauer, A. T., Moerschbacher, B. M., Schneider, S. W. & Gorzelanny, C. The endothelial glycocalyx anchors von Willebrand factor fibers to the vascular endothelium. *Blood Adv.* **2,** 2347–2357 (2018).

136. Gaertner, F., Ahmad, Z., Rosenberger, G., Fan, S., Nicolai, L., Busch, B., Yavuz, G., Luckner, M., Ishikawa-Ankerhold, H., Hennel, R., Benechet, A., Lorenz, M., Chandraratne, S., Schubert, I., Helmer, S., Striednig, B., Stark, K., Janko, M., Böttcher, R. T., Verschoor, A., Leon, C., Gachet, C., Gudermann, T., Mederos y Schnitzler, M., Pincus, Z., Iannacone, M., Haas, R., Wanner, G., Lauber, K., Sixt, M. & Massberg, S. Migrating Platelets Are Mechano-scavengers that Collect and Bundle Bacteria. *Cell* **171,** 1368-1382.e23 (2017).

137. Kolaczkowska, E., Jenne, C. N., Surewaard, B. G. J., Thanabalasuriar, A., Lee, W. Y., Sanz, M. J., Mowen, K., Opdenakker, G. & Kubes, P. Molecular mechanisms of NET formation and degradation revealed by intravital imaging in the liver vasculature. *Nat. Commun.* **6,** 1–13 (2015).

138. Cleuren, A. C. A., van der Ent, M. A., Jiang, H., Hunker, K. L., Yee, A., Siemieniak, D. R., Molema, G., Aird, W. C., Ganesh, S. K. & Ginsburg, D. The in vivo endothelial cell translatome is highly heterogeneous across vascular beds. *Proc. Natl Acad. Sci. USA* **116,** 23618–23624 (2019).

139. Yano, K., Liaw, P. C., Mullington, J. M., Shih, S., Okada, H., Bodyak, N., Kang, P. M.,

Toltl, L., Belikoff, B., Buras, J., Simms, B. T., Mizgerd, J. P., Carmeliet, P., Karumanchi, S. A. & Aird, W. C. Vascular endothelial growth factor is an important determinant of sepsis morbidity and mortality. *J. Exp. Med.* **203,** 1447–1458 (2006).

140. Escobar Galvis, M. L., Jia, J., Zhang, X., Jastrebova, N., Spillmann, D., Gottfridsson, E., van Kuppevelt, T. H., Zcharia, E., Vlodavsky, I., Lindahl, U. & Li, J. Transgenic or tumor-induced expression of heparanase upregulates sulfation of heparan sulfate. *Nat. Chem. Biol.* **3,** 773–778 (2007).

141. Coldewey, S. M., Benetti, E., Collino, M., Pfeilschifter, J., Sponholz, C., Bauer, M., Huwiler, A. & Thiemermann, C. Elevation of serum sphingosine-1-phosphate attenuates impaired cardiac function in experimental sepsis. *Sci. Rep.* **6,** 1–12 (2016).

142. Drost, C. C., Rovas, A., Kusche-Vihrog, K., Van Slyke, P., Kim, H., Hoang, V. C., Maynes, J. T., Wennmann, D. O., Pavenstädt, H., Linke, W., Lukasz, A., Hesse, B. & Kümpers, P. Tie2 Activation Promotes Protection and Reconstitution of the Endothelial Glycocalyx in Human Sepsis. *Thromb. Haemost.* **119,** E1 (2019).

143. Salmon, A. H. J., Neal, C. R., Sage, L. M., Glass, C. A., Harper, S. J. & Bates, D. O. Angiopoietin-1 alters microvascular permeability coefficients in vivo via modification of endothelial glycocalyx. *Cardiovasc. Res.* **83,** 24–33 (2009).

144. Oshima, K., Han, X., Ouyang, Y., Masri, R. El, Yang, Y., Haeger, S. M., McMurtry, S. A., Lane, T. C., Davizon-Castillo, P., Zhang, F., Yue, X., Vivès, R. R., Linhardt, R. J. & Schmidt, E. P. Loss of endothelial sulfatase-1 after experimental sepsis attenuates subsequent pulmonary inflammatory responses. *Am. J. Physiol. - Lung Cell. Mol. Physiol.* **317,** L6667–L677 (2019).

145. Mayr, F. B., Yende, S. & Angus, D. C. Epidemiology of severe sepsis. *Virulence* **5,** 1–11 (2014).

146. Durr, E., Yu, J., Krasinska, K. M., Carver, L. A., Yates, J. R., Testa, J. E., Oh, P. & Schnitzer, J. E. Direct proteomic mapping of the lung microvascular endothelial cell surface in vivo and in cell culture. *Nat. Biotechnol.* **22,** 985–992 (2004).

147. Amatschek, S., Kriehuber, E., Bauer, W., Reininger, B., Meraner, P., Wolpl, A., Schweifer, N., Haslinger, C., Stingl, G. & Maurer, D. Blood and lymphatic endothelial cell-specific differentiation programs are stringently controlled by the tissue environment. *Blood* **109,** 4777–4785 (2007).

148. Yini, S., Heng, Z., Xin, A. & Xiaochun, M. Effect of unfractionated heparin on endothelial glycocalyx in a septic shock model. *Acta Anaesthesiol. Scand.* **59,** 160–169 (2015).

149. Huang, X., Han, S., Liu, X., Wang, T., Xu, H., Xia, B., Kong, G., Li, J., Zhu, W., Hu, H., Hao, D. & Wang, X. Both UFH and NAH alleviate shedding of endothelial glycocalyx and coagulopathy in LPS-induced sepsis. *Exp. Ther. Med.* 913–922 (2019). doi:10.3892/etm.2019.8285

150. Chappell, D., Jacob, M., Hofmann-Kiefer, K., Rehm, M., Welsch, U., Conzen, P. & Becker, B. F. Antithrombin reduces shedding of the endothelial glycocalyx following ischaemia/reperfusion. *Cardiovasc. Res.* **83,** 388–396 (2009).

151. Rhodes, A., Evans, L. E., Alhazzani, W., Levy, M. M., Antonelli, M., Ferrer, R., Kumar, A., Sevransky, J. E., Sprung, C. L., Nunnally, M. E., Rochwerg, B., Rubenfeld, G. D., Angus, D. C., Annane, D., Beale, R. J., Bellinghan, G. J., Bernard, G. R., Chiche, J. D., Coopersmith, C., De Backer, D. P., French, C. J., Fujishima, S., Gerlach, H., Hidalgo, J. L., Hollenberg, S. M., Jones, A. E., Karnad, Di. R., Kleinpell, R. M., Koh, Y., Lisboa, T. C., MacHado, F. R., Marini, J. J., Marshall, J. C., Mazuski, J. E., McIntyre, L. A., McLean, A. S., Mehta, S., Moreno, R. P., Myburgh, J., Navalesi, P., Nishida, O., Osborn, T. M., Perner, A., Plunkett, C. M., Ranieri, M., Schorr, C. A., Seckel, M. A., Seymour, C. W., Shieh, L., Shukri, K. A., Simpson, S. Q., Singer, M., Thompson, B. T., Townsend, S. R., Van Der Poll, T., Vincent, J. L., Wiersinga, W. J., Zimmerman, J. L. & Dellinger, R. P. *Surviving Sepsis Campaign: International Guidelines for Management of Sepsis and Septic Shock: 2016. Crit. Care Med.* **45,** (2017).

152. Vandenbroucke, R. E. & Libert, C. Is there new hope for therapeutic matrix metalloproteinase inhibition? *Nat. Rev. Drug Discov.* **13,** 904–927 (2014).

153. Chappell, D., Hofmann-Kiefer, K., Jacob, M., Rehm, M., Briegel, J., Welsch, U., Conzen, P. & Becker, B. F. TNF-α induced shedding of the endothelial glycocalyx is prevented by hydrocortisone and antithrombin. *Basic Res. Cardiol.* **104,** 78–89 (2009).

154. Peng, Z., Pati, S., Potter, D., Brown, R., Holcomb, J. B., Grill, R., Wataha, K., Park, P. W., Xue, H. & Kozar, R. A. Fresh frozen plasma lessens pulmonary endothelial inflammation and hyperpermeability after hemorrhagic shock and is associated with loss of syndecan 1. *Shock* **40,** 195–202 (2013).

155. Wodicka, J. R., Chambers, A. M., Sangha, G. S., Goergen, C. J. & Panitch, A. Development of a glycosaminoglycan derived, selectin targeting anti-adhesive coating to treat endothelial cell dysfunction. *Pharmaceuticals* **10,** (2017).

156. Röst, H. L., Rosenberger, G., Navarro, P., Gillet, L., Miladinoviä, S. M., Schubert, O. T., Wolski, W., Collins, B. C., Malmström, J., Malmström, L. & Aebersold, R. OpenSWATH enables automated, targeted analysis of data-independent acquisition MS data. *Nat. Biotechnol.* **32,** 219–223 (2014).

157. Teuwen, L. A., Geldhof, V., Pasut, A. & Carmeliet, P. COVID-19: the vasculature unleashed. *Nat. Rev. Immunol.* **20,** 389–391 (2020).

158. Stahl, K., Gronski, P. A., Kiyan, Y., Seeliger, B., Bertram, A., Pape, T., Welte, T., Hoeper, M. M., Haller, H. & David, S. Injury to the Endothelial Glycocalyx in Critically Ill Patients with COVID-19. *Am. J. Respir. Crit. Care Med.* **202,** 1178–1181 (2020).

159. Rudd, K. E., Johnson, S. C., Agesa, K. M., Shackelford, K. A., Tsoi, D., Kievlan, D. R., Colombara, D. V, Kissoon, N., Finfer, S., Fleischmann-struzek, C., Ikuta, K. S., Machado, F. R., Reinhart, K. K., Rowan, K., Seymour, C. W., Watson, R. S., West, T. E., Marinho,

F., Hay, S. I., Lozano, R., Lopez, A. D., Angus, D. C., Murray, C. J. L. & Naghavi, M. Global, regional, and national sepsis incidence and mortality, 1990 – 2017: analysis for the Global Burden of Disease study. *Lancet* **6736,** 1–12 (2020).

160. Paoli, C. J., Reynolds, M. A., Sinha, M., Gitlin, M. & Crouser, E. Epidemiology and costs of sepsis in the United States-an analysis based on timing of diagnosis and severity level. *Crit. Care Med.* **46,** 1889–1897 (2018).

Chapter 2: Proteomic atlas of organ vasculopathies triggered by *Staphylococcus aureus* sepsis

2.1 Abstract

Sepsis is a life-threatening condition triggered by a dysregulated host response to microbial infection resulting in vascular dysfunction, organ failure and death. Here we provide a semi-quantitative atlas of the murine vascular cell-surface proteome at the organ level, and how it changes during sepsis. Using *in vivo* chemical labeling and high-resolution mass spectrometry, we demonstrate the presence of a vascular proteome that is perfusable and shared across multiple organs. This proteome is enriched in membrane-anchored proteins, including multiple regulators of endothelial barrier functions and innate immunity. Further, we automated our workflows and applied them to a murine model of methicillin-resistant *Staphylococcus aureus* (MRSA) sepsis to unravel changes during systemic inflammatory responses. We provide an organ-specific atlas of both systemic and local changes of the vascular proteome triggered by sepsis. Collectively, the data indicates that MRSA-sepsis triggers extensive proteome remodeling of the vascular cell surfaces, in a tissue-specific manner.

2.2 Introduction

The mammalian circulatory system is built of specialized tissues capable of specifying distinct vascular environments. Due to anatomical and histological constraints, the structure, morphology, and composition of the vasculature vary across different organs [1,2]. For example, the highly specialized blood–brain barrier (BBB) is built of continuous and rather impermeable brain capillaries, whereas the liver sinusoids or the kidney glomeruli are made of more permeable, discontinuous, or fenestrated blood vessels. The endothelial glycocalyx is a cell surface layer located at the luminal side of the blood vessels, and is mainly composed of glycans, glycolipids, glycoproteins, and proteoglycans [3]. The glycocalyx modulates organ-specific functions, vascular hemostasis, and multiple aspects of innate immunity [4].

Rapid remodeling of the vascular surfaces occurs during systemic inflammatory responses and sepsis [5,6], with increased degradation and shedding of glycocalyx components. Shed material can fuel dysregulated inflammatory loops, acting as damage-associated molecular patterns (DAMPs) or delaying glycocalyx reconstitution by blunting growth factor signaling [7]. Remodeling of the endothelial cell surface occurs during leukocyte recruitment and extravasation, and leads to activation of the coagulation and complement systems [8–11]. Infiltrating immune cells and soluble plasma proteins also modulate the final make-up of the endothelial glycocalyx.

The occurrence of multiple organ failure (MOF) is a cardinal sign of severe sepsis or "septic shock" [12–14]. However, the molecular mechanisms determining why certain organs are more prone to failure than others are not fully understood. Given its location between the blood and tissue compartments, the vascular glycocalyx is an attractive target for therapeutic intervention to prevent MOF in sepsis. In fact, it is possible that different vascular beds may respond differently to septic factors since they are equipped with unique and dynamic cell surface proteomes and

glycomes. Additionally, molecular remodeling of the vascular surfaces could also facilitate acute and adaptive immune responses. The ability to track these processes *in vivo* with temporal and spatial resolution is key to understanding early events during systemic inflammatory responses. Eventually, such insights might facilitate the molecular classification of sepsis subtypes based on specific pathogens and/or host vascular responses

Unfortunately, there is limited knowledge of the molecular composition of the vascular glycocalyx *in vivo*, its variation across different organs, and the changes that occur during disease. Most studies reported to date rely either on specialized fixation and staining techniques, or on indirect assays, for example tracking the levels of selected markers of endothelial dysfunction in plasma [15–17]. Proteomic approaches have also demonstrated changes in the glycocalyx of cultured endothelial cells after exposure to proinflammatory agents [18,19]. However, it is most likely that cell-based systems do not fully recapitulate the complex nature of the *in vivo* vascular glycocalyx due to the absence of perivascular cells and plasma components. In fact, ~40% of the proteins expressed on luminal endothelial cell plasma membranes isolated from rat lungs are totally absent in cultured rat lung microvascular endothelial cells, documenting the inadequacy of cell culture models to duplicate the natural environment of endothelial cells [20].

Terminal systemic perfusion of animals has been used to deliver reactive ester-derivatives of biotin to label cell surface proteins accessible from the vascular flow [21,22]. This approach is simple and effective, and depending on the chemistry of the linkers and the perfusion conditions, it can result in the specific labeling of tumors and identification of tumor biomarkers [23]. The use of biotin facilitates downstream affinity chromatography and can be easily interfaced with shotgun proteomics to dissect the vascular cell surface proteome. Studies have demonstrated the utility of these approaches to profile and quantify vascular anti- gens in metastatic lesions in the liver and

B-cell lymphomas, using time-of-flight (TOF) mass spectrometry [24,25]. However, new generation mass spectrometers with orbitrap-based technology are now widely available, providing increased sensitivity, scan speed, and mass accuracy compared to their predecessors. These instruments facilitate high-resolution measurements of fragment ions, improved proteome coverage, lower false discovery rates, and more robust absolute and semi-quantitative proteome analysis.

In this report, we apply a strategy based on systemic biotinylation of murine tissues, streptavidin affinity chromatography and high-resolution LC–MS/MS, all in a fully automated workflow, achieving high-throughput and reproducibility. The method was employed to generate a label-free semi-quantitative molecular atlas of the murine vascular cell surface proteome at the organ level (liver, kidney, brain, heart, and white adipose tissue) and how it changes during methicillin-resistant *Staphylococcus aureus* (MRSA) sepsis.

2.3 Materials and methods

2.3.1 Bacterial strain and preparation

Methicillin-resistant *Staphylococcus aureus* (MRSA USA300 TCH1516) was originally isolated from an outbreak in Houston, Texas and caused severe invasive disease in adolescents [26]. MRSA was routinely grown at 37°C on Todd-Hewitt agar (Difco) or in liquid cultures of Todd-Hewitt broth (THB, Difco) with agitation (200 rpm). Bacteria were inoculated into 5 mL of fresh THB and incubated overnight. 400 µL of overnight culture was inoculated into 6 mL of fresh THB and incubated to OD_{600} = 0.4. Bacteria were centrifuged, washed twice with PBS, and suspended in PBS at 5×10^8 cfu/mL.

2.3.2 Animal experiments

For MRSA infection, 8–10-week-old C57Bl/6 male and female mice were injected i.v. through the retroorbital sinus with 100 µL PBS as a control group or with 5×10^7 cfu (100 µL)

MRSA. At 24 h post-infection, animals were euthanized by isoflurane and immediately processed using systemic chemical perfusions. CFU in the MRSA inoculum were enumerated by serial dilution on Todd Hewitt Agar plates to ensure consistent CFU dosing across experiments. Animals were housed and bred in Individual Ventilated Cages in a Specific Pathogen Free background, in vivaria approved by the Association for Assessment and Accreditation of Laboratory Animal Care located in the School of Medicine, UC San Diego. All experiments were performed in accordance with relevant guidelines and regulations following standards and procedures approved by the UC San Diego Institutional Animal Care and Use Committee (protocol #S99127 and #S00227M).

2.3.3 Systemic chemical perfusions

In vivo biotinylation was essentially conducted as reported [22] with some minor changes. Briefly, animals were anesthetized using isoflurane in a closed chamber and a median sternotomy was performed. The left ventricle of the heart was punctured with a 25-gauge butterfly needle (BD Vacutainer) and a small cut was made in the right atrium to allow draining of perfusion solutions. All perfusion reagents were ice-cold and were infused using a perfusion pump (Fischer scientific). Blood components were quickly washed out with PBS for 5 min at a rate of 5 mL/min. A solution containing 100 mM EZ-link Sulfo-NHS-biotin (Thermo Fischer) in PBS, pH 7.4 was used to perfuse the animals at 3 ml/min for 10 min. Finally, animals were perfused with the quenching solution (50 mM Tris-HCl, pH 7.4) at 3 ml/min for 5 min. Control animals were perfused in exactly the same way but with PBS.

2.3.4 Organ preparations

Mouse organs were harvested and homogenized using zirconia/silica beads, (1 mm diameter, Biospec) in a benchtop MagNA Lyser instrument (Roche). Homogenization buffer contained 5 M urea, 0.25 M NaCl and 0.1% SDS. Samples were briefly centrifuged at 16100 ×g

for 5 min to sediment insoluble tissue debris. The clear supernatant was transferred to a new tube and protein was quantified by BCA assay (Thermo Scientific) as per manufacturer instructions and stored at −80°C until further analysis.

2.3.5 SDS-PAGE and in gel western blot

Organ homogenates were resolved by SDS–PAGE (Bis-tris 4–12%). After electrophoresis, gels were incubated with 50% isopropanol +5% acetic acid for 15 min, followed by a 15 min wash with ultrapure water. Gels were further incubated with streptavidin-IRDye680 (LI-COR Biosciences) for 1 h with gentle shaking in the dark. Gels were washed three more times for 10 min in PBS + 0.1% Tween 20. After a last wash with PBS for 5 min, the gel was imaged using an Odyssey Infrared Imaging System (LI-COR Biosciences).

2.3.6 Histological analysis and immunofluorescence

Tissues were fixed in 10% buffered formalin (Fischer Chemical) for 24 h, followed by submersion in 70% ethanol for at least 24 h. The samples were paraffin embedded and sectioned (3 µm), and stained with hematoxylin/eosin. For immunofluorescence of perfused tissues, organs were harvested immediately following systemic Sulfo-NHS-Biotin perfusion and fixed in ice-cold PBS + 4% paraformaldehyde for 18–24 h with gentle end-over-end agitation. Fixed organs were placed in 40% sucrose solution overnight. Saturated organs were then submerged in Optimal Cutting Temperature com- pound (OCT) (Sakura) and flash frozen in cassettes submerged in 2-methylbutane chilled with dry ice. Sections (20 µm) were permeabilized and stained for 1 h with 1 µg/mL Streptavidin Alexa Fluor 488 (Invitrogen) and 20 µg/mL Isolectin B4 Alexa Fluor 594 (Thermo Fischer Scientific), followed by mounting medium containing DAPI (Thermo Fischer Scientific). Lubricin/PRG4 Antibody (NBP1-19048, Novus Biologicals) was diluted 1/50 and detected with secondary goat anti rabbit Alexa Fluor 647 (A-21245, Invitrogen). Sections were

mounted on glass slides under #1.5 coverslips. All Z-stacks were acquired with an inverted Zeiss LSM 880 confocal with FAST AiryScan, using either a ×10 Plan-Apochromat 0.45NA objective or a ×40 LD LCI Plan-Apochromat 1.2NA immersion objective as indicated in the figure legend. Images were processed using the in line AiryScan processing module in Zen Black. For intensity comparisons, all acquisition parameters were standar- dized to the following: Red channel 561 nm, 721 master gain, 8.7% laser power, 3.7 AiryScan parameter; Green channel 488 nm, 676 master gain, 1.2% laser power, 4.1 AiryScan parameter; DAPI channel 405 nm, 732 master gain, 3.8% laser power, 3.8 AiryScan parameter.

2.3.7 qPCR analysis

mRNA was isolated from whole liver extracts, reverse transcribed, and quantitated by qRT-PCR using the following primers for murine PRG4:5′- CAG GAC AGC ACT CCA TGT AGT-3′ (reverse) and 5′-GGG TGG AAA ATA CTT CCC GTC-5′ (forward). mRNA was extracted using the RNeasy Kit (Qiagen). cDNA was synthetized using SuperScript III First-Stand Synthesis kit (Invitrogen). Expression was quantified using the $2^{-\Delta\Delta CT}$ method and TBP was used to normalize the expression of the target genes between samples.

2.3.8 Determination of hyaluronic acid concentration

Hyaluronan levels in plasma were measured using a Hyaluronan Quantikine Enzyme-Linked Immunosorbent Assays (ELISA) kit (R&D Systems) according to the manufacturer's recommendation.

2.3.9 Determination of plasma levels of ALT and AST

Blood was collected via cardiac puncture and placed in a pro-coagulant serum tube (BD Microtainer #365967) for 4 h at room temperature. Serum was isolated by spinning the tubes at 2000 xg and collecting the supernatant. All samples were frozen and thawed once before analysis.

ALT/AST was measured on a Cobas 8000 automated chemistry analyzer (Roche) with a general coefficient of variance of <5%.

2.3.10 Analysis of bacteria colony-forming unit counts

Organs of interest were placed in a 2 mL tube (Sarstedt #72.693.005) containing 1 mL ice-cold PBS and 1.0 mm diameter Zirconia/Silica beads (Biospec Products #11079110z). Samples were homogenized using a MagNA Lyzer (Roche) for 2 min at 6000 rpm. An aliquot of each organ sample was serially diluted in PBS and plated on Todd-Hewitt Agar to enumerate CFU.

2.3.11 Purification of biotinylated proteins

Biotinylated proteins were purified from homogenized organs (3 mg protein) using a Bravo AssayMap platform and AssayMap streptavidin cartridges (Agilent). Briefly, cartridges were prewashed with 50 mM ammonium bicarbonate (pH 8), and then samples were loaded. Non-biotinylated proteins were removed by extensively washing the cartridges with 8 M urea in 50 mM ammonium bicarbonate buffer (pH 8). Cartridges were washed with Rapid digestion buffer (Promega, Rapid digestion buffer kit) and bound proteins were subjected to on-column digestion using mass spec grade Trypsin/Lys-C Rapid digestion enzyme (Promega, Madison, WI) at 70 °C for 2 h. Released peptides were desalted in the Bravo platform using AssayMap C18 cartridges and the organic solvent was removed by vacuum centrifugation (SpeedVac). Samples were stored in −20°C prior to LC–MS/MS analysis.

2.3.12 LC-MS/MS analysis

Dried peptides were reconstituted with 2% acetonitrile, 0.1% formic acid, and quantified by modified BCA peptide assay (Thermo Fisher Scientific). Equal peptide amounts derived from each sample were injected and analyzed by LC-MS/MS using a Proxeon EASY nanoLC system (Thermo Fisher Scientific) coupled to a Q-Exactive Plus mass spectrometer (Thermo Fisher Sci-

entific). Peptides were separated using an analytical C18 Acclaim PepMap column (0.075 × 500 mm, 2 µm; Thermo Scientific) equilibrated with buffer A (0.1% formic acid in water) and eluted in a 93-min linear gradient of 2–28% solvent B (100% acetonitrile) at a flow rate of 300 nL/min. The mass spectrometer was operated in positive data-dependent acquisition mode. MS1 spectra were measured with a resolution of 70,000, an automated gain control (AGC) target of 1e6 and a mass range from 350 to 1700 m/z. Up to 12 MS2 spectra per duty cycle were triggered, fragmented by higher energy collisional dissociation (HCD), and acquired with a resolution of 17,500 and an AGC target of 5e4, an isolation window of 1.6 m/z and a normalized collision energy of 25. Dynamic exclusion was enabled with duration of 20 s.

2.3.13 2D-LC-MS/MS analysis

Dried samples were reconstituted in 0.1M ammonium formate pH ~10 and analyzed by 2D-LC–MS/MS using a 2D nanoACQUITY Ultra Performance Liquid Chromatography (UPLC) system (Waters corp., Milford, MA) coupled to a Q-Exactive Plus mass spectrometer (Thermo Fisher Scientific). Peptides were loaded onto the first-dimension column, XBridge BEH130 C18 NanoEase (300 µm × 50 mm, 5 µm) equilibrated with solvent A (20 mM ammonium formate, pH 10, first-dimension pump) at 2 µL/min. The first fraction was eluted at 17% of solvent B (100% acetonitrile) for 4 min and transferred to the second dimension Symmetry C18 trap column 0.180 × 20 mm (Waters corp., Milford, MA) using a 1:10 dilution with 99.9% second dimensional pump solvent A (0.1% formic acid in water) at 20 µL/min. Peptides were then eluted from the trap column and resolved on the analytical C18 Acclaim PepMap column (0.075 × 500 mm, 2 µm particles; Thermo Scientific) at low pH by increasing the composition of solvent B (100% acetonitrile) from 1 to 38% (non-linear) over 96 min at 300 nL/min. Subsequent fractions were generated with increasing concentrations of solvent B. The first-dimension fractions were eluted

at 19.5, 22, 26, and 65% solvent B, respectively. The mass spectrometer was operated in positive data-dependent acquisition mode. MS1 spectra were measured with a resolution of 70,000, an AGC target of 1e6 and a mass range from 350 to 1700 m/z. Up to 12 MS2 spectra per duty cycle were triggered, fragmented by HCD, and acquired with a resolution of 17,500 and an AGC target of 5e4, an isolation window of 1.6 m/z and a normalized collision energy of 25. Dynamic exclusion was enabled with duration of 20 s.

2.3.14 Mass spectrometry data analysis

MS Raw.files were processed in the MaxQuant platform [27](version 1.6.1.0) and searched by the Andromeda search engine [28] against the mouse UniProt FASTA database (downloaded 06–02–2017) and against a common contaminant database. Search parameters were set as follows: enzyme, trypsin/LysC with up to 2 potential missed cleavages; fixed modifications, carbamidomethyl on cysteines; variable modifications, oxidation of methionine and acetylation of protein N-terminus; minimum peptide length, 7. The false discovery rate (FDR) for both peptide and protein identifications was set to 1% and was calculated by searching the MS/MS data against a reversed decoy database. Allowed mass deviation for precursor ions was set to 5 ppm and for peptide fragments was set to 20 ppm. Label-free quantifications (LFQ) was based on a minimum of 2 counts, minimum number of neighbors was set to 3 and average number of neighbors was 6. The match between runs option was applied with a match time window of 0.7 min and an alignment time window of 20 min.

2.3.15 Statistical analysis

Bioinformatics and statistical analysis of proteomics results were conducted in the Perseus statistical suite (version 1.6.5.0) [29] of the MaxQuant computational platform. MaxQuant results were imported into Perseus and identified hits were filtered based on number of peptides (>2) and

number of MS/ MS scans for each peptide (>2). Missing values were addressed by requiring a cut-off corresponding to 75% valid values in at least one group (infected + biotin, uninfected + biotin, or PBS controls). Remaining missing values were imputed from the normal distribution using a width of 0.3 and a down shift of 1.8. Control samples from PBS-perfused samples were used to subtract the background, keeping protein identifications in labeled samples displaying at least a 2-fold change enrichment. Statistically significant changes between groups were assessed by two-way analysis of variance (ANOVA) with a permutation-based false discovery rate (FDR) for multiple test correction and truncation after 250 randomizations. Hierarchical clustering was applied using Euclidean distances and preprocessing with k-means. The statistical significance of the blood chemistry analysis was determined using a two-tailed Student's t-test in GraphPad prism (version 5.03). Pathway and GO term analysis were conducted using the online version of Metascape and DAVID server. Louvain clustering was performed in Python 3.6.6 using the python package python-Louvain located on the Python Package Index. Clustering was done running default parameter settings.

2.4 Results

2.4.1 Systemic labeling of vascular structures in murine organs

Due to its systemic nature, a septic response is difficult to recapitulate in vitro. Thus, a more universal approach is needed to track proteome changes triggered by a septic insult in vivo. We explored the labeling of murine vascular compartments using terminal systemic perfusion with ester derivatives of biotin to tag, purify, and identify proteins normally exposed to the vascular flow. The labeling conditions are summarized in Figure 2.1 and are similar to methods previously reported by Rybak, 2005 [21].We subjected wildtype C57BL/6J mice to this procedure using sulfo-

NHS-biotin as described in the Methods section, and verified the extent of labeling and localization of biotinylated material.

First, we harvested biotinylated organs, as well as control tissue derived from PBS-perfused animals. Tissues were homogenized, the homogenates run on SDS-PAGE, and tagged proteins were detected by blotting with streptavidin. As shown Figure 2.2, multiple protein bands were detected in the biotinylated samples, whereas only faint bands were observed in tissues from animals that were perfused with PBS. Tissue-specific differences were also observed, as suggested by differential mobility and intensity of the biotinylated protein bands detected in kidney and heart. These differences suggested that the accessibility and/or the composition of the vascular proteomes might differ among the organs.

To better resolve the tissue compartments targeted by sulfo-NHS-biotin perfusion, multiple organs were harvested, cryosectioned, and stained with fluorophore-conjugated streptavidin. Histological examination by confocal microscopy showed biotinylated proteins in close association with blood vessels (Figures 2.3A-D). For example, strong streptavidin reactivity was detected in the liver around the hepatic central veins and the sinusoidal microvasculature, but not in association with parenchymal hepatocytes (Figure 2.3A). In the kidney, biotinylated material was restricted to the glomerular compartments and proximal tubule (Figure 2.3B). In the heart (Figure 2.3C) and brain (Figure 2.3D), streptavidin reactivity localized primarily within the microvasculature, with no obvious penetration into deeper parenchymal regions.

To determine if the biotin labeling was specifically associated with endothelial cell surfaces, co-staining with Isolectin B4 (IB4) was performed (Figure 2.3A–D). IB4 is a glycoprotein derived from the African legume *Griffonia simplicifolia* that recognizes terminal alpha-linked galactose residues on the carbohydrates lining the endothelial lumen. Partial overlap

between the streptavidin and the IB4 staining patterns was observed in all tissues, confirming the presence of biotinylated material on the endothelial lumen. However, strong streptavidin reactivity was also detected at the basement membrane, and within the adjacent extracellular matrix (ECM) of the endothelial cells. Intracellular staining remained low, confirming the inability of sulfo-NHS-biotin to penetrate the cell membrane due to the charged character of its sulfate functionality.

2.4.2 Shared and organ-specific vascular proteomics signatures

To qualitatively explore the scope of the systemically labeled vascular proteome, two major organs (liver, kidney) were homogenized and subjected to streptavidin enrichment and trypsinization. Peptide digests were analyzed through an online 2D-LC-MS/MS workflow at high/low pH, as described in the Methods section, to perform deep fractionation of the samples and to increase proteome coverage. Briefly, samples were first separated by reverse phase chromatography on a C18-column at pH 10 and five consecutive fractions were collected by eluting at increasing acetonitrile concentrations (17%, 19.5%, 22%, 26% and 65%). The individual fractions were then separated at pH 3 on a C18-column and analyzed by LC-MS/MS (Figure 2.4A-B). Matching control tissue from PBS-perfused animals was subjected to the same analytical procedure to account for background signals (i.e. nonbiotinylated proteins that non-specifically interact with the streptavidin beads). Only peptides displaying at least a 2-fold enrichment compared to the PBS background of the respective organ were considered for further analysis. To add more stringency, a positive protein identification required a minimum of two unique peptides with two MS/MS scans each. The complete bioinformatic treatment of the data was performed as detailed in the Methods section.

After filtering the data, 409 non-redundant proteins were identified in the liver and 533 proteins were detected in kidney samples, at a 1% false discovery rate (Figure 2.4C). A number of

proteins (138) were shared between the tissues. We analyzed the subcellular localization of all protein identifications using hypergeometric enrichment tests on their associated Gene Ontology (GO) terms. In both liver and kidney datasets, we found a significant enrichment for proteins associated with the plasma membrane and the extracellular matrix (Figure 2.4D-E). This shared proteome included cadherins and cadherin-like proteins, integrins, collagens, laminins, proteoglycans, cellular receptors, and enzymes as well as a large repertoire of receptor-type protein tyrosine phosphatases. Classical endothelial markers such as VE-cadherin, endoglin, vascular cell adhesion molecule 1 (VCAM1), and intercellular adhesion molecule 1 (ICAM1) were also identified. Functional enrichment analysis of this signature retrieved pathways associated with cell adhesion, vascular morphogenesis, proteoglycan metabolism, and vascular endothelial growth factor (VEGF)-signaling pathways (Figure 2.4F).

Unique organ-specific proteomic signatures were also detected. For example, liver samples were characterized by the presence of multiple scavenger receptors such as C-type lectin family 4 F (Clec4F), Scavenger Receptor Class B Member 1 (Scarb1), stabilin 1 (Stab1), Stab2, and asialoglycoprotein receptor 2 (Asgr2), reflecting the filtering functions of the hepatic reticuloendothelial system. We also found a number of proteins involved in lipoprotein remodeling and clearance, including low density lipoprotein receptor (Ldlr), angiopoietin related protein 3 (Angptl3), hepatic triglyceride lipase precursor (Lipc), fatty acid binding protein 1 (Fabp1), and LDLR associated protein 1 (Ldlrap1), consistent with the role of the liver as the major target for lipoprotein metabolism and uptake. Clec4F is a marker for Kupffer cells, whereas Angptl3, Lipc, and Ldlrap1 are soluble proteins presumably bound to the glycocalyx. Similarly, kidney samples were specifically enriched in proteins involved in the regulation of blood pressure and fluid

balance, including components of the renin-angiotensin system, such as angiotensin converting enzyme (Ace), Ace2, glutamyl aminopeptidase (Enpep), and renin 2 (Ren2).

Finally, a network approach was applied to focus on potential protein-protein associations amongst the unique vascular proteomes. All proteins identified in each tissue were searched through the Search Tool for the Retrieval of Interacting Genes/Proteins (STRING) database to generate a network based on physical and functional interactions. Only high confidence protein–protein associations (STRING association scores >0.07) were retained in the network. The Louvain method was used to identify communities (or clusters) displaying a higher density of interconnected nodes than expected by random chance [30]. These clusters were further segregated via force-directed visualization algorithms and subjected to functional enrichment analysis. Roughly, 33% of the liver and 31% of the kidney proteins clustered into 4 and 5 distinct Louvain communities, respectively (Figure 2.5A–I). Each cluster covered several functional layers that were often enriched in distinct biological processes. The results from the Louvain clustering showed a clear pattern of functional commonalities between the biotinylated tissues. Interestingly, some of the clusters were enriched in organ-specific processes such as signaling through receptor tyrosine kinases and glutathione metabolism in the kidney (Figure 2.5B, E), or regulation of lipid metabolic pathways and lipoprotein particle clearance in the liver (Figure 2.5H).

2.4.3 MRSA-sepsis results in profound liver vasculopathy

Since sepsis is a systemic syndrome of vascular dysfunction, we reasoned that tracking specific molecular changes at the blood/tissue interface could generate new insights into sepsis-associated vasculopathies. To explore this idea, a proteomics workflow was applied to a murine model of sepsis triggered by MRSA bacteremia. Briefly, wildtype C57BL/6J mice were intravenously infected through the retroorbital route with 5×10^7 colony-forming units (CFU) of

MRSA, a model that induces lethality within 48 h post-infection [31], or with PBS as a control. Since changes in the vascular compartments are expected to precede organ damage and lethality, we focused on the early pre-mortality stages of the disease 24 h post-infection [32].

Analysis of the pathogen burden at this time point revealed dramatically different bacterial invasion and/or colonization across tissues. Liver, kidney, and heart samples exhibited the highest pathogen infiltration, followed by brain and WAT (Figure 2.6A). Gross pathology of the liver showed white necrotic plaques that were completely absent in control animals (Figure 2.6B), in line with previously published findings [33]. To confirm that the hepatic pathogen burden was linked to ongoing liver failure, we measured plasma levels of liver markers alanine aminotransferase (ALT) and aspartate aminotransferase (AST). Indeed, both markers were increased at 24 h post-infection (Figure 2.6C). Liver tissues showed leukocyte infiltrates, bacterial microabscesses, and severe signs of necrotic thrombosis (Figure 2.6D). Pathological hypercoagulation was characterized by the presence of large thrombi in the major veins of the liver, leading to blood vessel occlusion and disseminated tissue necrosis. Necrotic loci spread out over large areas adjacent to the thrombotic zones, and the thrombi were surrounded by layers of polymorphonuclear cells. To assess the suitability of the biotinylation perfusions for the analysis of vascular alterations during sepsis, liver cryosections from animals challenged with MRSA and systemic biotinylation, were probed with fluorescently labeled streptavidin. As shown in Figure 2.6E, streptavidin reactivity was detected in areas of thrombosis, around the blood vessels and at the surface of infiltrating immune cells. Notably, the thrombi were also intensely stained, whereas regions of tissue necrosis were streptavidin negative, consistent with occluded blood perfusion into those areas.

2.4.4 Proteomics profiling of vascular surfaces during sepsis

Given that the biotinylation perfusion was able to label protein targets within these key vasculopathic regions, the proteomics workflow was expected to render a molecular snapshot of the septic organ vasculatures, including the injured hepatic surfaces. For each experiment, 3 MRSA-infected and 3 uninfected mice were anesthetized and subjected to the systemic biotinylation protocol at 24 h post-infection. In addition, one infected and one uninfected mouse were perfused only with saline to account for potential background signals. Five different organs were selected for proteomics analysis based on their clinical relevance: liver, kidney, heart, brain, and white adipose tissue (WAT). In total, we performed four independent experiments resulting in a total of 160 LC-MS/MS runs. The samples were quantified using the MS label-free strategy described above. To minimize variability introduced by manual sample handling, the workflow was fully automated by transferring all sample preparations to a BRAVO liquid handling platform. To speed up the process and to be able to perform relative quantification, all samples were analyzed using a single run LC-MS/MS, instead of the 2D-LC-MS/MS approach used for deep fractionation. However, since sepsis is notoriously heterogenous, we also applied strict bioinformatic and statistical criteria to only focus on robust and reproducible changes, as specified in the method section.

The proteomics screening identified robust and reproducible alterations of a few hundred of proteins from each individual organ (liver: 272, kidney: 300, heart: 275, WAT: 185, and brain: 85), according to a two-way analysis of variance (ANOVA) with a permutation-based false discovery rate correction for multiple test comparisons. Missing values were addressed by requiring a cut-off corresponding to 75% valid values in at least one group (infected + biotin, uninfected + biotin, or PBS controls). Profile plots of proteins complying to strict criteria (see Methods) are shown in Figure 2.7A–E. In general, the identified proteome changes covered a wide

dynamic range. Notable interassay and intraassay variability was also observed across the samples as judge by profile plots of their Label-Free Quantification (LFQ)-normalized intensities (Figure 2.7A-E, upper panels). Nevertheless, plotting the LFQ-profiles of the top 10 proteins ranked by fold change(Figure 2.7A-E, lower panels), showed a clear separation between infected and non-infected samples in all tissues, indicating that the method can detect quantitative differences triggered by sepsis.

Closer inspection of the LFQ-normalized intensities showed strong correlations for replicates in the same group. For example, proteins identified across three infected livers, displayed high Pearson correlation coefficients (r = 0.93, 0.96 and 0.96) (Figure 2.8A), whereas correlations decreased when comparing infected vs non-infected controls (r = 0.91, 0.84, and 0.77) (Figure 2.8B). Even lower correlations were observed when comparing biotinylated samples with non-labeled PBS controls, independently of their infection status (infected vs. PBS, r = 0.62, 0.69, and 0.62; uninfected vs. PBS, r = 0.56, 0.71, and 0.74) (Figure 2.8C-D). Similar results were found in other tissues indicating that the identity of the proteome accessible through systemic biotinylation differs dramatically from uninfected and PBS-perfused tissues. More importantly, these findings also indicate that the methodology captures differences specifically associated with infection.

2.4.5 Global and organ-specific proteome changes

A comparative view of the proteomic changes taking place across the five organs revealed a consistent organ-specific hierarchy (Figure 2.9). In liver, kidney, and heart, many proteins were altered between infected, and non-infected samples, whereas in brain and WAT only a few proteins showed significant changes (Figure 2.9A). The liver pattern stood clearly out from the other organs. Also, some of the hepatic proteins that underwent dramatic changes in labeling included

lubricin/proteoglycan 4 (Prg4), macrophage receptor with collagenous structure (Marco), C-X-C motif chemokine ligand 9 (Cxcl9), as well as others. We subjected the data to principal component analysis (PCA) to determine if the organ protein patterns combined with their LFQ-intensities could segregate the data into meaningful groups. Liver samples were clearly separated by PCA analysis into infected and non-infected clusters (Figure 2.9B). Kidney and brain also stratified in a similar fashion. On the other hand, PCA analysis of WAT and heart samples did not separate the infected and uninfected groups from each other. Unsupervised hierarchical clustering of the proteomics data revealed complex expression patterns. Heat maps generated to visualize the clustered data showed that all tissues had large clusters of proteins enriched or depleted by infection (Figure 2.9C).

A shared group of 57 proteins was consistently found to undergo changes in all examined organs, whereas other proteins were changing in a tissue-specific manner (liver: 88, kidney: 75, heart: 85, brain: 8, and WAT: 18) (Figure 2.10A). Functional enrichment analysis of the shared proteome retrieved biological pathways associated with coagulation, complement, ECM-remodeling, and Staphylococcus aureus infection (Figure 2.10B). This proteome signature consisted of acute phase reactants (e.g. Hp, Saa2), members of the alternative pathway of the complement cascade, for example complement factor b (Cfb), Cfh, and the matrix proteins basal cell adhesion molecule (Bcam) and nidogen 1 (Nid1). Interestingly, some of these shared proteins experienced very large fold-changes in all organs (e.g. fold-change of haptoglobin (HP) >100 in all tissues) whereas other proteins had a more scattered expression, with large fold-changes in one organ and modest induction in the others (e.g. >30-fold change of alpha-1-acid glycoprotein 2 (Orm2) in WAT, whereas ~2–6-fold in all other tissues) (Figure 2.10C).

The fold-changes associated with the top 50 differential proteins in each tissue were ranked and visualized as Circos plots (Figure 2.10D). In this representation, each protein corresponds to one ribbon, and the width of the ribbon indicates the normalized fold-change of an individual protein as a percentage of the summed fold-changes of all identified proteins in a particular organ. Strong induction of Hp was observed in all tissues accounting for 7% of all proteome changes in the liver, 36% in kidney, 34% in heart, 45% in brain, and 23% in WAT (Figure 2.10D). This is clearly shown in the Hp ribbon, which further divides into 5 sub-ribbons that connects back to the protein distribution of each organ. Interestingly, the pattern of the liver was unique because it was largely dominated by liver-specific markers, as opposed to the other organs where the largest fold-changes were instead associated with the shared vascular proteome. Proteoglycan 4 (Prg4) accounted for 34% of all liver vascular surface proteome alterations but remained undetected in the other tissues, except for the heart where it corresponded to 1% of the cardiac proteome changes.

We identified other tissue-specific markers, which were further subjected to pathway enrichment analysis to delineate organ-specific pathologies (Figure 2.11A-E). In the liver, neutrophil degranulation was the most enriched biological process, reflecting the presence of multiple neutrophil-derived proteins such as myeloperoxidase (MPO), an essential factor for neutrophil antimicrobial responses [34,35]. Other liver-specific pathways were related to cell-adhesion, integrin signaling, and glycosaminoglycan metabolism, especially hyaluronan/hyaluronic acid (HA). Kidney samples were enriched in multiple renal adhesion proteins such as the kidney-specific cadherin-16, nephronectin, and nephrin, as well as in markers of renal epithelium morphogenesis (Figure 2.11B). Similarly, heart-specific processes were highly enriched in proteins related to muscle contraction and markers of hypertrophic cardiomyopathy (HCM), reflecting potential ongoing heart failure (Figure 2.11C). Finally, a smaller number of

organotypic proteins and hence a smaller number of differential pathways were detected in brain and WAT tissues, compared with liver, kidney and heart (Figure 2.11D-E).

2.4.6 Changes in hyaluronan turnover and recognition

As mentioned above, some liver-specific markers could be grouped based on their ability to influence HA recognition and turnover. HA is a megadalton acidic polysaccharide involved in many immunomodulatory processes, including recruitment of activated neutrophils to the liver during inflammatory responses [36]. Among the proteins enriched in HA metabolism and function, we found CD44, one of the main HA receptors that regulates leukocyte trafficking and extravasation; the lymphatic vessel endothelial hyaluronan receptor 1 (Lyve1), the primary HA receptor in lymphatic endothelium; Tmem2, an endothelial cell surface hyaluronidase; and Prg4, a lubricating and anti-inflammatory competitor for HA binding to CD44 (Figure 2.12A)[37]. Notably, endothelial HA binds only weakly to CD44, unless the former becomes cross-linked to one or more of the inter-alpha-trypsin inhibitor heavy chains [36]. Cross-linked HA constitutes a high-affinity ligand for neutrophil CD44 during leukocyte extravasation in the liver sinusoids. However, the identity of the heavy chains involved in this modification remains unknown. At least 6 closely related heavy chains are expressed by many cell types, but only Itih1, Itih2, and Itih3 can be cross-linked to HA [38]. Interestingly, we detected these three heavy chains in both normal and septic livers, but no significant differences were observed regarding the levels of Itih1 and Itih2 during infection. In contrast, a 5-fold increase in Itih3 was consistently detected in liver samples, suggesting a potential role in HA-maturation during liver inflammation. Moreover, increased HA plasma levels has been identified as a sensitive marker of glycocalyx remodeling and liver dysfunction during sepsis [39,40]. Indeed, at 24 h post-infection, plasma HA levels were elevated more than 6-fold in MRSA-infected samples compared to controls (Figure 2.12B).

We focused on Prg4, since this HA-binding protein displayed the largest induction of all detected liver proteins, in all liver replicates, and across all independent experiments. Also known as lubricin, Prg4 is a secreted high molecular weight glycoprotein composed of globular domains connected by an extended mucin region. Prg4 is abundantly expressed in synovial fluid and its glycosylation plays an important role in the lubrication of articular joints. Although extra-articular expression of Prg4 is known to occur, its physiological role or involvement in liver disease has never been reported.

Expression and localization studies of Prg4 by immunofluorescence microscopy showed dramatic increase and deposition of Prg4 in the microvasculature of septic livers (Figure 2.12C-D) compared with uninfected control liver. Strong Prg4-immunoreactivity was detected both in vascular and perivascular regions, in agreement with the results from the biotinylation experiments. Of note, Prg4-staining was also detected in the periphery of large thrombi in the vicinity of necrotic areas, and in association with ly6G- positive neutrophils (Figure 2.12E-F). Finally, quantitative PCR analysis of liver tissue at 12 h post-infection revealed a 4.2-fold increase in PRG4 mRNA compared to uninfected controls (Figure 2.12G). Taken together, these signatures suggest that remodeling of HA and HA-modifying proteins is a liver-specific phenomenon activated during MRSA sepsis.

2.5 Discussion

Remodeling of the vascular glycocalyx is a hallmark of devastating diseases such as atherosclerosis, cancer and dysregulated inflammatory responses. Both glycocalyx shedding and repair (remodeling) are tightly regulated by a variety of mechanisms that can be triggered in response to physiological and/or pathological stimuli. A mechanistic understanding of these processes has been hampered by a general lack of tools to properly address their molecular basis.

Prior studies have demonstrated the use of systemic perfusion to tag murine vascular surfaces in vivo, using ester derivatives of biotin [21,22]. In principle, this delivery route creates a window to track molecular events at the blood/tissue interface and to gain insights into changes in the vascular proteome in a broad spectrum of diseases. However, these previous studies were based on labor-intensive protocols, with limited reproducibility and throughput. Additionally, chemical labeling has mainly been interfaced with off-line chromatographic separations and low-resolution MS. Nevertheless, these techniques have potential as generic tools to interrogate preclinical models of vascular diseases such as sepsis, where multiple host tissues are simultaneously engaged.

In the present study, we combined systemic biotinylation of murine tissues with an automated proteomics workflow to profile the vascular surfaces in a more robust and quantitative fashion. Indeed, multidimensional chromatography and high-resolution proteomics profiling of murine organs confirmed the presence of a complex protein landscape embedded in the vascular glycocalyx. In keeping with previous reports, proteins accessible to the vascular flow comprised a large number of adhesion molecules (including many classical endothelial markers), receptor tyrosine kinases, enzymes, scavenger receptors, proteoglycans, and plasma proteins. Notably, we observed the presence of a shared core proteome, probably essential to basic vascular functions of most tissues, along with concomitant organ-specific vascular signatures. Phenotypic heterogeneity of the vasculature is a phenomenon that has become widely recognized [41,42]. Organotypic specification of vascular tissues allows the organs to meet basic requirements of oxygenation, nutrient acquisition, hemodynamic regulation, and immunosurveillance, across a wide range of local environments. Organs such as the liver or kidney are specifically involved in regulating the rate of exchange and/or clearance of ions, metabolites, proteins, and bacterial toxins from circulation, and thus some organ-specific functions need to be wired at the vascular level.

Consistent with this idea, we found proteomic signatures specific to hepatic or renal vascular surfaces that reflected specific functions of those organs. For example, in the liver multiple proteins involved in lipid clearance were detected together with a large repertoire of scavenger receptors. In contrast, kidney displayed proteome signatures consistent with its role in controlling fluid balance and blood pressure. Recently, in vivo phage display assays facilitated identification of peptides capable of homing to specific vascular beds in vivo [43]. These approaches have been useful in generating tools for targeted delivery of compounds to specific vascular "zip codes", and they highlight the tremendous organotypic heterogeneity of the vascular surfaces. Similarly, recent developments in single cell sequencing have facilitated detailed profiling of the brain vasculature, revealing specific molecular signatures associated with zonation along the arteriovenous axis [44].

To obtain a holistic picture of vascular changes taking place during sepsis, we adapted a murine model of MRSA-sepsis and subjected the animals to chemical labeling and a proteomics workflow, selecting several organs for molecular profiling. We constructed a label-free semi-quantitative proteomics atlas of the murine vascular cell surface proteome at the organ level (liver, kidney, heart, brain, and WAT), and demonstrated that a septic insult triggered by MRSA bacteremia causes substantial remodeling of the vascular surfaces. More specifically, we demonstrated that MRSA-sepsis results in enrichment of acute-phase reactants and specific matrix proteins in the vasculature of multiple tissues. Interestingly, some of the identified proteins, such as Hp and the serum amyloid proteins Saa1 and Saa2, have already demonstrated predictive value for diagnosis of systemic inflammatory processes, including neonatal sepsis [45]. We also identified alterations of an array of proteins and biological processes in particular tissues, including potentially novel pathways associated with hepatic HA-recognition and turnover. Our proteomics screening singled out the liver as a hotspot for MRSA sepsis pathology, a pattern further confirmed

by blood chemistry and histopathological evidence of liver dysfunction, necrosis and thrombosis. The levels of many proteins in the hepatic vasculature changed during infection. One in particular, Prg4, consistently dominated the global pattern of proteome changes in the liver. Prg4 can oligomerize and deposit in the superficial zone of the articular cartilage, acting as a lubricating gel to reduce friction [46]. Due to the large amount of negatively charged carbohydrates decorating its mucin domain, Prg4 can impact the adhesion properties of synovial cell populations, bacteria and immune cells [47]. Interestingly, Pgr4 is also expressed in the liver but a role in basic liver physiology or pathology has never been described. Here we report that *PRG4* gene expression is rapidly induced during MRSA bacteremia, resulting in its secretion and abundant vascular deposition in the liver. Notably, Prg4 was also detected in association with the surface of neutrophil populations, adhering to the edges of large necrotizing thrombi, partially occluding the perfusion of the liver. It is conceivable that vascular deposition of Prg4 during liver inflammation might impact the adhesion of bacteria to the glycocalyx and influence how immune cells such as neutrophils interact with the activated endothelium. A mechanistic understanding of the role of Prg4 during acute hepatic injury, and especially during MRSA sepsis, warrants future studies.

Circulating glycocalyx fragments are most likely good markers of organ-specific pathologies. However, we do not know if some of the proteome alterations reported in this study can also be detected in plasma. Plasma proteomics has been widely applied to identify fluid biomarkers of sepsis [32,48]. One major challenge with these analyses though is the broad dynamic range of plasma proteins, which exceeds 10 orders of magnitude [49]. Profiling molecular changes in the vascular compartment can aid in the search for novel plasma markers by defining molecular targets undergoing remodeling at the vascular wall. Having pre-knowledge of what kind of candidate molecules to seek might facilitate the application of targeted proteomic assays to the

plasma proteome to increase sensitivity and coverage. Indeed, future studies will be directed to the validation of promising candidates in plasma samples to assess their predictive value. Finally, this study focused on a single time-point, but the dynamic nature of the sepsis response can only be fully addressed with temporal-spatial resolution. Tracking some of these markers over time will be imperative to achieve that final goal.

2.6 Acknowledgements

Chapter 2 was published as a manuscript in *Nature Communications* (2019) 10:4656. A Gómez Toledo, GJ Golden, A Rosa Campos, H Cuello, J Sorrentino, N Lewis, N Varki, V Nizet, JW Smith & JD Esko. The dissertation author was a primary investigator and author of this material. Proteomics analysis was done at the Proteomics Core Facility, Sanford-Burnham-Prebys Medical Discovery Institute, La Jolla, CA, USA. A.G.T. and J.D.E. conceived the study and designed it together with G.G. and J.W.S.; A.G.T., G.G., A.R.C. and H.C. performed all the experiments. A.G.T., G.G., J.S., V.N., N.L. and J.D.E. interpreted the data. N.V. performed the histopathological analysis. A.G.T. and J.D.E. wrote the paper with significant input from all the coauthors. This work was supported by grant P01HL131474 to J.D.E. and J.W.S. N.L. and J.S. also acknowledge support from NIGMS R35 GM119850. J.W.S. was supported by R01 GM107523. G.G. was supported by Microbial Sciences Graduate Research Fellowship Awards 1-F17GG and 1-F18GG.

2.7 Figures

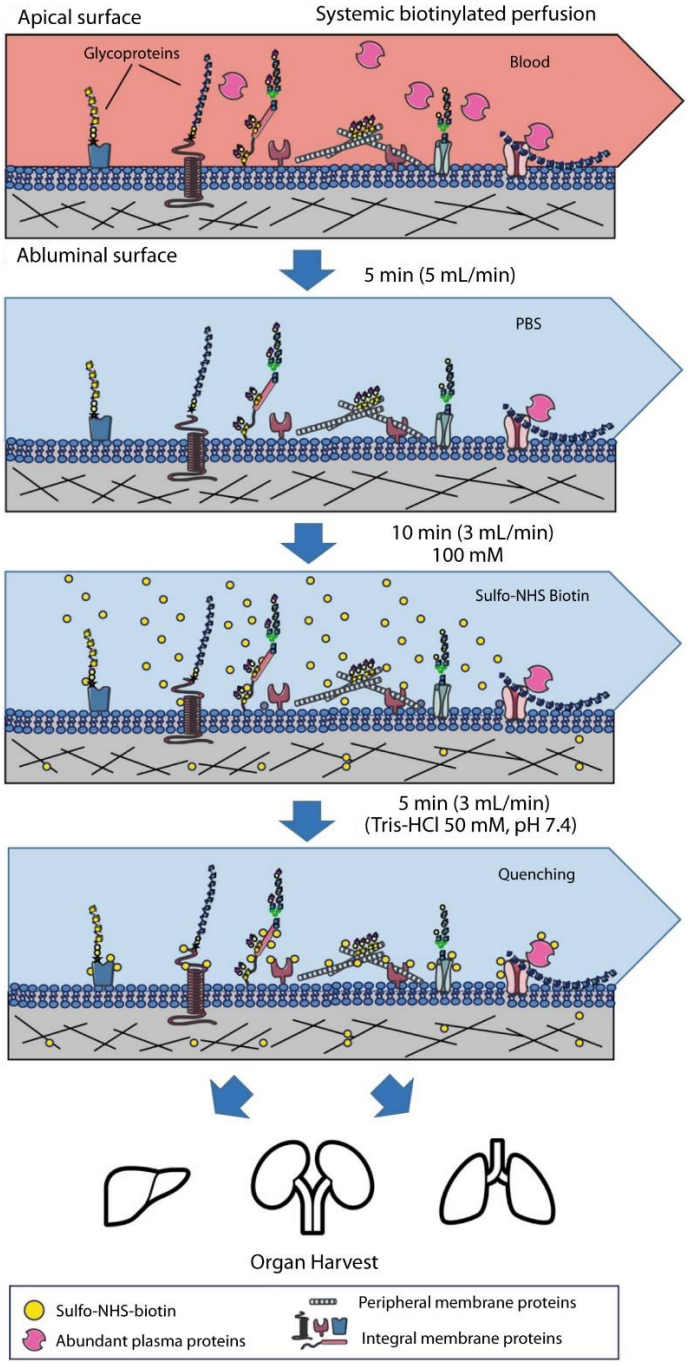

Figure 2.1 Workflow for *in vivo* biotinylation of vascular antigens. Animals were first perfused with saline (PBS) to remove blood, followed by biotinylation using an isotonic solution of sulfo-NHS-biotin. Unreacted NHS-groups were quenched by perfusion with a Tris-HCl buffer (pH 7.4). All buffers were kept ice-cold and the perfusion times were kept as short as possible to minimize potential tissue damage and disruption. After biotinylation, multiple organs were harvested and preserved for histological analysis, or immediately homogenized and subjected to proteomics analysis.

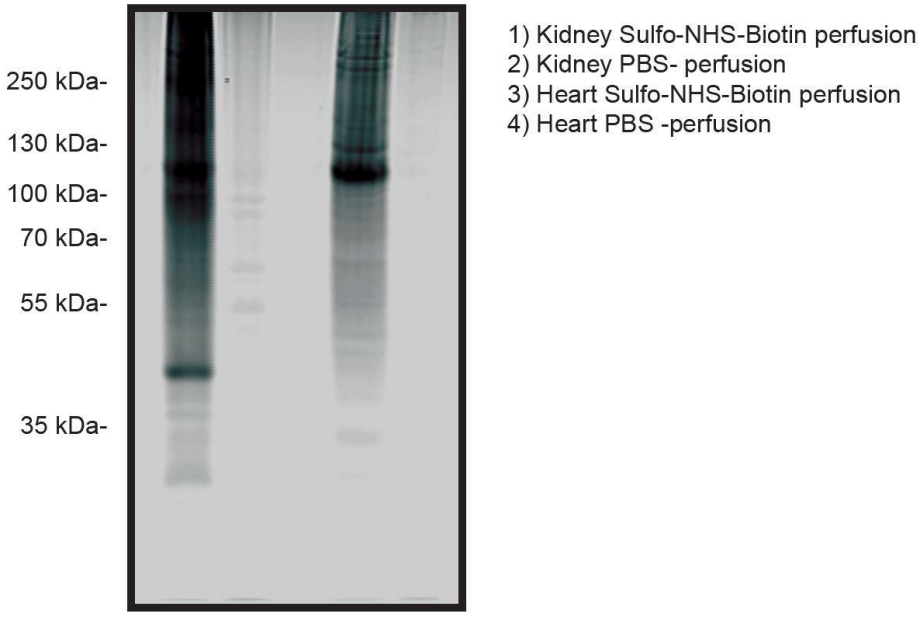

Figure 2.2 Western blotting analysis of organ lysates derived from systemically biotinylated mice. Kidney and heart tissues from animals subjected to perfusion with sulfo-NHS-biotin were homogenized and resolved by SDS-PAGE. Protein signals were detected by incubating with a streptavidin probe conjugated to an infrared dye. Strong streptavidin reactivity was detected in the biotinylated samples (lanes 1 and 3). Only faint signals were observed in control tissue derived from animals perfused with PBS (lanes 2 and 4).

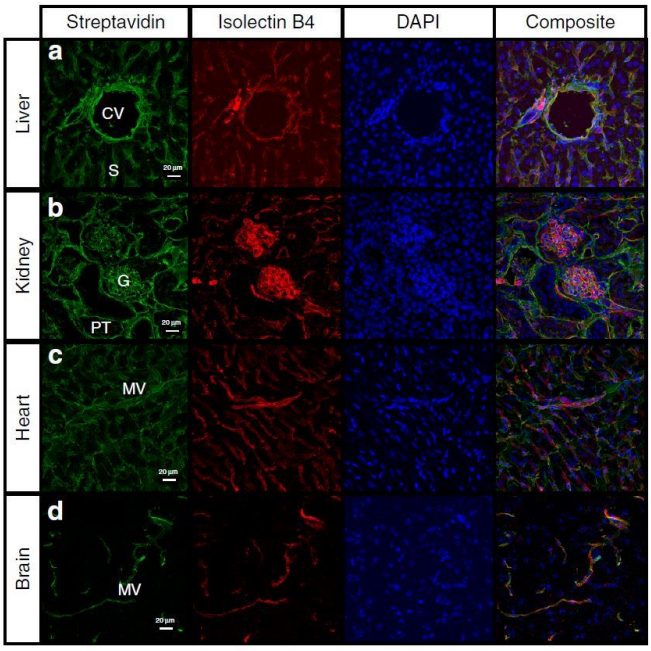

Figure 2.3 Protein biotinylation is primarily associated with vascular compartments. Murine tissues from animals perfused with sulfo-NHS-biotin were excised and subjected to cryosectioning, followed by histological analysis using fluorescently labeled streptavidin. Cryosections from liver (A), kidney (B), heart (C), and brain (D) were imaged using confocal microscopy. Most of the streptavidin reactivity was closely associated with vascular tissue structures such as the liver sinusoid or the kidney glomerular microvasculature. Tissue slides were also co-stained with IB4 to visualize the endothelial lumen. Partial co-localization between streptavidin and IB4 stains indicated incorporation of biotin into the endothelial glycocalyx but also in the nearby extracellular matrix and the vascular extracellular space. Histological analysis was conducted in biological triplicates, but only representative slides are shown. CV: hepatic central veins, S: sinusoids, G: glomeruli, PT: proximal tubules, MV: microvasculature. Scale bar, 20 μm.

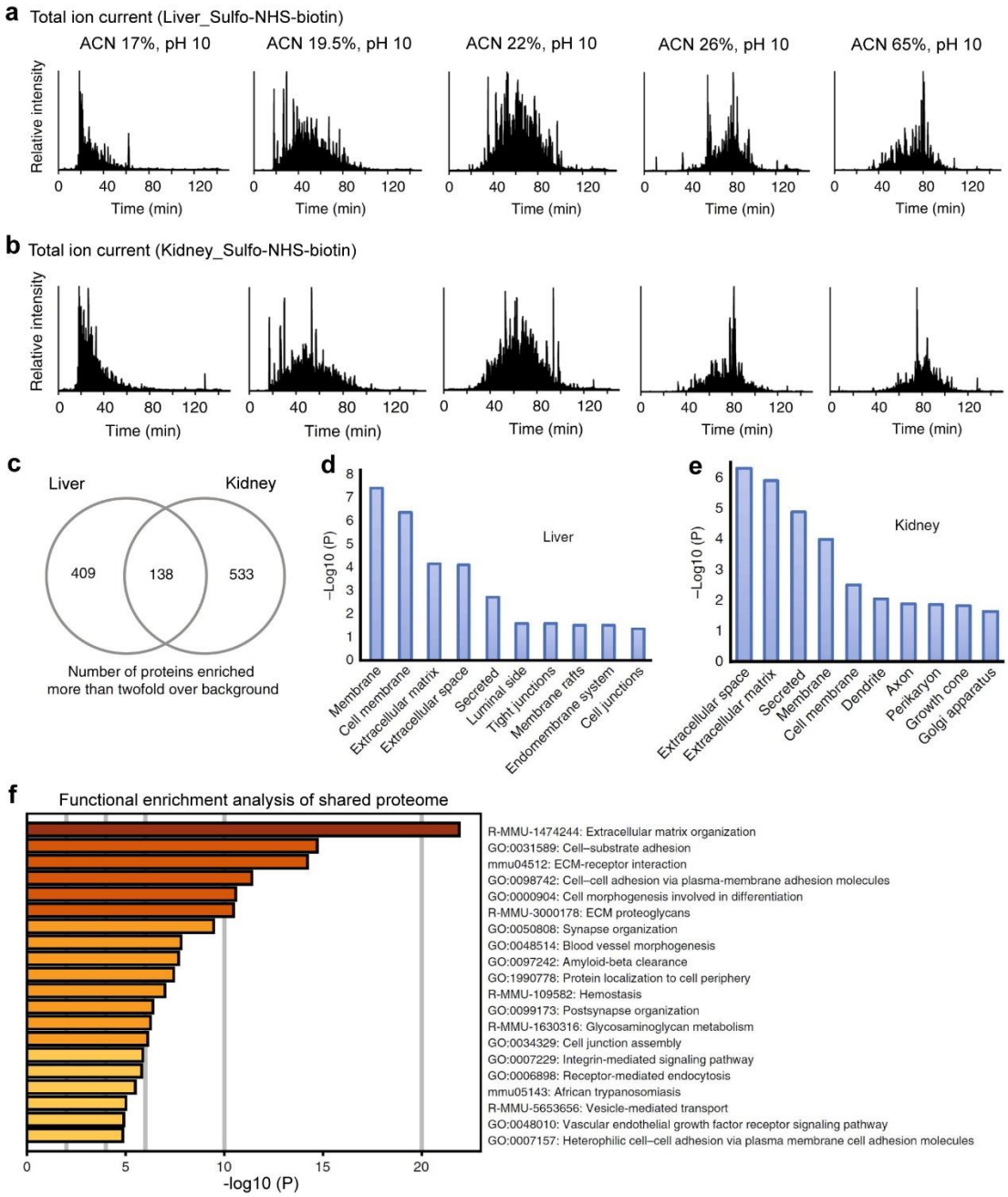

Figure 2.4 Online 2D-LC-MS/MS proteomics analysis of liver and kidney proteins. Biotinylated proteins from one liver and one kidney samples were enriched on streptavidin columns, trypsinized and subjected to an online 2D-LC-MS/MS workflow on a C18 column at high/low pH. Total ion chromatograms for 5 consecutive fractions from liver (A) and kidney (B) peptide digests are shown, indicating that proteins eluting from the C18 column at high pH and at increasing acetonitrile concentrations display different chromatographic behaviors when separated at low pH, consistent with an orthogonal fractionation strategy. Venn diagrams showing unique and shared protein components (C). Hypergeometric enrichment test for subcellular localization showed significant enrichment for proteins located in the cell membrane and extracellular matrix in both liver (D) and kidney (E). Functional enrichment analysis of shared proteome signatures is shown in (F).

Figure 2.5 Network analysis of systemically biotinylated proteins from liver and kidney tissues. Proteins identified through proteomics analysis were used to generate a protein-protein association network through the STRING database. Protein interactions were limited to high confidence physical or functional associations (association score > 0.7). The final network was subjected to Louvain clustering to identify highly interconnected communities. The identified clusters were further segregated via force-directed visualization algorithms and subjected to functional enrichment analysis using the web-based version of Metascape. Kidney proteins were clustered into 5 different communities (A-E) whereas liver samples were segregated into 4 different cluster (F-I). Some of these clusters were enriched in specific functions and organ specific biological pathways.

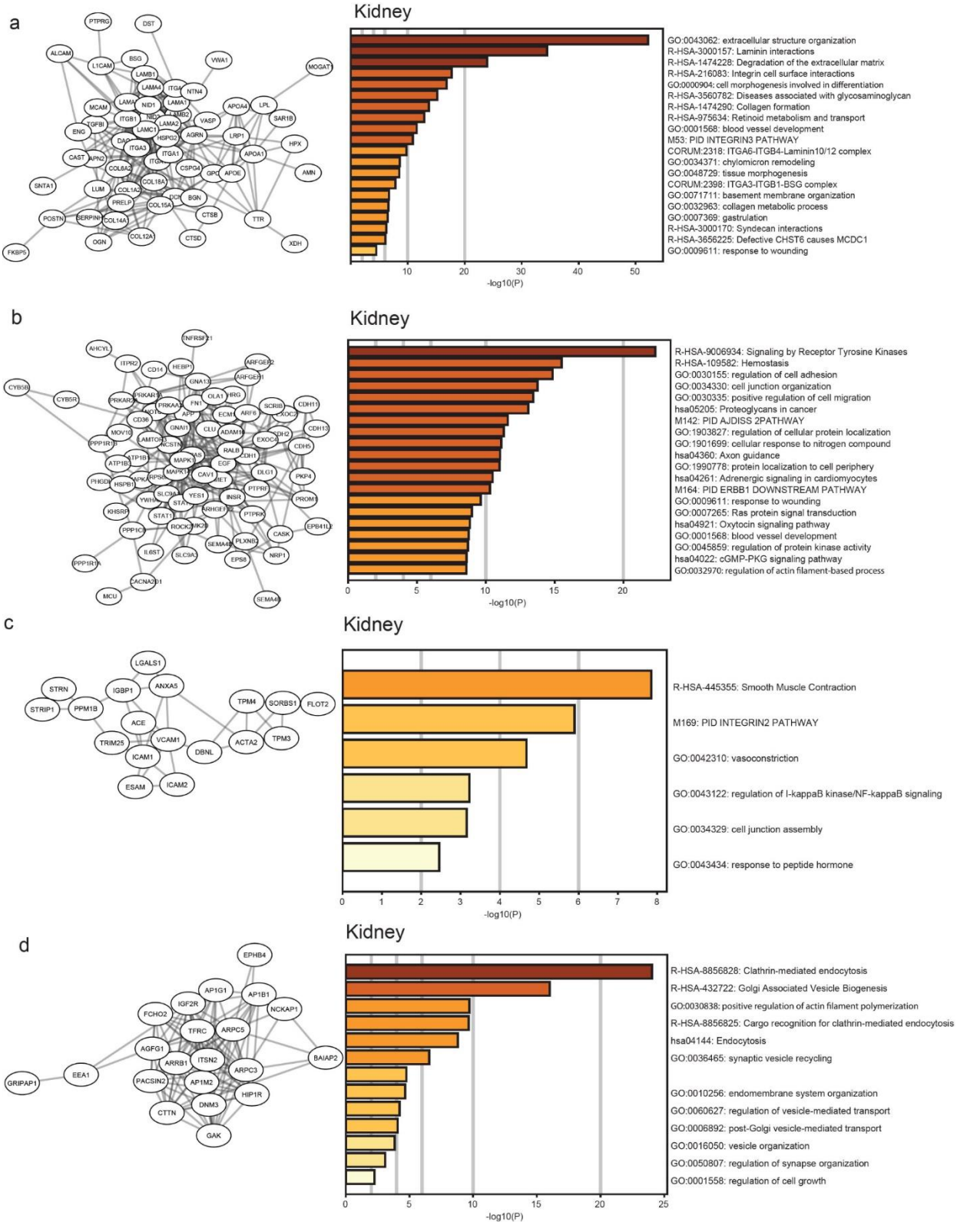
a
Kidney
GO:0043062: extracellular structure organization
R-HSA-3000157: Laminin interactions
R-HSA-1474228: Degradation of the extracellular matrix
R-HSA-216083: Integrin cell surface interactions
GO:0000904: cell morphogenesis involved in differentiation
R-HSA-3560782: Diseases associated with glycosaminoglycan
R-HSA-1474290: Collagen formation
R-HSA-975634: Retinoid metabolism and transport
GO:0001568: blood vessel development
M53: PID INTEGRIN3 PATHWAY
CORUM:2318: ITGA6-ITGB4-Laminin10/12 complex
GO:0034371: chylomicron remodeling
GO:0048729: tissue morphogenesis
CORUM:2398: ITGA3-ITGB1-BSG complex
GO:0071711: basement membrane organization
GO:0032963: collagen metabolic process
GO:0007369: gastrulation
R-HSA-3000170: Syndecan interactions
R-HSA-3656225: Defective CHST6 causes MCDC1
GO:0009611: response to wounding
-log10(P)
b
Kidney
R-HSA-9006934: Signaling by Receptor Tyrosine Kinases
R-HSA-109582: Hemostasis
GO:0030155: regulation of cell adhesion
GO:0034330: cell junction organization
GO:0030335: positive regulation of cell migration
hsa05205: Proteoglycans in cancer
M142: PID AJDISS 2PATHWAY
GO:1903827: regulation of cellular protein localization
GO:1901699: cellular response to nitrogen compound
hsa04360: Axon guidance
GO:1990778: protein localization to cell periphery
hsa04261: Adrenergic signaling in cardiomyocytes
M164: PID ERBB1 DOWNSTREAM PATHWAY
GO:0009611: response to wounding
GO:0007265: Ras protein signal transduction
hsa04921: Oxytocin signaling pathway
GO:0001568: blood vessel development
GO:0045859: regulation of protein kinase activity
hsa04022: cGMP-PKG signaling pathway
GO:0032970: regulation of actin filament-based process
-log10(P)
c
Kidney
R-HSA-445355: Smooth Muscle Contraction
M169: PID INTEGRIN2 PATHWAY
GO:0042310: vasoconstriction
GO:0043122: regulation of I-kappaB kinase/NF-kappaB signaling
GO:0034329: cell junction assembly
GO:0043434: response to peptide hormone
-log10(P)
d
Kidney
R-HSA-8856828: Clathrin-mediated endocytosis
R-HSA-432722: Golgi Associated Vesicle Biogenesis
GO:0030838: positive regulation of actin filament polymerization
R-HSA-8856825: Cargo recognition for clathrin-mediated endocytosis
hsa04144: Endocytosis
GO:0036465: synaptic vesicle recycling
GO:0010256: endomembrane system organization
GO:0060627: regulation of vesicle-mediated transport
GO:0006892: post-Golgi vesicle-mediated transport
GO:0016050: vesicle organization
GO:0050807: regulation of synapse organization
GO:0001558: regulation of cell growth
-log10(P)

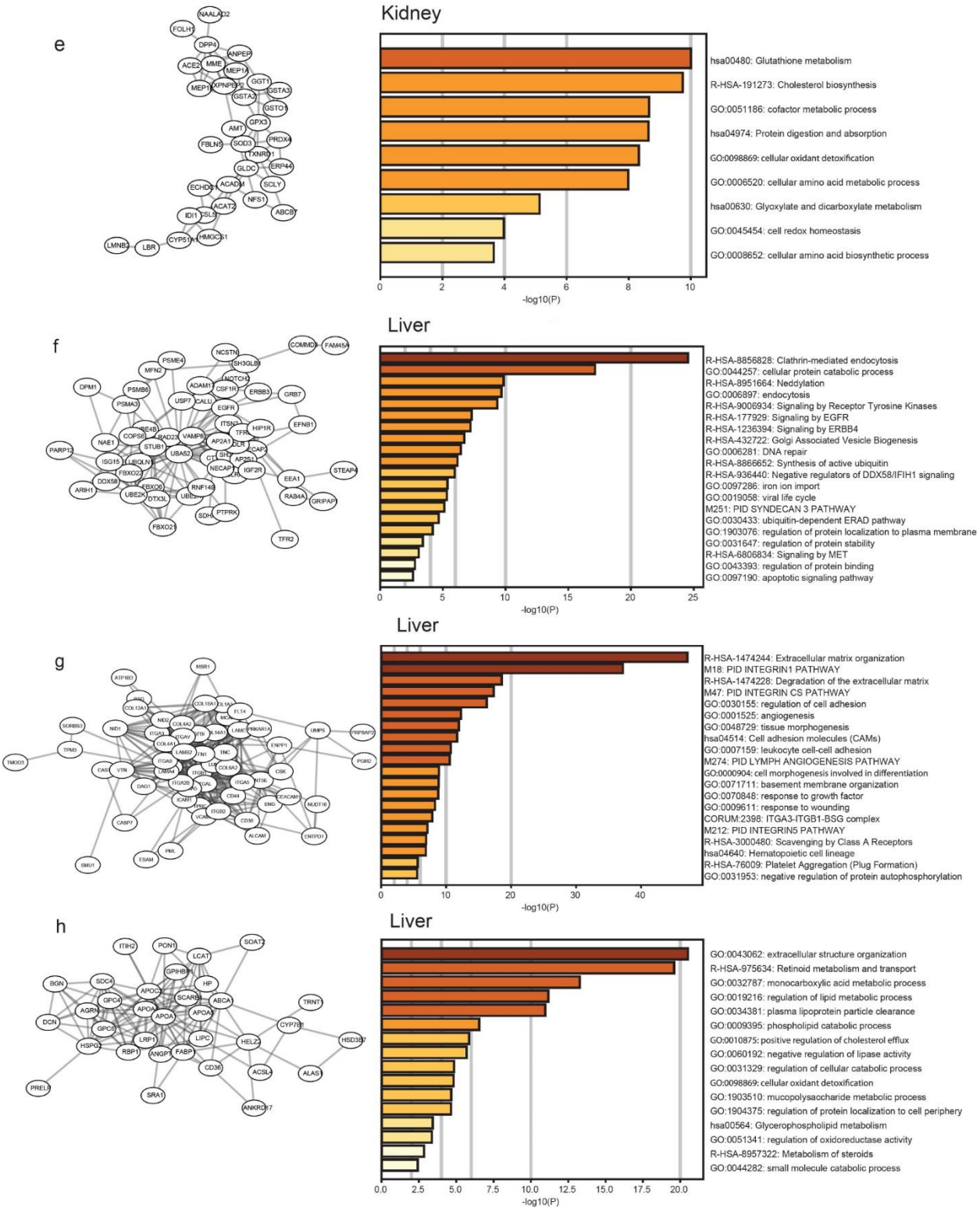

Figure 2.5 Network analysis of systemically biotinylated proteins from liver and kidney tissues (continued)

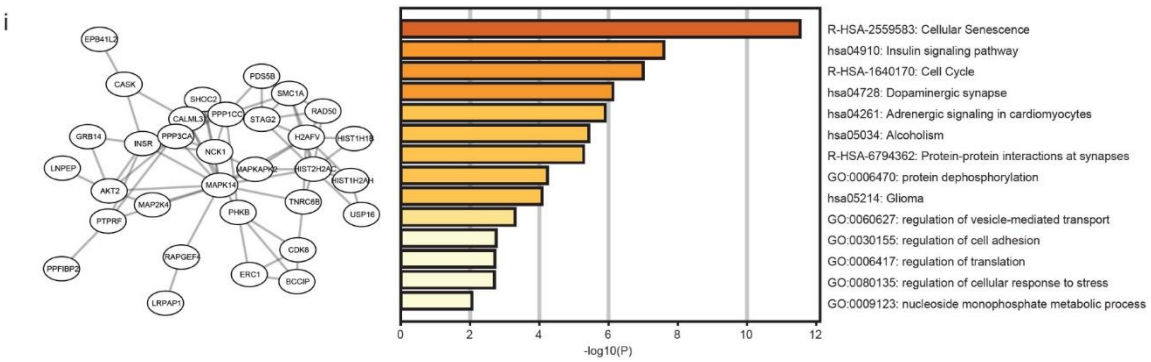

Figure 2.5 Network analysis of systemically biotinylated proteins from liver and kidney tissues (continued)

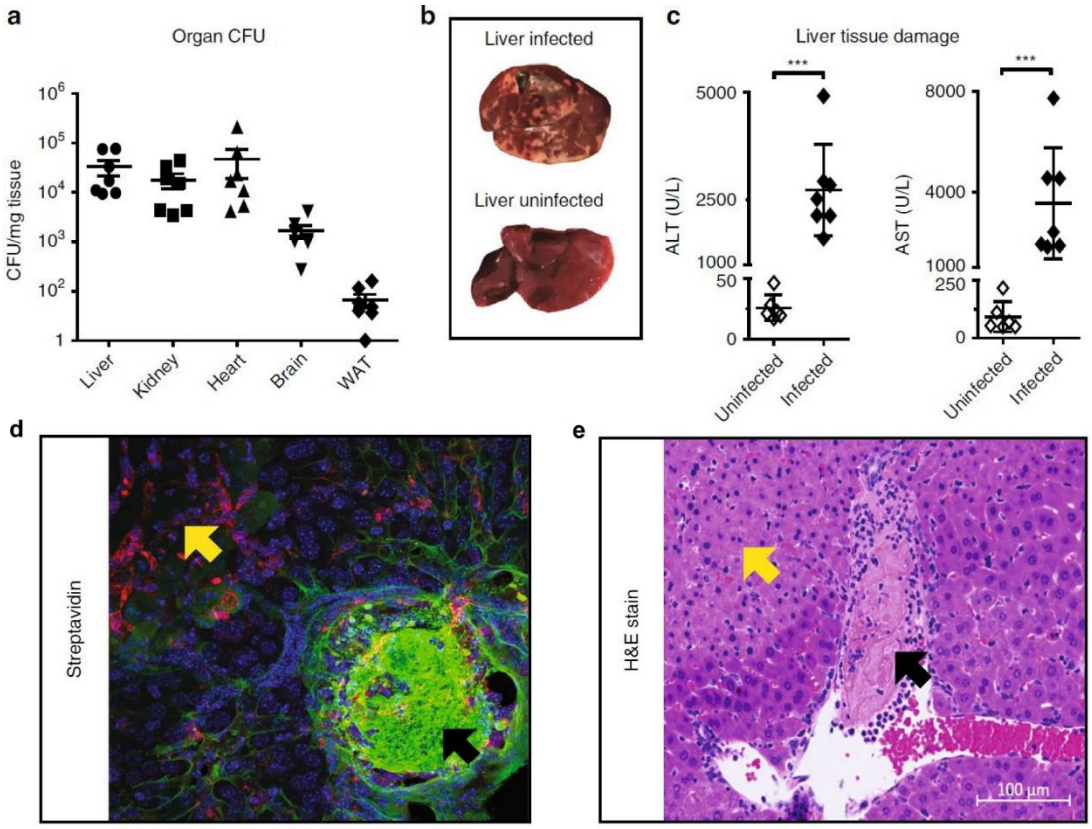

Figure 2.6 The murine model of MRSA-sepsis has a profound liver vasculopathic phenotype. Analysis of the pathogen burden expressed as colony-forming units (CFUs) at 24 h post-infection (A). A representative image of liver gross pathology in uninfected and infected mice at 24 h post-infection shows the presence of white areas corresponding to necrotic areas across the liver parenchyma (b). Quantification of soluble markers of liver damage alanine aminotransferase (ALT) and aspartate aminotransferase (AST) in serum collected 24 h post-infection (c). Hematoxylin and eosin staining of representative liver sections from infected animals showing signs of necrosis (yellow arrow) and thrombosis (black arrows), scale bar, 100 µm. d Representative liver section from mice challenged with MRSA, subjected to systemic biotinylation, and stained with streptavidin (green), IB4 (red) and DAPI (blue) (e). For a and c, data was pooled from two independent experiments with n = 3 and n = 4 mice per experiment, where mice were infected but not subjected to biotinylation perfusion. Data are represented as mean ± SD. ***$p < 0.001$ by two-sided Student's t-test.

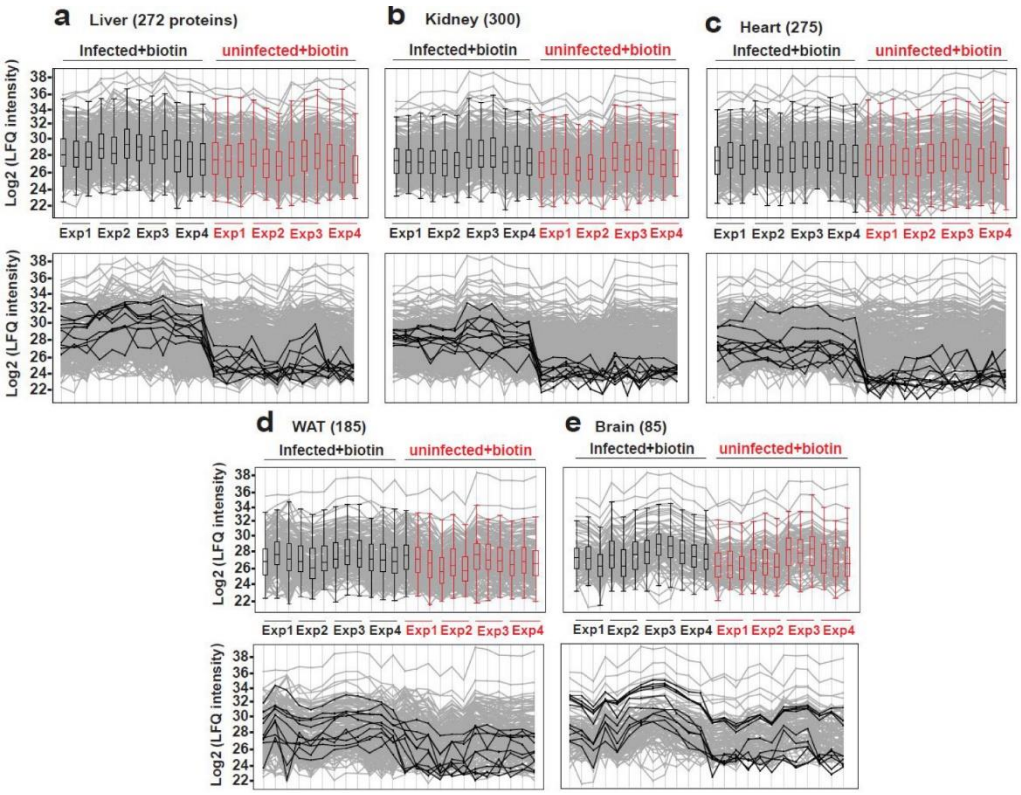

Figure 2.7 Profile plots of the label-free quantification (LFQ) normalized intensities of significant protein targets detected in the organ vasculatures. Combined proteomics datasets of MRSA infected (n=12) and uninfected (n=12) biological replicates of liver (A), kidney (B), heart (C), WAT (D) and brain (E) show that the proteome changes detected by the method encompassed a broad dynamic range. There was a notable intrassay (within the same group) and interassay (within experiments) variability in the LFQ-values (A-E, upper panels). However, plotting the top 10 differential proteins identified in each tissue makes evident that the changes during infection largely exceed the experimental error since the method is still capable of differentiating between infected and uninfected samples (A-E, lower panels).

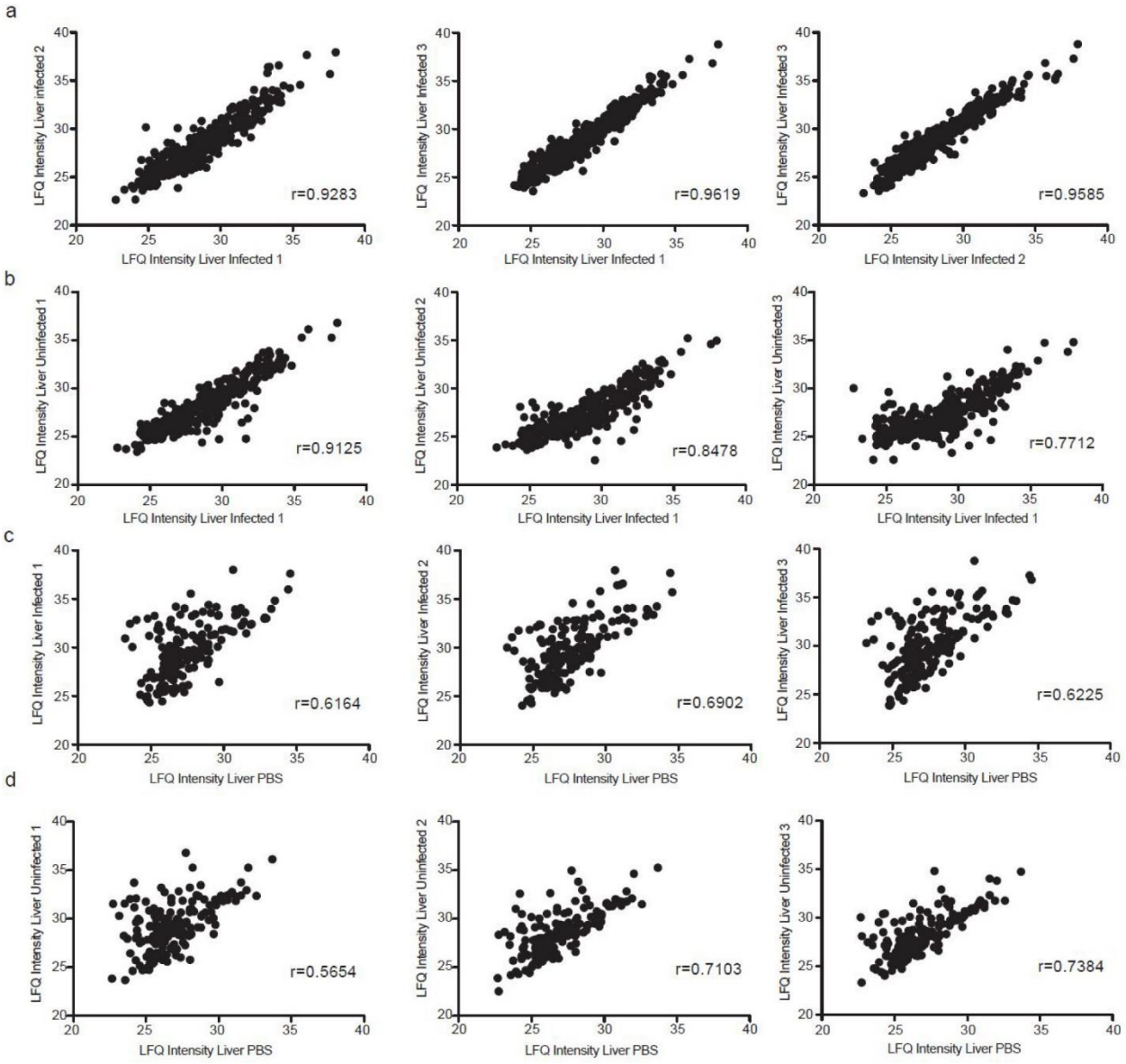

Figure 2.8. Multiple correlation plots of the label-free quantification intensities across liver samples analyzed in the same individual experiment. Pearson correlation coefficients were derived from the plots and compared across biological replicates of infected, uninfected and PBS-control liver tissues. Infected replicates (A) showed high Pearson correlation coefficients, whereas correlations were decreases when comparing infected vs uninfected (B). Even lower correlations were observed when comparing labeled samples with the PBS controls independently of their infection status (C-D).

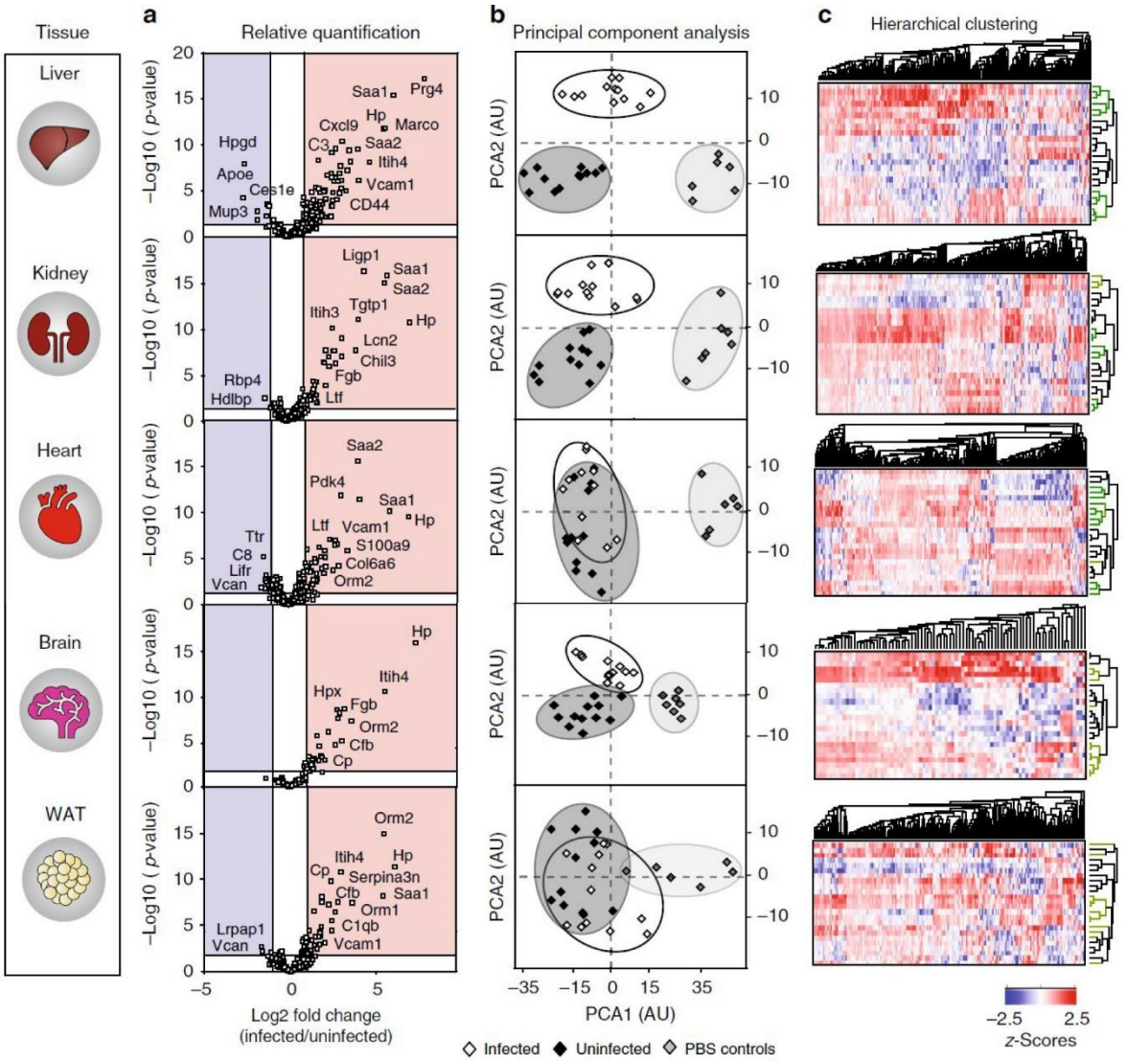

Figure 2.9 Changes in the vascular cell surface proteome in a murine model of MRSA-sepsis. Biotinylation perfusions were coupled to an automated shotgun proteomics workflow to identify organ-specific vascular targets changing in a murine model of MRSA-sepsis. We performed 4 separate experiments, which resulted in the simultaneous proteomics profiling of infected (n =12) and uninfected (n =12) mice across 5 major organs (liver, kidney, heart, brain, and WAT). (A) Differential expression analysis of proteins significantly changing during infection showed that the examined organs displayed a clear hierarchy in terms of the type and amounts of vascular proteome that was altered during sepsis, with liver samples being among the most severely affected. (B) Principal component analysis (PCA) of the identified proteins segregated the liver, kidney, and brain tissues into infected and uninfected groups, but was less specific for WAT and heart stratification. (C) Unsupervised hierarchical clustering of the data revealed dramatic proteome changes at 24 h post-infection with large protein clusters being differentially regulated across all examined organs.

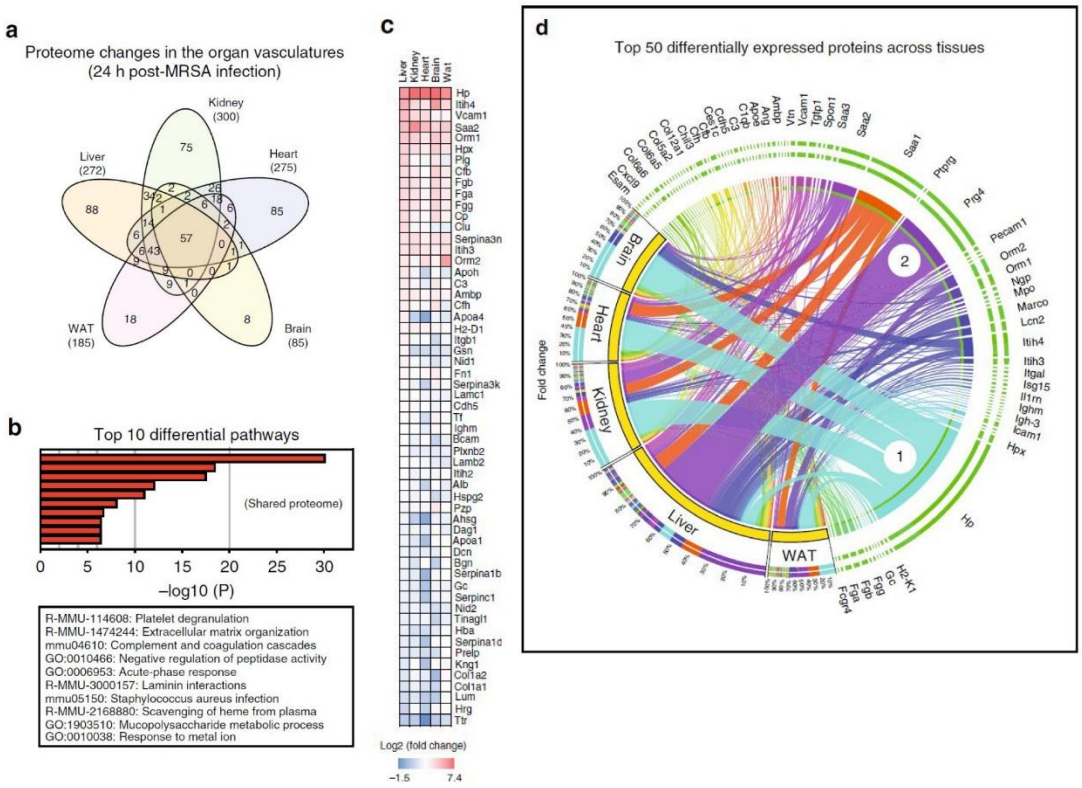

Figure 2.10 Remodeling of the vascular surfaces during MRSA-sepsis. (A) Venn diagrams of significant proteins hits across the organs (infected n =12, uninfected n= 12) revealed that a total of 57 proteins were shared among all examined tissues, whereas other targets were changing in a tissue-specific fashion. (B) Functional enrichment analysis using the Metascape tool indicate that biological processes related to coagulation, acute phase responses and ion hemostasis are highly enriched in the shared proteome across all organs. (C) Heat map of the organ average fold-change values for all proteins in the shared category. (D) Circos plot depicting the normalized fold-changes of the top 50 differential proteins across five organs. Each protein value is expressed as a ribbon with a unique color, the width of which corresponds to the normalized fold-change of that protein as a percentage of the summed fold-changes of all identified proteins in each tissue. Haptoglobin (Hp) is marked with an encircled number 1 to illustrate proteins displaying large induction in all tissues, whereas proteoglycan 4 (Prg4) is marked with an encircled number 2 to highlight proteins displaying very large fold-changes in a tissue-specific fashion.

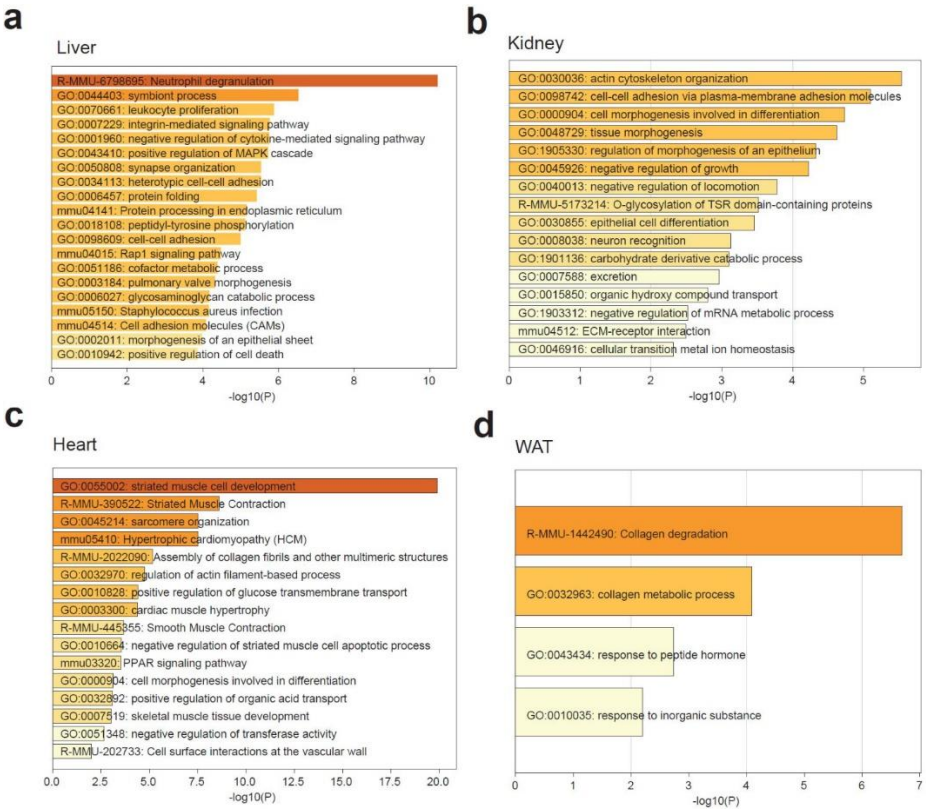

Figure 2.11 Proteomics and functional enrichment analysis of the vascular cell surface proteome identified multiple shared and organ-restricted biological pathways dysregulated during sepsis. All significantly changing proteins across liver (A), kidney (B), heart (C), brain (D) and white adipose tissue (WAT) (E) were analyzed by Metascape resulting in enrichment in particular biological pathways.

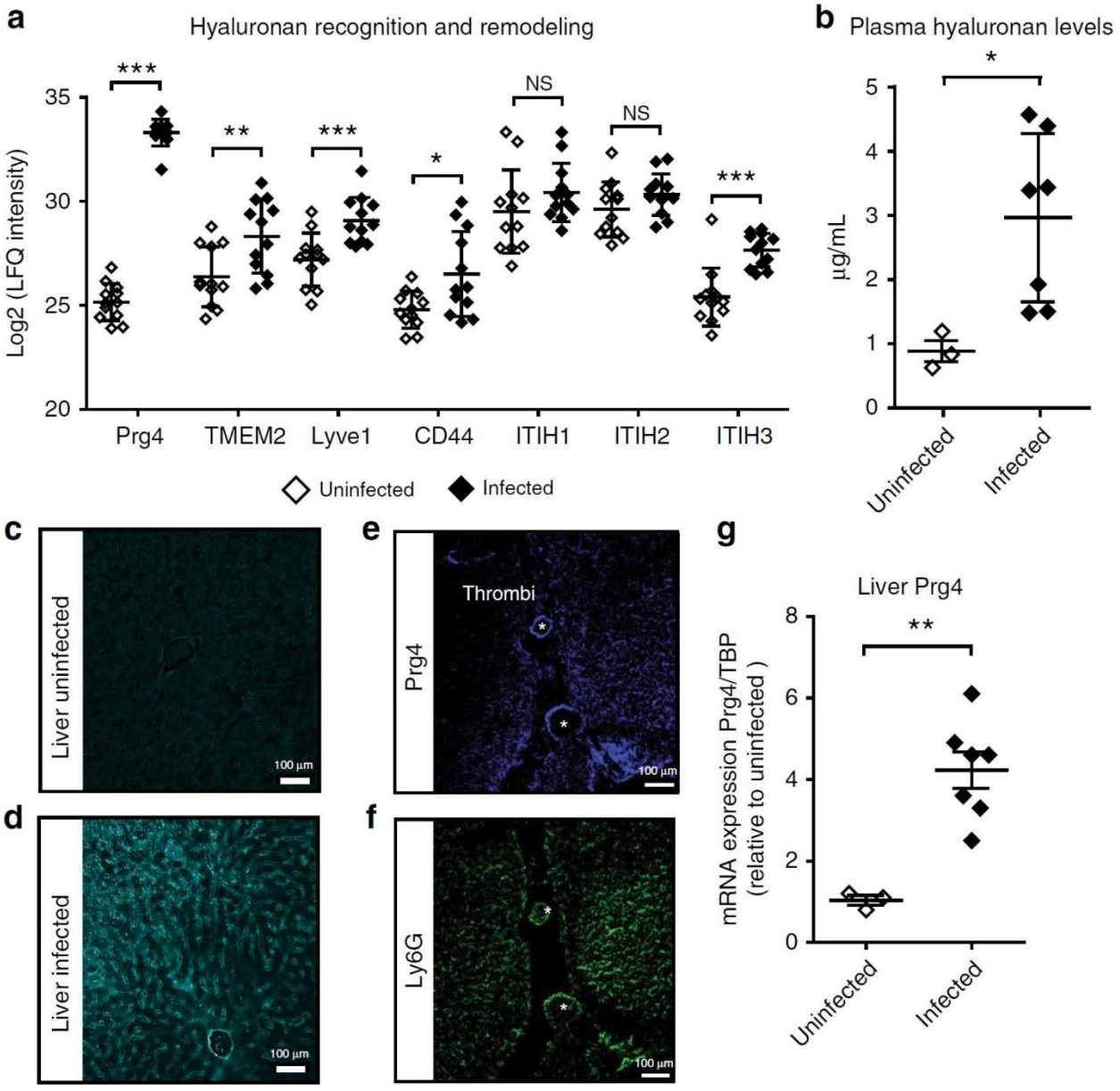

Figure 2.12 Changes in hyaluronan and hepatic hyaluronan-binding proteins. (A) Relative label-free quantification (LFQ) analysis of proteomic changes in the hepatic vasculature during sepsis reveals differential abundance of multiple targets involved in hyaluronic acid recognition and turnover. (B) The levels of circulating hyaluronic acid in plasma at 24 h post-infection were also significantly increased in a separate cohort of MRSA-infected animals (n=7) compared with controls (n = 3). (C,D) MRSA infection increases expression and deposition of Prg4 along the central veins and the sinusoidal microvasculature. (E,F) Prg4-immunoreactivity was also found at the edges of large necrotic thrombi in association with Ly6G+ neutrophils. (G) qPCR analysis in a separate cohort of mice (infected livers n=7, uninfected controls n=3) demonstrated increased expression of hepatic Prg4-mRNA levels already at 12 h post-infection. Data are represented as mean ± SD. ***$p<0.001$, **$p<0.01$ and *$p<0.05$ by two-sided Student's t-test. Scale bar, 100µm

2.8 References

1. Aird, W. C. Phenotypic heterogeneity of the endothelium: I. Structure, function, and mechanisms. *Circ. Res.* **100,** 158–173 (2007).

2. Aird, W. C. Phenotypic heterogeneity of the endothelium: II. Representative vascular beds. *Circ. Res.* **100,** 174–190 (2007).

3. Reitsma, S., Slaaf, D. W., Vink, H., Van Zandvoort, M. A. M. J. & Oude Egbrink, M. G. A. The endothelial glycocalyx: Composition, functions, and visualization. *Pflugers Arch. Eur. J. Physiol.* **454,** 345–359 (2007).

4. Zhang, X., Sun, D., Song, J. W., Zullo, J., Lipphardt, M., Coneh-Gould, L. & Goligorsky, M. S. Endothelial cell dysfunction and glycocalyx – A vicious circle. *Matrix Biol.* **71–72,** 421–431 (2018).

5. Uchimido, R., Schmidt, E. P. & Shapiro, N. I. The glycocalyx: a novel diagnostic and therapeutic target in sepsis. *Crit. Care* **23,** 1–12 (2019).

6. Iba, T. & Levy, J. H. Derangement of the endothelial glycocalyx in sepsis. *J. Thromb. Haemost.* **17,** 283–294 (2019).

7. Yang, Y., Haeger, S. M., Suflita, M. A., Zhang, F., Dailey, K. L., Colbert, J. F., Ford, J. A., Picon, M. A., Stearman, R. S., Lin, L., Liu, X., Han, X., Linhardt, R. J. & Schmidt, E. P. Fibroblast growth factor signaling mediates pulmonary endothelial glycocalyx reconstitution. *Am. J. Respir. Cell Mol. Biol.* **56,** 727–737 (2017).

8. Marki, A., Esko, J. D., Pries, A. R. & Ley, K. Role of the endothelial surface layer in neutrophil recruitment. *J. Leukoc. Biol.* **98,** 503–515 (2015).

9. Finigan, J. H. The coagulation system and pulmonary endothelial function in acute lung injury. *Microvasc. Res.* **77,** 35–38 (2009).

10. Wang, L., Fuster, M., Sriramarao, P. & Esko, J. D. Endothelial heparan sulfate deficiency impairs L-selectin- and chemokine-mediated neutrophil trafficking during inflammatory responses. *Nat. Immunol.* **6,** 902–10 (2005).

11. Fischetti, F. & Tedesco, F. Cross-talk between the complement system and endothelial cells in physiologic conditions and in vascular diseases. *Autoimmunity* **39,** 417–428 (2006).

12. Balk, R. A. Pathogenesis and Management of Multiple Organ Dysfunction or Failure in Severe Sepsis and Septic Shock. *Crit. Care Clin.* **16,** 337–352 (2000).

13. Rossaint, J. & Zarbock, A. Pathogenesis of multiple organ failure in sepsis. *Crit. Rev. Immunol.* **35,** 277–291 (2015).

14. Singer, M., Deutschman, C. S., Seymour, C. W., Shankar-Hari, M., Annane, D., Bauer,

M., Bellomo, R., Bernard, G. R., Chiche, J.-D., Coopersmith, C. M., Hotchkiss, R. S., Levy, M. M., Marshall, J. C., Martin, G. S., Opal, S. M., Rubenfeld, G. D., van der Poll, T., Vincent, J. & Angus, D. C. The Third International Consensus Definitions for Sepsis and Septic Shock (Sepsis-3). *JAMA* **315,** 801–10 (2016).

15. Inagawa, R., Okada, H., Takemura, G., Suzuki, K., Takada, C., Yano, H., Ando, Y., Usui, T., Hotta, Y., Miyazaki, N., Tsujimoto, A., Zaikokuji, R., Matsumoto, A., Kawaguchi, T., Doi, T., Yoshida, T., Yoshida, S., Kumada, K., Ushikoshi, H., Toyoda, I. & Ogura, S. Ultrastructural Alteration of Pulmonary Capillary Endothelial Glycocalyx During Endotoxemia. *Chest* **154,** 317–325 (2018).

16. Okada, H., Takemura, G., Suzuki, K., Oda, K., Takada, C., Hotta, Y., Miyazaki, N., Tsujimoto, A., Muraki, I., Ando, Y., Zaikokuji, R., Matsumoto, A., Kitagaki, H., Tamaoki, Y., Usui, T., Doi, T., Yoshida, T., Yoshida, S., Ushikoshi, H., Toyoda, I. & Ogura, S. Three-dimensional ultrastructure of capillary endothelial glycocalyx under normal and experimental endotoxemic conditions. *Crit. Care* **21,** 1–10 (2017).

17. Wiesinger, A., Peters, W., Chappell, D., Kentrup, D., Reuter, S., Pavenstädt, H., Oberleithner, H. & Kümpers, P. Nanomechanics of the endothelial glycocalyx in experimental sepsis. *PLoS One* **8,** 1–14 (2013).

18. Slany, A., Bileck, A., Kreutz, D., Mayer, R. L., Muqaku, B. & Gerner, C. Contribution of human fibroblasts and endothelial cells to the hallmarks of inflammation as determined by proteome profiling. *Mol. Cell. Proteomics* **15,** 1982–1997 (2016).

19. Mohr, T., Haudek-Prinz, V., Slany, A., Grillari, J., Micksche, M. & Gerner, C. Proteome profiling in IL-1β and VEGF-activated human umbilical vein endothelial cells delineates the interlink between inflammation and angiogenesis. *PLoS One* **12,** 1–23 (2017).

20. Durr, E., Yu, J., Krasinska, K. M., Carver, L. A., Yates, J. R., Testa, J. E., Oh, P. & Schnitzer, J. E. Direct proteomic mapping of the lung microvascular endothelial cell surface in vivo and in cell culture. *Nat. Biotechnol.* **22,** 985–992 (2004).

21. Ryback, J. N., Ettorre, A., Kaissling, B., Giavazzi, R., Neri, D. & Elia, G. In vivo protein biotinylation for identification of organ-specific antigens accessible from the vasculature. *Nat. Methods* **2,** 291–298 (2005).

22. Castronovo, V., Waltregny, D., Kischel, P., Roesli, C., Elia, G., Rybak, J. N. & Neri, D. A chemical proteomics approach for the identification of accessible antigens expressed in human kidney cancer. *Mol. Cell. Proteomics* **5,** 2083–2091 (2006).

23. Kischel, P., Waltregny, D. & Castronovo, V. Identification of accessible human cancer biomarkers using ex vivo chemical proteomic strategies. *Expert Rev. Proteomics* **4,** 727–739 (2007).

24. Schliemann, C., Roesli, C., Kamada, H., Borgia, B., Fugmann, T., Klapper, W. & Neri, D. In vivo biotinylation of the vasculature in B-cell lymphoma identifies BST-2 as a target for antibody-based therapy. *Blood* **115,** 736–744 (2010).

25. Borgia, B., Roesli, C., Fugmann, T., Schliemann, C., Cesca, M., Neri, D. & Giavazzi, R. A proteomic approach for the identification of vascular markers of liver metastasis. *Cancer Res.* **70,** 309–318 (2010).

26. Hultén, K. G., Kaplan, S. L., Gonzalez, B. E., Hammerman, W. A., Lamberth, L. B., Versalovic, J. & Mason, E. O. Three-year surveillance of community onset health care-associated Staphylococcus aureus infections in children. *Pediatr. Infect. Dis. J.* **25,** 349–353 (2006).

27. Tyanova, S., Temu, T. & Cox, J. The MaxQuant computational platform for mass spectrometry-based shotgun proteomics. *Nat. Protoc.* **11,** 2301–2319 (2016).

28. Cox, J., Neuhauser, N., Michalski, A., Scheltema, R. A., Olsen, J. V. & Mann, M. Andromeda: A peptide search engine integrated into the MaxQuant environment. *J. Proteome Res.* **10,** 1794–1805 (2011).

29. Tyanova, S., Temu, T., Sinitcyn, P., Carlson, A., Hein, M. Y., Geiger, T., Mann, M. & Cox, J. The Perseus computational platform for comprehensive analysis of (prote)omics data. *Nat. Methods* **13,** 731–740 (2016).

30. Blondel, V. D., Guillaume, J. L., Lambiotte, R. & Lefebvre, E. Fast unfolding of communities in large networks. *J. Stat. Mech. Theory Exp.* **2008,** 0–12 (2008).

31. Kim, H. K., Missiakas, D. & Schneewind, O. Mouse models for infectious diseases caused by Staphylococcus aureus. *J. Immunol. Methods* **410,** 88–99 (2014).

32. Pimienta, G., Heithoff, D. M., Rosa-campos, A., Tran, M., Esko, J. D., Mahan, M. J., Marth, J. D. & Smith, J. W. Plasma Proteome Signature of Sepsis: a functionally connected protein network. *Proteomics* **19,** (2019).

33. Kolaczkowska, E., Jenne, C. N., Surewaard, B. G. J., Thanabalasuriar, A., Lee, W. Y., Sanz, M. J., Mowen, K., Opdenakker, G. & Kubes, P. Molecular mechanisms of NET formation and degradation revealed by intravital imaging in the liver vasculature. *Nat. Commun.* **6,** 1–13 (2015).

34. Klinke, A., Nussbaum, C., Kubala, L., Friedrichs, K., Rudolph, T. K., Rudolph, V., Paust, H. J., Schröder, C., Benten, D., Lau, D., Szocs, K., Furtmüller, P. G., Heeringa, P., Sydow, K., Duchstein, H. J., Ehmke, H., Schumacher, U., Meinertz, T., Sperandio, M. & Baldus, S. Myeloperoxidase attracts neutrophils by physical forces. *Blood* **117,** 1350–1358 (2011).

35. Metzler, K. D., Fuchs, T. A., Nauseef, W. M., Reumaux, D., Roesler, J., Schulze, I., Wahn, V., Papayannopoulos, V. & Zychlinsky, A. Myeloperoxidase is required for neutrophil extracellular trap formation: Implications for innate immunity. *Blood* **117,** 953–959 (2011).

36. Mcdonald, B., Mcavoy, E. F., Lam, F., Gill, V., Motte, C. De, Savani, R. C. & Kubes, P. Interaction of CD44 and hyaluronan is the dominant mechanism for neutrophil sequestration in inflamed liver sinusoids. *J. Exp. Med.* **205,** 915–927 (2008).

37. Al-Sharif, A., Jamal, M., Zhang, L. X., Larson, K., Schmidt, T. A., Jay, G. D. & Elsaid, K. A. Lubricin/proteoglycan 4 binding to CD44 receptor: A mechanism of the suppression of proinflammatory cytokine-induced synoviocyte proliferation by lubricin. *Arthritis Rheumatol.* **67,** 1503–1513 (2015).

38. Zhuo, L. & Kimata, K. Structure and function of inter-α-trypsin inhibitor heavy chains. *Connect. Tissue Res.* **49,** 311–320 (2008).

39. Yagmur, E., Koch, A., Haumann, M., Kramann, R., Trautwein, C. & Tacke, F. Hyaluronan serum concentrations are elevated in critically ill patients and associated with disease severity. *Clin. Biochem.* **45,** 82–87 (2012).

40. Jensen, J. U. S., Peters, L., Itenov, T. S., Bestle, M., Thormar, K. M., Mohr, T. T., Lundgren, B., Grarup, J. & Lundgren, J. D. Biomarker-assisted identification of sepsis-related acute liver impairment: A frequent and deadly condition in critically ill patients. *Clin. Chem. Lab. Med.* **57,** 1422–1431 (2019).

41. Augustin, H. G. & Koh, G. Y. Organotypic vasculature: From descriptive heterogeneity to functional pathophysiology. *Science (80-.).* **357,** (2017).

42. Rajotte, D., Arap, W., Hagedorn, M., Koivunen, E., Pasqualini, R. & Ruoslahti, E. Molecular heterogeneity of the vascular endothelium revealed by in vivo phage display. *J. Clin. Invest.* **102,** 430–437 (1998).

43. Arap, W., Kolonin, M. G., Trepel, M., Lahdenranta, J., Cardó-Vila, M., Giordano, R. J., … Pasqualini, R. Steps toward mapping the human vasculature by phage display. *Nat. Med.* **8,** 121–127 (2002).

44. Vanlandewijck, M., He, L., Mäe, M. A., Andrae, J., Ando, K., Del Gaudio, F., Nahar, K., Lebouvier, T., Laviña, B., Gouveia, L., Sun, Y., Raschperger, E., Räsänen, M., Zarb, Y., Mochizuki, N., Keller, A., Lendahl, U. & Betsholtz, C. A molecular atlas of cell types and zonation in the brain vasculature. *Nature* **554,** 475–480 (2018).

45. Mithal, L. B., Palac, H. L., Yogev, R., Ernst, L. M. & Mestan, K. K. Cord blood acute phase reactants predict early onset neonatal sepsis in preterm infants. *PLoS One* **12,** 1–16 (2017).

46. Ruan, M. Z. C., Erez, A., Guse, K., Dawson, B., Bertin, T., Chen, Y., Jiang, M. M., Yustein, J., Gannon, F. & Lee, B. H. L. Proteoglycan 4 expression protects against the development of osteoarthritis. *Sci. Transl. Med.* **5,** (2013).

47. S.M. Iqbal, C. Leonard, S. C. Regmi, D. De Rantere, P. Tailor, G. Ren, H. Ishida, CY. Hsu, S. Abubacker, D. SJ. Pang, P. T. Salo, H.J. Vogel, D.A. Hart, C.C. Waterhouse, G.D Jay, T.A. Schmidt, R. J. K. Lubricin/Proteoglycan 4 binds to and regulates the activity of Toll-Like Receptors In Vitro. *Sci. Rep.* **6,** (2015).

48. Malmström, E., Kilsgård, O., Hauri, S., Smeds, E., Herwald, H., Malmström, L. & Malmström, J. Large-scale inference of protein tissue origin in gram-positive sepsis

plasma using quantitative targeted proteomics. *Nat. Commun.* **7,** (2016).

49. Wu, L. & Han, D. K. Overcoming the dynamic range problem in mass spectrometry-based shotgun proteomics. *Expert Rev. Proteomics* **3,** 611–619 (2006).

Chapter 3: Sepsis and infection in mice altered in endothelial heparan sulfate

3.1 Introduction

Heparan sulfate (HS) is ubiquitously expressed by all animal cells and impacts native immune responses [1]. HS is a polyanionic linear polysaccharide composed of repeating disaccharide subunits generated from glucuronic acid, GlcA, and *N*-acetylglucosamine, GlcNAc [2]. HS chains assemble while covalently attached to core proteins to form heparan sulfate proteoglycans (HSPGs). HSPGs include syndecan 1-4, which are anchored to cells via their transmembrane core protein, and glypican 1-6, which have their core protein covalently linked to a glycosylphosphatidylinositol anchor. Cell surface syndecans and glypicans have HS bound only to the extracellular domain of the core protein [2]. There is considerable heterogeneity in the structure of HS. The initial modification reaction, *N*-deacetylation and *N*-sulfation of GlcNAc, is catalyzed by *N*-deacetylase-*N*-sulfotransferase 1 (*Ndst1*)[3]. Subsequent HS sulfation relies on *Ndst1* activity, and *Ndst1* deletion results in reduced overall HS sulfation [4]. As the HS chain polymerizes, O-sulfation of carbon 6 (C6) and C3 of glucosamine units and C2 on uronic acids occurs [5]. Addition of sulfate groups to HS occurs in short interspersed segments with intervening long tracts of unmodified sugars [2]. Very distinct modifications in HS, defined by arrangements of IdoA and sulfate groups, and non-specific arrangements of sulfate groups govern protein-HS interactions [6].

HSPGs expressed on the cell surface are involved in inflammation [1], and may be involved in sepsis pathophysiology (Table 1). HS binds to a large cohort of chemokines and cytokines [7], which increase dramatically during inflammation and sepsis [8]. Endothelial HS is important for chemokine presentation and transport, as well as neutrophil extravasation [4,9] and lymphocyte homing to peripheral lymph nodes [10]. Directional crawling of neutrophils on venular endothelium is mediated by chemokine gradients bound to HS [11]. Inflammation upregulates HSPG expression in monocytes and macrophages [12]. Other studies show that HS and HSPGs influence bacterial

infection. Group B Streptococcus (GBS) uses HS to invade the blood brain barrier and cause meningitis [13]. Neutrophils derived from mice lacking in 2-O sulfation are deficient in neutrophil extracellular trap formation, rendering the mice more susceptible to GBS sepsis [14]. Syndecan-1 knockout mice (*Sdc1*$^{-/-}$) mice have increased resistance to *Pseudomonas aeruginosa* [15] and *Staphylococcus aureus* lung infection [16]. *Sdc1*$^{-/-}$ mice are also protected from *S. aureus* corneal infection [17]. It was recently found that 2-*O*-sulfated HS moieties bind CRAMP, the murine cathelicidin antimicrobial peptide (and homologue of human LL-37), during *S. aureus* infection of the corneal epithelium, inhibiting neutrophil killing of bacteria [18]. Additionally, *Sdc1*$^{-/-}$ mice with a *P. aeruginosa*-infected burn wound have decreased mortality, bacterial systemic spread, and pro-inflammatory cytokine levels [19].

The role of HSPGs in the immune response becomes even more complex as they undergo shedding from the endothelial cell surface. Shedding occurs through proteolysis of the HSPG ectodomain proximal to the plasma membrane via matrix metalloproteases [20] and cleavage of the chains can occur by extracellular heparanase, an endogenous heparan sulfate-specific β-glucuronidase [21]. Upon shedding, HS and HSPGs, along with bound proteins, enter the surrounding environment and/or bloodstream where they mediate several processes. Additionally, shed HSPGs can act as a sink to "soak up" excess cytokines in circulation. Changes in HSPG and HS shedding are observed in sepsis (Table 1). *S. aureus* α- and β- toxins activate Sdc1 shedding in cultured cells [22,23]. SEB, another toxin of *S. aureus*, also induces Sdc1 shedding and high mortality in mice. Further, heparanase-deficient (*Hpse*$^{-/-}$) mice are protected from sepsis [21].

However, HSPGs do not always exacerbate infection and sepsis. *Sdc1*$^{-/-}$ mice have increased mortality and organ damage in lipopolysaccharide (LPS) [24] and staphylococcal enterotoxin B (SEB) [25] induced sepsis. *Sdc4*$^{-/-}$ mice are also more susceptible to LPS-mediated

sepsis [26]. Intraperitoneal (i.p.) injection of HS with SEB greatly decreases mortality, blood cytokine levels, and organ damage [25]. Considering the conflicting influence of HS/HSPGs on sepsis outcome (Table 1), there is currently no unifying explanation of their function in this context.

Although previous studies focusing on HS or HSPGs show the importance of these host factors during infection, most of them utilize strategies that do not specifically study how HS in the VGC affects infection outcome. In fact, very few studies have used targeted deletion of VGC components to study how altering the VGC impacts sepsis outcome. Our preliminary results shown below provide a new path for studying connections between the VGC, HS, and sepsis. Selective *Ndst1* deletion in endothelial and myeloid cells in *Ndst1$^{f/f}$Tie2Cre* mice was utilized to structurally alter HS in the VGC. Sepsis responses in mice with altered HS in the VGC were stratified across several sepsis-causing agents. Further, individual cell populations from *Ndst1$^{f/f}$Tie2Cre* mice were isolated to characterize how altering HS affects infection in cell populations relevant to sepsis.

3.2 Materials and methods

3.2.1 Animal model

Ndst1$^{f/f}$Tie2Cre animals were bred according to Wang, 2015 [4]. Briefly, *Ndst1$^{f/f}$* mice were bred to transgenic mice expressing Cre recombinase under control of the *Tek* promoter-enhancer (*Tie2Cre*). Male *Ndst1$^{f/f}$Tie2Cre+* mice were bred with female *Ndst1$^{f/f}$* mice to yield mutant mice (*Ndst1$^{f/f}$Tie2Cre+*) and wild-type littermate controls (*Ndst1$^{f/f}$Tie2Cre-*). All experiments used age- and sex-matched littermates. Offspring were genotyped by PCR with genomic DNA isolated from tail clip tissue.

3.2.2 Bacterial culture and sepsis models

Staphylococcus aureus USA300 TCH1516, *Streptococcus pyogenes* M1 5448 (Group A streptococcus, GAS), and *Streptococcus agalactiae* 10/84 (Group B streptococcus, GBS) were cultured from frozen 25% glycerol stocks in 5 mL overnight cultures in Todd-Hewitt Broth (THB, Difco) with agitation (200 rpm) at 37°C. 400 uL of overnight *S. aureus* culture was subcultured in 6 mL of fresh THB and grown to 0.4 OD_{600}, whereupon bacteria were centrifuged and washed with sterile PBS twice and resuspended at $5x10^8$ cfu/mL. To induce *S. aureus* sepsis, 100 µL of *S. aureus* was injected via intra-venous retroorbital injection. For both GAS and GBS culture, 1 mL of overnight culture was diluted in 9 mL fresh THB and incubated with agitation (200 rpm) at 37°C until 0.4 OD_{600}. The 10 mL culture was centrifuged and washed twice in PBS, which was concentrated to $7x10^8$ cfu/mL for GBS and $5x10^8$ cfu/mL for GAS. 100 µL of bacteria was i.p. injected to induce GBS or GAS sepsis. For *S. pneumoniae* strain D39 culture, frozen stocks were inoculated into 5 mL Todd-Hewitt broth containing 2% yeast extract (Difco) and incubated without shaking at 37°C in a 5% CO2 incubator. After overnight incubation, bacteria are re-inoculated into fresh broth and cultured to 0.4 OD_{600}. Bacteria was washed in PBS twice and diluted to 1 $x10^6$ cfu/mL, and 100 uL was injected i.p. to induce *S. pneumoniae* sepsis. For culture of *Salmonella typhimurium* 14028 and *E. coli* ATCC 25922, frozen 25% glycerol stocks were inoculated in 5 mL LB (Difco) overnight with agitation (200 rpm) at 37°C. *S. typhimurium* and *E. coli* were diluted 1:10 in fresh LB, grown to 0.4 OD_{600}, and centrifuged and washed twice in PBS. *S. typhimurium* was concentrated to $1x10^8$ cfu/mL in PBS and injected via oral gavage. *E. coli* was diluted to $1x10^8$ cfu/mL and 100 µL was injected i.p. to induce sepsis. Infection inoculum colony forming units (CFUs) for all bacterial strains was determined by serial dilution in PBS and plating on agar plates with growth media used to subculture the respective bacterial strains. *S. pneumoniae* was the exception, which was enumerated on 5% sheep blood agar plates (Hardy Diagnostics). Mice were

monitored twice daily and sacrificed upon severe morbidity as determined by inability to grasp with their forelimbs.

3.2.3 Endothelial Entry of Bacteria

Endothelial cells were isolated, immortalized, and *Ndst1* inactivated as described in Wang, 2005 [4]. Endothelial cells were plated in DMEM (Gibco) with 20% heat-inactivated fetal bovine serum (FBS). Endothelial cells were plated at 50% confluency in 24 well plates 3 days prior to infection. To infect endothelial cells, bacteria were added at 10 multiplicity of infection (MOI) and spun at 160 xg for 3 minutes to initiate bacteria-endothelial contact. After 2 hours of incubation at 5% CO_2, gentamycin was added to 100 µg/mL and penicillin was added to 5 µg/mL. The culture was incubated for an additional 30 min to kill extracellular bacteria. After the 30 min incubation, the plate was spun at 500 xg for 5 minutes, wells were washed with 100 uL PBS, then spun down again. PBS was removed, and 100 uL of 0.05% TritonX in PBS was incubated on the cells for 10 minutes at room temperature. 20 uL of the lysis mixture, as well as sequential dilutions of 1:10, 1:100, 1:1000, were plated on appropriate solid media to enumerate intracellular CFU.

3.2.4 Macrophage entry of bacteria

Tie2 driven inactivation of genes can result in recombination of "floxed" genes in the hematopoietic lineage in addition to the endothelium [27]. Therefore, infection parameters were also examined in myeloid-lineage cells including macrophages. Macrophages were isolated and matured from the bone marrow of *Ndst1$^{f/f}$Tie2Cre* mice as described in Gordts, 2014 [28]. Mature macrophages were plated in 96 well plates at $3x10^5$ cells/well in RPMI (Gibco) with 10% FBS. 24 hours later, freshly cultured bacteria were added at 10 MOI and the plate was spun at 160 xg for 3 minutes to initiate bacteria-macrophage contact and incubated for the desired amount of time. Gentamycin was added to the media and incubated for 30 minutes. Dead extracellular cells were

washed away with PBS, and intracellular bacteria were liberated via host cell lysis and enumerated with serial dilution. PBS was removed, and 100 uL of 0.05% TritonX in PBS was incubated on the cells for 3 minutes at room temperature followed by vigorous pipetting. 20 uL of the lysis mixture, as well as sequential dilutions of 1:10, 1:100, 1:1000, were plated on appropriate solid media to enumerate intracellular CFU.

3.2.5 Whole blood killing of bacteria

Whole blood was isolated via cardiac puncture of *Ndst1$^{f/f}$Tie2Cre* mice with hirudin anticoagulant pre-loaded in the syringe. 5x10^5 CFU of freshly cultured bacteria were added to 200 uL of blood in 2 mL siliconized tubes and incubated end-over-end for 3 hours in 5% CO_2 at 37°C. 20 uL of the whole blood mixture, as well as sequential dilutions of 1:10, 1:100, 1:1000, were plated on appropriate solid media to enumerate intracellular CFU.

3.2.6 Neutrophil killing of bacteria

Neutrophils were isolated from *Ndst1$^{f/f}$ Tie2Cre* mice bone marrow suspensions spun over a 62% Percoll gradient. 1x10^5 neutrophils were added to each well of a 96 well plate in RPMI with 2% FBS. Bacteria was added to neutrophils at 0.1 MOI, and the plate was centrifuged at 1600 rpm for 5 minutes to put bacteria into contact with neutrophils. The co-culture was incubated in 5% CO_2 at 37°C for up to 1 hour. CFU was enumerated as in Section 3.2.5.

3.2.7 Platelet killing of bacteria

Blood was isolated from *Ndst1$^{f/f}$ Tie2Cre* mice as in Section 3.2.5. The platelet-rich plasma (PRP) was isolated by centrifugation of blood at 180 xg and pipetting the plasma off the top of the separated cell populations. The PRP was placed in siliconized tubes and spun at 100 xg to pellet leukocytes. The platelet-enriched supernatant was isolated and spun down at 400 xg for 10 minutes to pellet the platelets. Platelets were resuspended in RPMI, counted, and placed in 96 well plates.

Bacteria were added at 0.01 MOI and incubated in 5% CO_2 at 37°C for 2 hours. CFU was enumerated as in Section 3.2.5.

3.3 Results

3.3.1 Mouse survival and pathology during sepsis

Our hypothesis was that altering VGC HS would impact sepsis outcome. Sepsis was induced with an LD_{50} to LD_{100} bacterial dose via i.p. injection for common sepsis causing pathogens *S. pneumoniae, S. pyogenes* (Group A *Streptococcus*, GAS), *S. agalactiae* (Group B *Streptococcus,* GBS), and *E. coli*, i.v. injection for *S. aureus*, or oral gavage for *S. typhimurium*. These routes of infection were chosen based upon their infection efficacy. After injection, sepsis outcome was assessed by survival. Altering HS increases host susceptibility to *S. aureus* (Figure 3.1A, Table 3.2) while decreasing susceptibility to *S. pneumoniae* (Figure 3.1B, Table 3.2). Importantly, altering HS did not impact sepsis outcome in the other microbial infections (Figure 3.1C-F, Table 3.2).

3.3.2 Bacterial entry into endothelial cells and macrophages

Pathogenic bacteria often colonize or cross the endothelium to invade tissues. For example, GBS uses HS to cross the blood brain barrier and colonize the brain [13]. *S. aureus* uses the endothelium as a site to escape host defense systems [29]. Macrophages can also be used as sites of bacterial replication, which can help bacteria hide from host defense systems, disseminate through the host, and increase inflammation through intracellular PAMP signaling [30,31]. Our hypothesis was that endothelial and macrophage HS impacts entry into these cell types. Immortalized *Ndst1*$^{f/f}$ and *Ndst1*$^{-/-}$ lung endothelial cells were used for endothelial invasion assays. Macrophages were derived and matured from isolated *Ndst1*$^{f/f}$*Tie2Cre* bone marrow. Bacteria were added to confluent cells at MOI 10, centrifuged to initiate contact, and incubated for 2 hours. Gentamycin was added

to the media and incubated for 30 minutes to kill extracellular bacteria. Dead extracellular cells were washed away, and intracellular bacteria were liberated via host cell lysis and enumerated with serial dilution. *Ndst1*$^{-/-}$ endothelial cells and macrophages contained fewer amount of GBS and *S. typhimurium* than *Ndst1*$^{f/f}$ host cells (Figure 3.2-3.3, Table 3.2).

3.3.3 Bactericidal activity of whole blood, neutrophils, and platelets

Bacteremia often occurs in sepsis, with 20% of sepsis cases presenting with bacteremia [32]. Whole blood does have bactericidal activity, which can be altered by changing HS. Whole blood deficient in 2-*O* sulfation has impaired bactericidal activity against GBS [14]. Neutrophils also have decreased killing ability when deficient in HS 2-*O* sulfation [14]. Specific blood cell populations have been shown to have antimicrobial activity. Platelets are well known for their role in clotting and vascular repair, but their role as direct antimicrobial agents against *S. aureus* has recently been established [33]. Neutrophils circulate in blood until activated by infection and inflammation, whereupon they promote bacterial killing and clearance [34]. Our hypothesis was HS sulfation impacts bactericidal activity in whole blood, neutrophils, and platelets. Bacteria were added *Ndst1*$^{f/f}$*Tie2Cre* whole blood with end-over-end movement to mimic blood flow turbulence. Neutrophils were isolated from *Ndst1*$^{f/f}$*Tie2Cre* bone marrow, while platelets were purified from the buffy coat of centrifuged whole blood. Bacteria was added to platelets and neutrophil cultures, and live bacteria were counted after co-incubation. Altering myeloid HS increased whole blood killing of GBS and *S. typhimurium* and not in other species (Figure 3.4A-F, Table 3.2). *Ndst1*$^{-/-}$ neutrophils had deficient microbicidal activity against *S. aureus* (Figure 3.5A), and increased killing of GBS and *S. typhimurium* (Figure 3.5A-F, Table 3.2). Altering platelet HS had no effect on microbicidal activity (Figure 3.6A-F, Table 2).

3.4 Discussion

By using tissue-specific HS mutant animal models to study sepsis and infection outcomes across several pathogens, several new novelties and insights were gained. First, few studies have used tissue-specific alteration of HS or HSPGs, or any VGC component, to study how these VGC components impact sepsis outcome. Our studies suggest that VGC HS is important to infection, depending upon the infectious agent. Considering this, these studies are the first example of stratifying sepsis outcome from several bacterial pathogens based upon VGC status. Host tolerance to septic challenge after VGC alteration can vary depending upon the pathogen, indicating that sepsis progression is not uniform across septic insults. Last, this phenotypic screen highlighted that HS can differentially impact infection in depending upon the host cell type and pathogen. Further studies can determine if these phenotypes are critical to sepsis outcome.

The phenotypic screen revealed that modifying VGC HS affected sepsis outcomes in two pathogens tested, *S. aureus* and *S. pneumoniae* (Figure 3.1, Table 3.2). Interestingly, altering vascular HS increased susceptibility to *S. aureus* while having the opposite affect in *S. pneumoniae* sepsis. HS mutant hypersensitivity to *S. aureus* infection was very pronounced by 24 hours post-infection, while protection from *S. pneumoniae* was less striking. Further, *S. aureus* infection of HS mutant neutrophils showed a correlative phenotype with a defect in neutrophil killing while *S. pneumoniae* infection showed no phenotypes in cells with altered HS (Figure 3.5, Table 3.2). Although *S. typhimurium* and GBS had mirrored phenotypes across every cell type tested, sepsis caused by these pathogens was not impacted by HS status. Therefore, further studies investigating the impact of altering VGC HS in sepsis focused solely on the *S. aureus* model.

3.5 Acknowledgments

Chapter 3 is not being prepared for publication. The dissertation author is the primary author of this material. Thank you to Joshua Olson for assistance with culture and mouse sepsis

methods, and Satoshi Uchiyama and Joshua Sun for cell killing assay assistance. These studies were supported by the National Institute of Health (P01- HL131474) and the UCSD Microbiome Center for Innovation (Microbial Sciences Graduate Research Fellowship Award 1-F17GG and 1-F18GG).

3.6 Figures

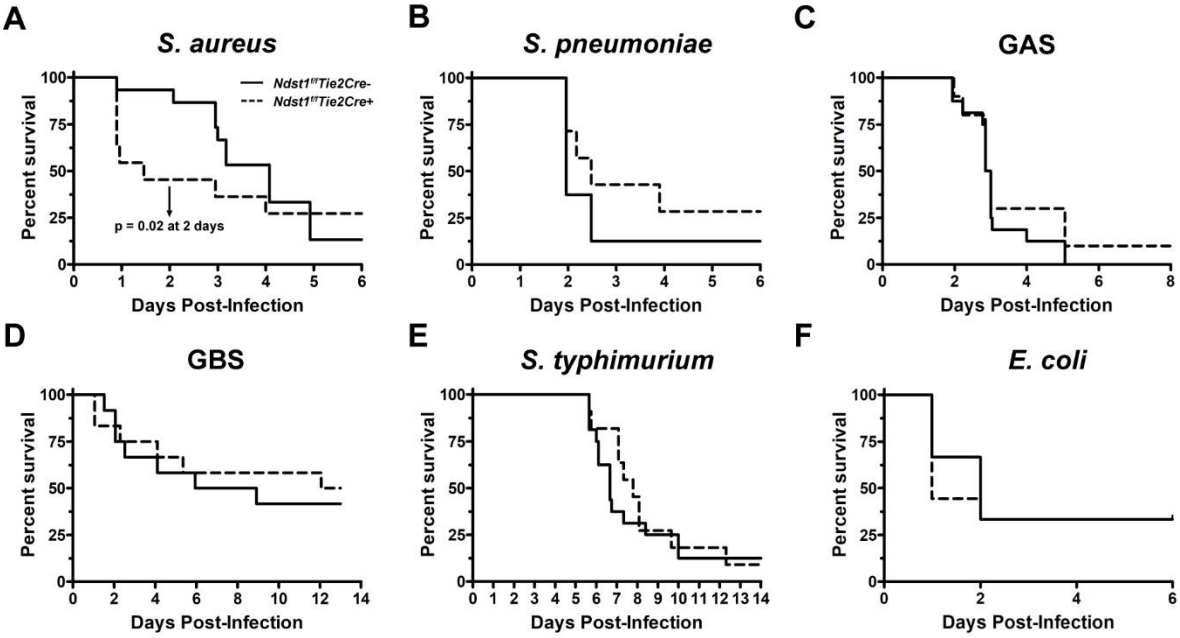

Figure 3.1 Susceptibility of *Ndst1$^{f/f}$Tie2Cre* mice to septic challenge with common sepsis-causing agents. Mice were infected with LD_{50} to LD_{100} of the indicated bacterial pathogens and survival was measured. At least 8 mice were used per genotype. *p* value determined by Log-rank Mantel-Cox test. *p* value in (A) determined using data exclusively from the first two days of infection.

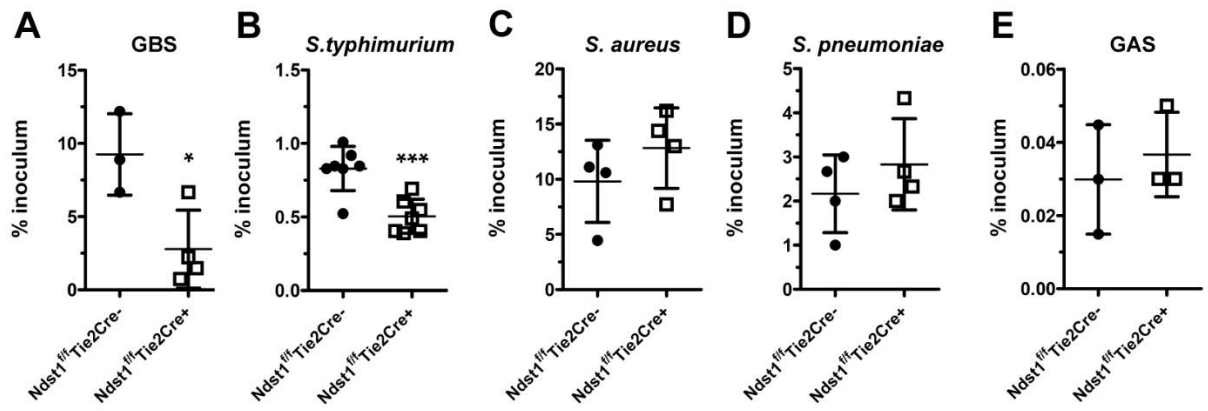

Figure 3.2 Bacterial entry into *Ndst1$^{f/f}$Tie2Cre* endothelial cells. Levels of intracellular bacteria inside endothelial cells 2.5 hours post-infection. Bacterial CFU is normalized to the percent of the input inoculum. Values are representative of one experiment. *E. coli* values could not be determined because endothelial cells lysed in response to bacterial insult. *p* value determined with Student's T-test. * is $p < 0.05$ and *** is $p < 0.001$.

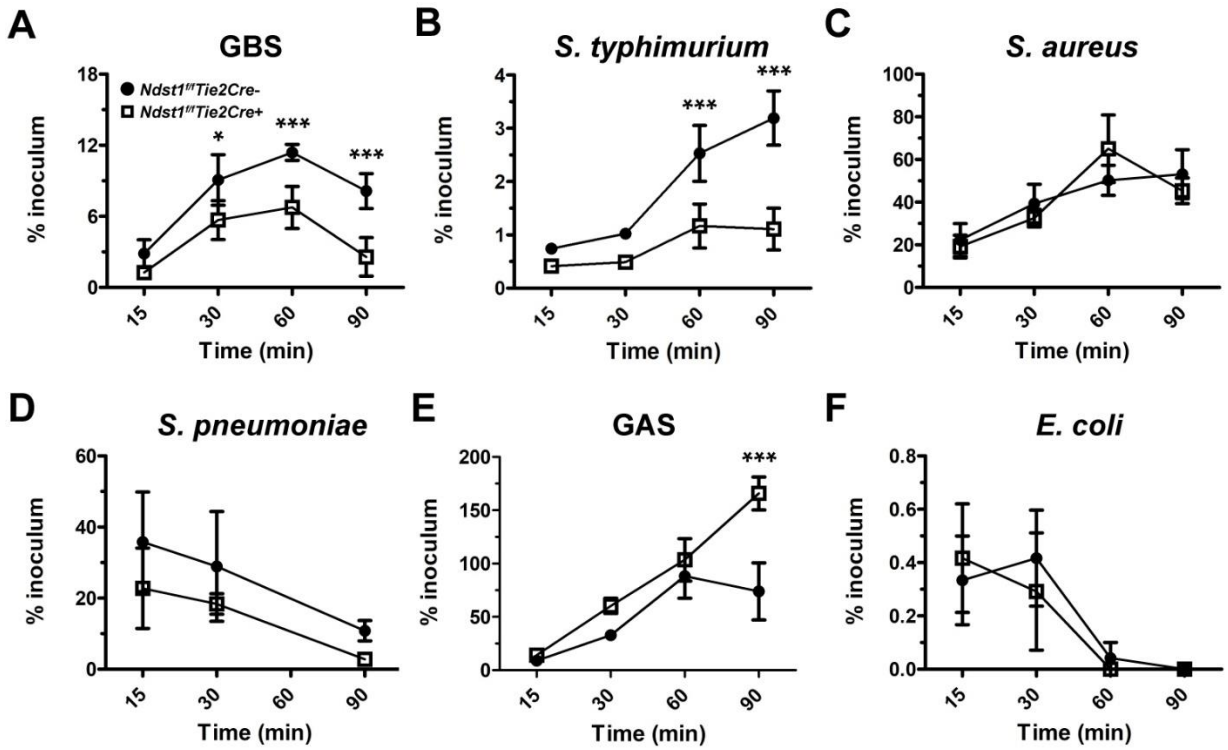

Figure 3.3 Intracellular bacterial burden in *Ndst1$^{f/f}$Tie2Cre* bone marrow derived macrophages. Bacterial CFU were enumerated at the indicated timepoints and normalized to the percent of the input inoculum. Values are representative of one experiment. *p* value determined with two-way ANOVA with Bonferroni post-test between genotypes within one timepoint. * is $p < 0.05$ and *** is $p < 0.001$.

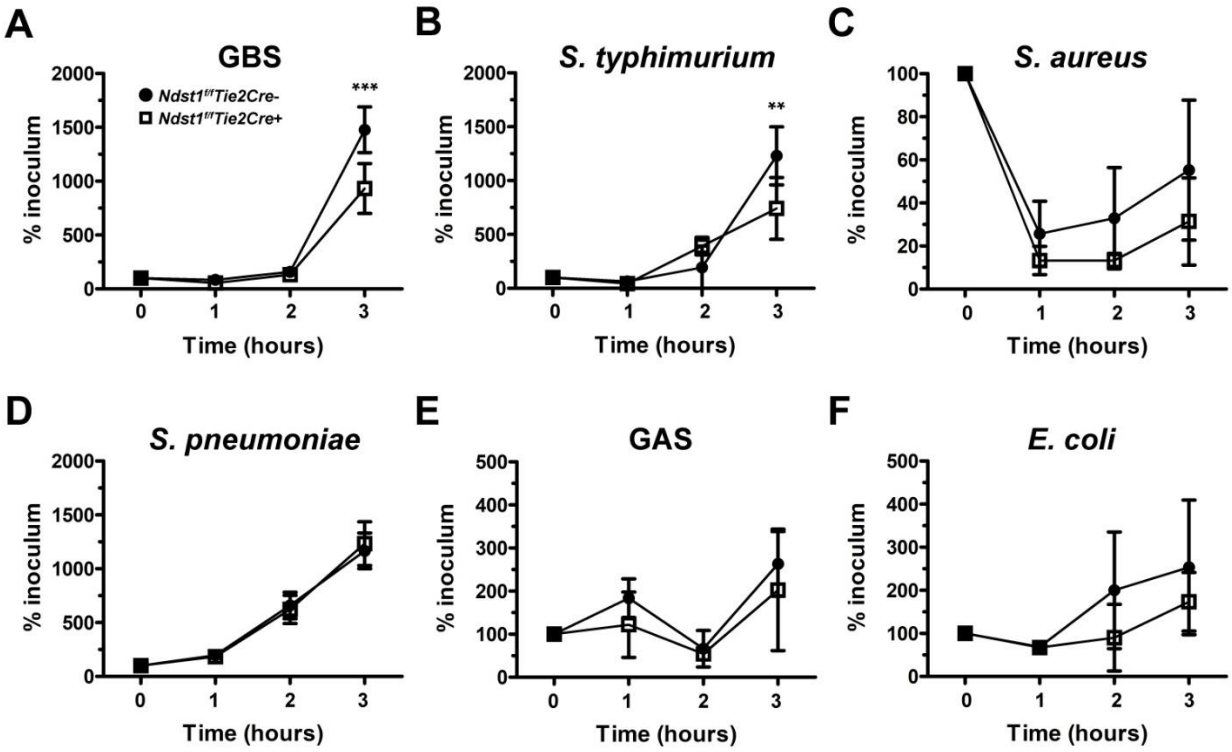

Figure 3.4 *Ndst1$^{f/f}$Tie2Cre* whole blood bactericidal activity. Bacterial CFU were enumerated at the indicated timepoints and normalized to the percent of the input inoculum. Values are representative of one experiment. *p* value determined with two-way ANOVA with Bonferroni post-test between genotypes within one timepoint. ** is $p < 0.01$ and *** is $p < 0.001$.

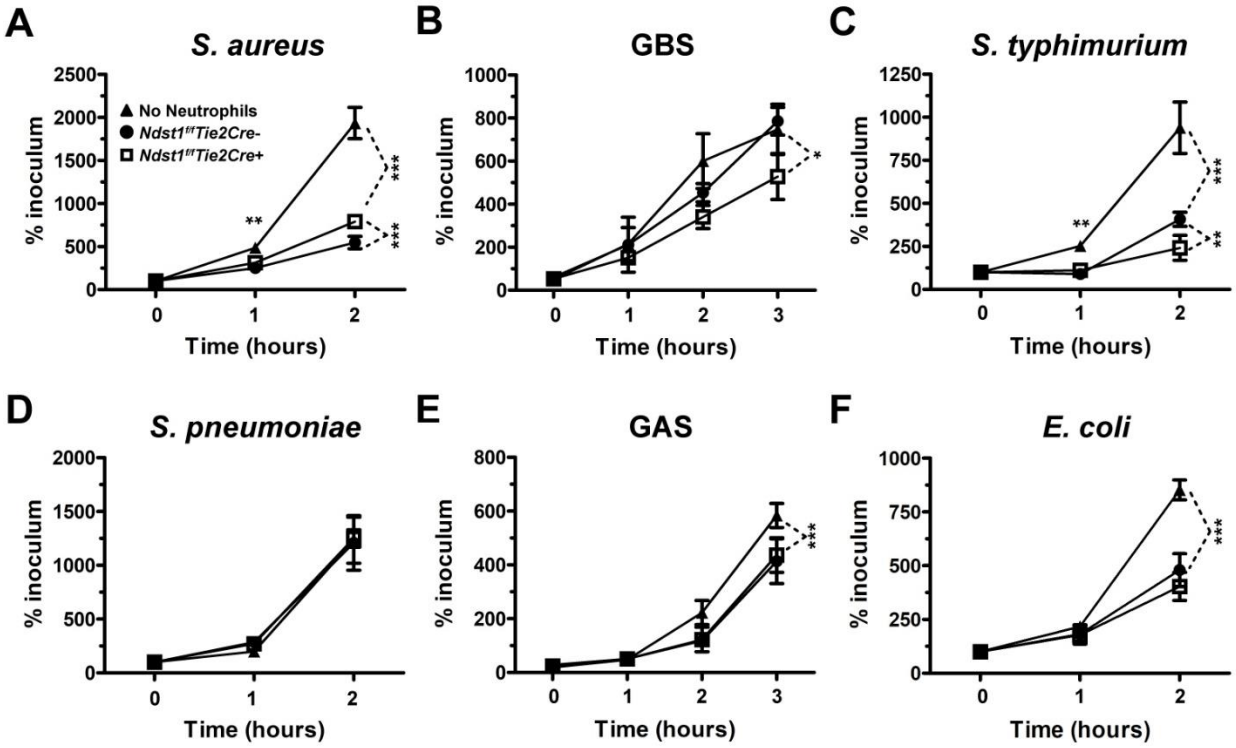

Figure 3.5 Bactericidal activity of *Ndst1$^{f/f}$Tie2Cre* neutrophils. Bacterial CFU were enumerated at the indicated timepoints and normalized to the percent of the input inoculum. 3 hour timepoints are excluded from some pathogens due to overgrowth of the culture. Values are representative of one experiment. *p* value determined with two-way ANOVA with Bonferroni post-test between genotypes within one timepoint. * is $p < 0.05$, ** is $p < 0.01$, and *** is $p < 0.001$.

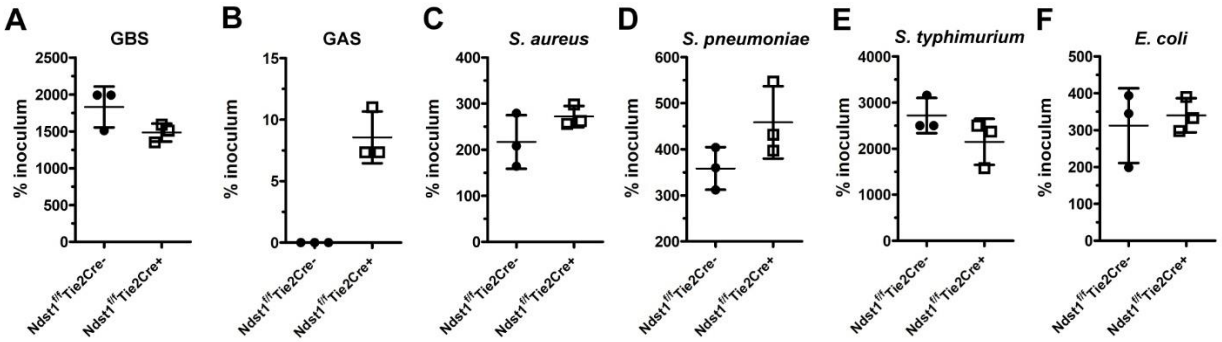

Figure 3.6 Bactericidal activity of *Ndst1$^{f/f}$Tie2Cre* platelets. Bacterial CFU were enumerated at the 2 hours post-infection and normalized to the percent of the input inoculum. 0 CFU indicates bacteria was below the detection limit. Values are representative of one experiment. Statistical significance as tested with Student's T-test was not reached with any pathogen.

3.7 Tables

Table 3.1: Stratification of HS/HSPG influence on sepsis

	Context of infection/insult	Effect on Immune Response/Sepsis	Ref.
Studies that show HS/HSPGs increase susceptibility to sepsis	Sdc1-/- mice, P. aeruginosa lung infection	Increased host resistance to infection	[15]
	Sdc1-/- mice, S. aureus lung infection	Increased host resistance to infection	[16]
	Sdc1-/- mice, S. aureus corneal infection	Increased host resistance to infection	[17]
	Sdc1-/- mice, P. aeruginosa burn wound infection	Increased host resistance to infection, decreased inflammatory response	[19]
	Sdc1-/- mice, P. aeruginosa burn wound infection + injected heparin	Heparin increased host susceptibility to infection	[19]
	WT mice, S. aureus corneal infection	2-O sulfation binds CRAMP, increased host susceptibility	[18]
	Human sepsis patients, urine samples	Increased urine HS levels correlate with death	[35]
	WT mice, P. aeruginosa lung infection	HS shedding increased host susceptibility to infection	[15]
	Heparanase-/- mice, cecal ligation and puncture	Increased host resistance	[21]
	Mouse epithelium, P. aeruginosa LasA and S. aureus α/β toxins	Increased Sdc1 shedding	[22,23]
	WT mice, LPS injection	Increased ECM shedding	[21]
Studies that show HS/HSPGs decrease susceptibility to sepsis	Hs2stf/f Tie2Cre+ mice, GBS sepsis	Increased host susceptibility	[14]
	Sdc1-/- mice, LPS and SEB injection	Increased host susceptibility to toxic shock	[25]
	Sdc4-/- mice, LPS injection	Increased host susceptibility to toxic shock	[26]
	WT mice, HS + SEB i.p. injection	Increased host resistance to toxic shock, decreased inflammatory response	[25]

Table 3.2 Sepsis and infection model Screen in a Heparan Sulfate Mutant Background

Bacteria	Mouse Survival	Endothelial Entry	Macrophage Entry	Whole Blood Killing	Neutrophil Killing	Platelet Killing
Streptococcus pneumoniae	Enhanced survival in *Ndst1$^{f/f}$Tie2Cre+* mice	No difference	No difference	No difference	No difference	No difference
Staphylococcus aureus	Decreased survival in *Ndst1$^{f/f}$Tie2Cre+* mice	No difference	No difference	No difference	Decreased killing by *Ndst1$^{-/-}$* neutrophils	No difference
Salmonella typhimurium	No difference	Reduced invasion of *Ndst1$^{-/-}$* cells	Decreased entry into *Ndst1$^{-/-}$* cells	Increased killing by *Ndst1$^{f/f}$Tie2Cre+* blood	Increased killing by *Ndst1$^{-/-}$* neutrophils	No difference
Streptococcus pyogenes	No difference	No difference	Increased entry into *Ndst1$^{-/-}$* cells	No difference	No difference	No difference
Streptococcus agalactiae	No difference	Reduced invasion of *Ndst1$^{-/-}$* cells	Decreased entry into *Ndst1$^{-/-}$* cells	Increased killing by *Ndst1$^{f/f}$Tie2Cre+* blood	Increased killing by *Ndst1$^{-/-}$* neutrophils	No difference
Escherichia coli	No difference	No difference	No difference	No difference	No difference	No difference

3.8 References

1. Parish, C. R. The role of heparan sulphate in inflammation. *Nat. Rev. Immunol.* **6,** 633–643 (2006).

2. Bishop, J. R., Schuksz, M. & Esko, J. D. Heparan sulphate proteoglycans fine-tune mammalian physiology. *Nature* **446,** 1030–1037 (2007).

3. Kusche-Gullberg, M. & Kjellén, L. Sulfotransferases in glycosaminoglycan biosynthesis. *Curr. Opin. Struct. Biol.* **13,** 605–611 (2003).

4. Wang, L., Fuster, M., Sriramarao, P. & Esko, J. D. Endothelial heparan sulfate deficiency impairs L-selectin- and chemokine-mediated neutrophil trafficking during inflammatory responses. *Nat. Immunol.* **6,** 902–10 (2005).

5. Esko, J. D. & Lindahl, U. Molecular diversity of heparan sulfate. *J. Clin. Invest.* **108,** 169–173 (2001).

6. Xu, D. & Esko, J. D. Demystifying heparan sulfate-protein interactions. *Annu. Rev. Biochem.* **83,** 129–157 (2014).

7. Ori, A., Wilkinson, M. C. & Fernig, D. G. A systems biology approach for the investigation of the heparin/heparan sulfate interactome. *J. Biol. Chem.* **286,** 19892–19904 (2011).

8. Rittirsch, D., Flierl, M. A. & Ward, P. A. Harmful molecular mechanisms in sepsis. *Nat. Rev. Immunol.* **8,** 776–87 (2008).

9. Axelsson, J., Xu, D., Kang, B. N., Nussbacher, J. K., Handel, T. M., Ley, K., Sriramarao, P. & Esko, J. D. Inactivation of heparan sulfate 2- O -sulfotransferase accentuates neutrophil infiltration during acute inflammation in mice. *Blood* **120,** 1742–1751 (2012).

10. Tsuboi, K., Hirakawa, J., Seki, E., Imai, Y., Yamaguchi, Y., Fukuda, M. & Kawashima, H. Role of high endothelial venule-expressed heparan sulfate in chemokine presentation and lymphocyte homing. *J Immunol* **191,** 448–455 (2013).

11. Massena, S., Christoffersson, G., Hjertström, E., Zcharia, E., Vlodavsky, I., Ausmees, N., Rolny, C., Li, J. P. & Phillipson, M. A chemotactic gradient sequestered on endothelial heparan sulfate induces directional intraluminal crawling of neutrophils. *Blood* **116,** 1924–1931 (2010).

12. Srivastava, M., Jung, S., Wilhelm, J., Fink, L., Bühling, F., Welte, T., Bohle, R. M., Seeger, W., Lohmeyer, J. & Maus, U. a. The inflammatory versus constitutive trafficking of mononuclear phagocytes into the alveolar space of mice is associated with drastic changes in their gene expression profiles. *J. Immunol.* **175,** 1884–93 (2005).

13. Chang, Y. C., Wang, Z., Flax, L. A., Xu, D., Esko, J. D., Nizet, V. & Baron, M. J. Glycosaminoglycan binding facilitates entry of a bacterial pathogen into central nervous

systems. *PLoS Pathog.* **7,** (2011).

14. Xu, D., Olson, J., Cole, J. N., van Wijk, X. M., Brinkmann, V., Zychlinsky, A., Nizet, V., Esko, J. D. & Chang, Y. C. Heparan sulfate modulates neutrophil and endothelial function in antibacterial innate immunity. *Infect. Immun.* **83,** 3648–3656 (2015).

15. Park, P. W., Pier, G. B., Hinkes, M. T. & Bernfield, M. Exploitation of syndecan-1 shedding by Pseudomonas aeruginosa enhances virulence. *Nature* **411,** 98–102 (2001).

16. Hayashida, A., Bartlett, A. H., Foster, T. J. & Park, P. W. Staphylococcus aureus beta-toxin induces lung injury through syndecan-1. *Am. J. Pathol.* **174,** 509–18 (2009).

17. Hayashida, A., Amano, S. & Park, P. W. Syndecan-1 promotes Staphylococcus aureus corneal infection by counteracting neutrophil-mediated host defense. *J. Biol. Chem.* **286,** 3288–3297 (2011).

18. Hayashida, A., Amano, S., Gallo, R. L., Linhardt, R. J., Liu, J. & Park, P. W. 2-O-sulfated domains in syndecan-1 heparan sulfate inhibit neutrophil cathelicidin and promote Staphylococcus aureus corneal infection. *J. Biol. Chem.* **290,** 16157–16167 (2015).

19. Haynes, A., Ruda, F., Oliver, J., Hamood, A. N., Griswold, J. A., Park, P. W. & Rumbaugh, K. P. Syndecan 1 shedding contributes to Pseudomonas aeruginosa sepsis. *Infect. Immun.* **73,** 7914–7921 (2005).

20. Manon-Jensen, T., Itoh, Y. & Couchman, J. R. Proteoglycans in health and disease: The multiple roles of syndecan shedding. *FEBS J.* **277,** 3876–3889 (2010).

21. Schmidt, E. P., Yang, Y., Janssen, W. J., Gandjeva, A., Perez, M. J., Barthel, L., Zemans, R. L., Bowman, J. C., Koyanagi, D. E., Yunt, Z. X., Smith, L. P., Cheng, S. S., Overdier, K. H., Thompson, K. R., Geraci, M. W., Douglas, I. S., Pearse, D. B. & Tuder, R. M. The pulmonary endothelial glycocalyx regulates neutrophil adhesion and lung injury during experimental sepsis. *Nat Med* **18,** 1217–1223 (2012).

22. Park, P. W., Pier, G. B., Preston, M. J., Goldberger, O., Fitzgerald, M. L. & Bernfield, M. Syndecan-1 Shedding Is Enhanced by LasA, a Secreted Virulence Factor of Pseudomonas aeruginosa. *J. Biol. Chem.* **275,** 3057–3064 (2000).

23. Park, P. W., Foster, T. J., Nishi, E., Duncan, S. J., Klagsbrun, M. & Chen, Y. Activation of Syndecan-1 Ectodomain Shedding by Staphylococcus aureus α-Toxin and β-Toxin. *J. Biol. Chem.* **279,** 251–258 (2004).

24. Hayashida, K., Parks, W. C. & Pyong, W. P. Syndecan-1 shedding facilitates the resolution of neutrophilic inflammation by removing sequestered CXC chemokines. *Blood* **114,** 3033–3043 (2009).

25. Hayashida, K., Chen, Y., Bartlett, A. H. & Pyong, W. P. Syndecan-1 is an in vivo suppressor of gram-positive toxic shock. *J. Biol. Chem.* **283,** 19895–19903 (2008).

26. Ishiguro, K., Kadomatsu, K., Kojima, T., Muramatsu, H., Iwase, M., Yoshikai, Y., Yanada, M., Yamamoto, K., Matsushita, T., Nishimura, M., Kusugami, K., Saito, H. & Muramatsu, T. Syndecan-4 Deficiency Leads to High Mortality of Lipopolysaccharide-injected Mice. *J. Biol. Chem.* **276,** 47483–47488 (2001).

27. Tang, Y., Harrington, A., Yang, X., Friesel, R. E. & Liaw, L. The contribution of the Tie2+ lineage to primitive and definitive hematopoietic cells. *Genesis* **48,** 563–567 (2010).

28. Gordts, P. L. S. M., Foley, E. M., Lawrence, R., Sinha, R., Lameda-Diaz, C., Deng, L., Nock, R., Glass, C. K., Erbilgin, A., Lusis, A. J., Witztum, J. L. & Esko, J. D. Reducing macrophage proteoglycan sulfation increases atherosclerosis and obesity through enhanced type i interferon signaling. *Cell Metab.* **20,** 813–826 (2014).

29. Tong, S. Y. C., Davis, J. S., Eichenberger, E., Holland, T. L. & Fowler, V. G. Staphylococcus aureus infections: Epidemiology, pathophysiology, clinical manifestations, and management. *Clin. Microbiol. Rev.* **28,** 603–661 (2015).

30. Mitchell, G., Chen, C., Portnoy, D. A. & Biology, C. Strategies used by bacteria to grow in macrophages. *Microbiol. Spectr.* **4,** (2016).

31. Surewaard, B. G. J., Deniset, J. F., Zemp, F. J., Amrein, M., Otto, M., Conly, J., Omri, A., Yates, R. M. & Kubes, P. Identification and treatment of the Staphylococcus aureus reservoir in vivo. *J. Exp. Med.* **213,** 1141–1151 (2016).

32. Mayr, F. B., Yende, S. & Angus, D. C. Epidemiology of severe sepsis. *Virulence* **5,** 1–11 (2014).

33. Ali, R. A., Wuescher, L. M., Dona, K. R. & Worth, R. G. Platelets Mediate Host Defense against *Staphylococcus aureus* through Direct Bactericidal Activity and by Enhancing Macrophage Activities. *J. Immunol.* **198,** 344–351 (2017).

34. Kobayashi, S. D., Malachowa, N. & DeLeo, F. R. Neutrophils and Bacterial Immune Evasion. *J. Innate Immun.* **10,** 432–441 (2018).

35. Schmidt, E. P., Overdier, K. H., Sun, X., Lin, L., Liu, X., Yang, Y., Ammons, L. A., Hiller, T. D., Suflita, M. A., Yu, Y., Chen, Y., Zhang, F., Burlew, C. C., Edelstein, C. L., Douglas, I. S. & Linhardt, R. J. Urinary glycosaminoglycans predict outcomes in septic shock and ARDS. *Am. J. Respir. Crit. Care Med.* **Published,** (2016).

Chapter 4: Endothelial heparan sulfate mediates hepatic neutrophil trafficking and injury during *Staphylococcus aureus* sepsis

4.1 Abstract

Staphylococcus aureus sepsis causes profound hepatic vasculopathy, hypercoagulation, and organ failure. Liver dysfunction is driven by pro-inflammatory neutrophils that traffic to the liver dependent on vascular hyaluronan. In peripheral tissues heparan sulfate (HS), a sulfated glycosaminoglycan in the vascular glycocalyx, facilitates leukocyte recruitment during inflammation. To examine if reducing the overall sulfation of HS in the vasculature might mitigate hepatic damage induced by *S. aureus*, we inactivated the HS biosynthetic enzyme *N-deacetylase-N-sulfotransferase 1* in endothelial and myeloid cells by crossing *Ndst1*$^{f/f}$ and *Tie2Cre* mice. *Ndst1*$^{f/f}$*Tie2Cre*$^{+}$ mice displayed lower levels of liver damage and less intravascular coagulation compared to wildtype littermate controls. Both the degree of hepatic infarction and liver pathogen burden were significantly diminished. In contrast, *Ndst1*$^{f/f}$*LysMCre*$^{+}$/*PF4Cre*$^{+}$ mice were unaffected. Impaired neutrophil trafficking was observed in models of liver injury using flow cytometry and intravital microscopy. Importantly, neutrophil recruitment was diminished in both septic and sterile injury, which utilize different mechanisms for neutrophil recruitment. These findings suggest that HS regulates rapid neutrophil trafficking to the liver in multiple types of injury and that the fine-structure of vascular HS modulates hepatic coagulopathy and organ pathogenesis during *S. aureus* sepsis.

4.2 Introduction

Sepsis is a life-threatening organ dysfunction due to a dysregulated host response to infection [1]. Inappropriate responses to infection by the host vasculature and immune system fuel vascular dysfunction, leading to inadequate nutrient delivery to vital organs and subsequent organ failure [1–3]. Organ failure is a critical aspect of sepsis, yet historically sepsis treatment studies have aimed at inhibiting systemic inflammation with little clinical success [4,5]. Understanding the mechanistic ties between vascular dysfunction and organ failure in sepsis may lead to improved organ support and better outcome in patients [4].

The vascular surface is covered in a layer of glycans, glycolipids, glycoproteins, and glycosaminoglycans (GAGs) termed the glycocalyx [6]. The vascular glycocalyx can be as thick as the endothelial cell layer and forms the interface between the lumen and the endothelium, modulating vascular function [7,8]. Sepsis dramatically alters the vascular glycocalyx, promoting leukocyte adherence, vascular dysfunction and inflammation [9–12]. Until recently, a comprehensive *in vivo* analysis of the vascular glycocalyx, in health or in a disease-state, was lacking. We developed an organ-specific proteomic atlas of the murine vascular glycocalyx, demonstrating that it changes dramatically in an organotypic fashion during *Staphylococcus aureus* sepsis [13]. A vast majority of these proteins are glycoproteins, indicating that each glycocalyx undergoes extensive remodeling during sepsis.

The liver undergoes the most dynamic and extensive changes in the vascular glycocalyx during *Staphylococcus aureus* sepsis [13]. We and others have shown that *S. aureus* primarily colonizes the liver [13,14], where tissue-resident macrophage Kupfer cells (KCs) filter circulating bacteria [15,16]. Upon bacterial sequestration by KCs, neutrophils rapidly traffic to the liver sinusoids to clear the infection. Activated neutrophils release neutrophil extracellular traps in the liver

sinusoids, triggering an immunothrombotic response in the liver vasculature that can help ensnare bacteria [14,17]. However, we and others have shown that this neutrophilic immunothrombosis aberrantly develops into a pathological thrombotic response that occludes the liver vasculature and ultimately cause parenchymal necrosis and organ failure [13,14]. Importantly, blocking neutrophil trafficking into the liver completely protects the liver from this damage [14]. During infection, neutrophil trafficking into the liver depends on CD44 on neutrophils binding to sinusoidal hyaluronan, a class of GAG that is abundant in the vascular glycocalyx [14,18]. Additionally, we showed the liver vascular glycocalyx has a marked increase in HA, HA binding and processing proteins, as well as neutrophil activation markers [13]. In contrast, during sterile inflammation, neutrophils chemotax intravascularly through the sinusoids via an integrin-dependent mechanism [19]. The adhesion molecules and chemotactic signals that govern neutrophil chemotaxis in the liver, in sterile or septic inflammation, reside in the vascular glycocalyx. Understanding the components of the vascular glycocalyx that regulate neutrophil chemotaxis in the liver is valuable for understanding how liver inflammatory processes develop.

Heparan sulfate (HS), another type of GAG, is a major component of the glycocalyx and is ubiquitously expressed in the vasculature [20]. HS is a polyanionic linear polysaccharide composed of repeating disaccharide subunits of alternating uronic acids and glucosamine units that can be modified with sulfate groups. Addition of sulfate groups to HS occurs in short interspersed segments with intervening long tracts of unmodified sugars [21]. The initial modification reaction, N-deacetylation and N-sulfation of GlcNAc, is catalyzed by N-deacetylase-N-sulfotransferase 1 (*Ndst1*). Further modification includes specific O-sulfation of uronic acids and N-sulfated glucosamine units [22,23]. The arrangement of uronic acids and sulfated sugars and the high negative charge of the chains govern protein-HS interactions and HS function [24].

HS directly impacts multiple aspects of vascular inflammation and sepsis. Endothelial HS binds chemokines and participates in chemokine transcytosis as well as chemokine gradient formation that attracts leukocytes toward sites of inflammation [25–33]. HS mediates neutrophil extravasation by interacting with neutrophil selectins during rolling [26,27]. Exogenous synthetic HS oligosaccharides block neutrophil influx and inflammation in acetaminophen-induced liver failure [34], while intravenous injection of the recombinant GAG-binding domain of CXCL9 competes with native chemokine binding to blunt neutrophil trafficking [35–37]. HS chains are normally covalently bound to core proteins to form heparan sulfate proteoglycans (HSPGs). HSPGs can promote damaging inflammation during bacterial infection [38–41]. During sepsis, HS fragments and HSPG ectodomains are enzymatically shed from the vascular glycocalyx and can fuel pathological processes [9,42–44].

In this report, we modified vascular HS fine structure to study how selective alteration of the vascular glycocalyx affects organ pathology during *S. aureus* sepsis. Genetic manipulation of vascular HS specifically affects liver pathology by diminishing neutrophil trafficking and subsequent pathological thrombosis in the liver vasculature.

4.3 Materials and Methods

4.3.1 Bacterial Strains and Preparation

As previously described [13], *Staphylococcus aureus* (strain USA300 TCH1516) was originally isolated from an outbreak in Houston, Texas and caused severe invasive disease in adolescents [45]. *S. aureus* was routinely grown at 37°C on Todd-Hewitt agar (Difco) or in liquid cultures of Todd-Hewitt broth (THB, Difco) with agitation (200 rpm). Bacteria were inoculated into 5 mL of fresh THB and incubated overnight. 400 uL of overnight culture was inoculated into 6 mL of fresh THB and incubated to OD_{600}= 0.4. Bacteria were centrifuged, washed twice with

PBS, and suspended in PBS at $5x10^8$ cfu/mL. *S. aureus* USA300 TCH1516 constitutively expressing GFP [46] was cultured using the same method.

4.3.2 Animal Studies

Ndst1$^{f/f}$ transgenic C57bl/6 mice were crossed with *Tie2Cre* transgenic C57bl/6 mice to generate *Ndst1$^{f/f}$Tie2Cre* mice [26]. To generate *Ndst1$^{f/f}$LysM/PF4Cre* mice, B6.129P2-*Lyz2$^{tm1(cre)Ifo}$*/J (LysMCre, Jackson Labs) were crossed to *Ndst1$^{f/f}$* transgenic C57bl/6 mice to generate *Ndst1$^{f/f}$LysMCre* mice, and C57BL/6-Tg(Pf4-icre)Q3Rsko/J (PF4Cre, Jackson Labs) were crossed to *Ndst1$^{f/f}$* transgenic C57bl/6 mice to generate *Ndst1$^{f/f}$PF4Cre* mice. Then, the double-Cre line was generated by crossing *Ndst1$^{f/f}$LysMCre* and *Ndst1$^{f/f}$PF4Cre* mice as described elsewhere [47]. As previously described [13], for *S. aureus* infection, 8-10-week-old C57Bl/6 male and female mice were injected i.v. through the retroorbital sinus with $5x10^7$ cfu (100µL) *S. aureus*. At 24 hr post-infection, animals were euthanized by isoflurane and immediately processed for sample collection. CFU in the *S. aureus* inoculum were enumerated by serial dilution on Todd Hewitt Agar plates to ensure consistent CFU dosing across experiments. Animals were housed and bred in Individual Ventilated Cages in a Specific Pathogen Free background, in vivaria approved by the Association for Assessment and Accreditation of Laboratory Animal Care located in the School of Medicine, UC San Diego. All experiments were performed in accordance with relevant guidelines and regulations following standards and procedures approved by the UC San Diego Institutional Animal Care and Use Committee (protocols #S99127 and #S00227M) and the La Jolla Institute for Immunology Department of Laboratory Animal Care (protocol #AP00001019).

4.3.3 Blood Chemistry and Complete Blood Count

To collect serum for blood chemistry, blood was collected via cardiac puncture and placed in a pro-coagulant serum tube (BD Microtainer #365967) for 4 hours at room temperature. Serum was isolated by spinning the tubes at 2000xg and collecting the supernatant. All samples were frozen and thawed once before analysis. Blood chemistry parameters were measured on a Cobas 8000 automated chemistry analyzer (Roche) with a general coefficient of variance of <5%. All samples were frozen and thawed no more than two times before analysis. For complete blood count, blood was isolated in a 1:9 citrate dextrose solution (Millipore Sigma #C3821) to blood ratio and a Hemavet 950FS Multi-Species Hematology System (Drew Scientific, CT) programmed to mouse settings was used to collect complete blood count.

4.3.4 Histological Analysis

Tissues were fixed in 10% buffered formalin (Fischer Chemical) for 24 hr, followed by submersion in 70% ethanol for at least 24 hr. The samples were paraffin embedded and sectioned (3 µm) and stained with hematoxylin/eosin. Sections underwent blinded scoring to measure liver inflammation and necrosis, with scores ranging from 0 – 4 (4 representing the most inflamed and necrotic tissue).

4.3.5 Bacterial Colony Forming Units (CFU) Counts

As previously described, organs of interest were placed in a 2 mL tube (Sarstedt #72.693.005) containing 1 mL ice cold PBS and 1.0 mm diameter Zirconia/Silica beads (Biospec Products #11079110z). Samples were homogenized using a MagNA Lyzer (Roche) for 2 minutes at 6000 rpm. An aliquot of each organ sample was serially diluted in PBS and plated on Todd-Hewitt Agar to enumerate CFU.

4.3.6 Single Cell Suspension and Flow Cytometry

Mice were perfused before livers were isolated for flow cytometry. Briefly, mice were humanely euthanized with isoflurane and immediately perfused at 7 mL/minute for 2 minutes with ice cold PBS through the left ventricle, with a small cut made in the right ventricle for drainage of perfusion materials. The left lobe of the liver was isolated from each mouse and homogenized with scissors in ice cold petri dishes. An equal weight of each individual homogenate was further processed. Organs were then resuspended in 5 mL of ice cold HBSS with Ca^{2+}/Mg^{2+} (ThermoFischer Scientific #14025092) + 3 mM $CaCl_2$ in a 50 mL conical tube. To digest organs, 0.3 Units/mL of Liberase TL (Roche #5401020001) and 40 Units/mL DNaseI (Millipore Sigma #D4263) where added to each suspended homogenate, and the homogenates were shaken at 37°C for 30 min at 150 rpm. Digested homogenates were filtered through a 70 µM strainer to make single cell suspensions. Single cell suspensions were spun at 50 xg for 3 min at 4°C to pellet hepatocytes, while the supernatant was collected for further processing. The supernatant was spun down and resuspended in 20 mL ACK lysis buffer for 5 minutes at 25°C to lyse remaining red blood cells. After 2 washes in HBSS + 0.1% BSA + 0.5 mM EDTA (Flow Buffer), $2.5x10^5$ cells were blocked with α-CD16/32 antibody (Biolegend #101302) for 15 minutes on ice. After one wash with Flow Buffer, cells were incubated with Violet LIVE/DEAD Stain (ThermoFisher L34963) and ~0.25 µg/mL antibodies for 30 minutes on ice to stain for cells of interest (α-CD45 – Biolegend #103132; α-CD11b – Biolegend #101226; α-Ly6G – Biolegend #127606, α-Ly6C). To ensure equal volumes of sample were run through flow, absolute counting beads (Fisher Scientific #NC0318024) were used to normalize cell counts. Cells were subsequently washed 2 times with Flow Buffer and analyzed on a BD FACSCanto II. Data was analyzed via FlowJo software package version 16.0 (FlowJo, LLC).

4.3.7 Immunofluorescence

Organs were harvested and fixed in ice-cold PBS + 4% paraformaldehyde for 18–24 h with gentle end- over-end agitation. Fixed organs were placed in 40% sucrose solution overnight. Saturated organs were then submerged in Optimal Cutting Temperature compound (OCT) (Sakura) and flash frozen in cassettes submerged in 2-methylbutane chilled with dry ice. Sections (10 µm) were permeabilized and stained with ~1 µg/mL rabbit anti-myeloperoxidase (Abcam #ab9535), 5 µg/mL rat anti-mouse CD68 (ThermoFisher Scientific #14-0681-82), followed by incubation with goat anti-rabbit AF594 (ThermoFisher Scientific #A11012) and goat anti-rabbit AF488 (ThermoFisher Scientific #A11006). Nuclei were visualized using mounting medium containing DAPI (ThermoFisher Scientific). Sections were mounted on glass slides under #1.5 coverslips. Images were acquired with an inverted Zeiss LSM 880 confocal with FAST AiryScan, using either a 10X Plan-Apochromat 0.45NA objective or a 40X LD LCI Plan-Apochromat 1.2NA immersion objective as indicated in the figure legend. Images were processed using the in line AiryScan processing module in Zen Black.

4.3.8 Intravital Microscopy

Mice were anesthetized with isoflurane inhalation and were kept on a 37°C heating pad throughout the experiments. All images were taken with an Leica SP8 Upright Confocal DM600 CFS confocal microscope equipped with a resonant scanner via a cover slip corrected x25, 0.95 NA water immersion objective (Leica Microsystems, Buffalo Groove, IL).In the sterile injury experiments, mice were injected retro-orbitally with 5 µl (2.5 µg) Ly6G-AF647 antibody (Clone 2A8, Biolegend, San Diego, CA) in 100 µl sterile Ca2+/Mg2+-free PBS (Gibco, Thermo Fisher Scientific, USA). The abdominal wall was opened with a transverse scission along the costal margin and the left liver lobe was immobilized against a coverslip with a suction ring [48]. Around the suction ring, the wound was covered with sterile wet gauze to mitigate desiccation. An area in

the sinusoids with little motion artefact was chosen and a focal burn injury was applied via 2 sec long illumination with high-power two-photon laser beam on a ~250 μm^2 area. An ~40,000 μm^2 area with the burned injury centered was imaged in GFP and AF647 channels over 3 hr in a time-serial, z-stack scanning mode. In septic injury experiments, the left femoral artery was cannulated with a PE-10 tube and the left liver lobe was exteriorized for confocal imaging as described above. The mouse was injected through the femoral artery cannule with 5 µl (2.5 µg) Ly6G-AF647 (Biolegend #127610) in 100 µl of PBS. Four fields of view with low motion artefact and centered on the sinusoids were selected. Imaging was conducted for 3 hr in GFP and Ly6G-AF647 channels in a multi-position, time-serial, z-stack scanning mode. Immediately following imagining initiation, $5x10^7$ cfu of GFP expressing *S. aureus* (described above) suspended in 100 µl Ca2+/Mg2+-free PBS was injected into the femoral artery cannule. Videos were analyzed for neutrophil and *S. aureus* accumulation with the Imaris software (Bitplane, Concord, MA). Neutrophils were tracked via applying area modeling on the AF647 signal. Only neutrophils present in 3 consecutive frames were counted. *S. aureus* was counted via applying spot modeling on the GFP signal.

4.3.9 Statistical Analysis

All statistical analyses were performed in GraphPad Prism Version 8, with a p value < 0.05 considered statistically significant. Unless otherwise indicated, normally distributed pairwise comparisons were performed using a two tailed students T-test, and non-normal distributions were compared using the Mann-Whitney U Test.

4.4 Results

4.4.1 Endothelial heparan sulfate mediates hepatic injury during *S. aureus* sepsis

To examine how vascular HS affects organ pathology, we inactivated *Ndst1* by Tie2-driven expression of Cre recombinase (*Ndst1$^{f/f}$Tie2Cre*) [26]. In prior studies we showed that HS in the vasculature is significantly undersulfated, thereby disrupting native HS-protein interactions that govern HS biological function [26,49]. Incomplete desulfation of the chains occurs because most tissues also express *Ndst2* [50]. Removal of both genes or systemic inactivation of *Ndst1* leads to embryonic or perinatal lethality, respectively, thus necessitating the use of conditional mutants [51–53].

Ndst1$^{f/f}$Tie2Cre mice were challenged with a septic *S. aureus* dose and colony forming units (CFU) were measured in several tissues at multiple time points. Under these conditions, about 50-75% of the animals succumb within 48 hours. *S. aureus* bacteremia and organ CFU were readily detectable 6 hr post-infection (Figure 4.1A-C). Consistent with previous findings, the liver contained the most CFU early in infection (Figure 4.1C) [13,14]. Although bacteremia is stable, organ CFU increased ~8-fold in the kidney and liver by 24 hr post-infection. Interestingly, *Ndst1$^{f/f}$Tie2Cre+* mice did not exhibit as dramatic an increase in liver CFU (≤2-fold on average), with several mice not exhibiting any increase in CFU (Figure 4.1C). Both *Ndst1$^{f/f}$Tie2Cre-* and *Ndst1$^{f/f}$Tie2Cre+* mice exhibited similar increases in kidney CFU and had similar bacteremia, indicating that modification of vascular HS differentially impacts *S. aureus* infection depending upon the organ.

Liver pathology was analyzed to explore the impact of altering vascular HS. After *S. aureus* challenge, the liver undergoes significant coagulopathy that occludes the vasculature and leads to subsequent necrosis of the surrounding parenchyma that is readily visible by gross pathology (Figure 4.1D) [13]. Strikingly, *Ndst1$^{f/f}$Tie2Cre+* exhibited fewer visible necrotic lesions 24 hr post-infection (Figure 4.1D). In *S. aureus* infected *Ndst1$^{f/f}$Tie2Cre-* mice, liver thromboses begin to

develop early after infection. At 6 hr post-infection, *Ndst1$^{f/f}$Tie2Cre-* mice have neutrophilic collections in larger vessels that propagate thromboses (Figure 4.1E) [54,55]. At 12 hr post-infection, intense thromboses are readily apparent, with neutrophils surrounding the thrombi, and the beginnings of hepatic necrosis are observable. At 24 hr post-infection, there is complete occlusion of many vessels with large areas of necrosis that often contain bacterial colonies, which correlates with the large increase in *S. aureus* CFU at 24 hr post-infection. In *Ndst1$^{f/f}$Tie2Cre+* mice, liver pathology is reduced at all observed stages of infection, with tissue perfusion still occurring 24 hr post-infection and a lack of necrotic regions (Figure 4.1E-F). Liver damage serum markers coincided with liver pathology (Figure 4.1G-H). *Ndst1$^{f/f}$Tie2Cre-* mice exhibited dramatic increases in serum alanine aminotransferase (ALT) and aspartate aminotransferase (AST) at 12 and 24 hr post-infection. *Ndst1$^{f/f}$Tie2Cre+* mice also had increases in these markers, albeit significantly less than *Ndst1$^{f/f}$Tie2Cre-* mice (Figure 4.1G-H). Importantly, reducing vascular HS sulfation did not affect kidney damage markers in the serum during sepsis, which indicates that altering vascular HS does not impact damage across all organs (Figure 4.1I).

Tie2 driven inactivation of genes can result in recombination of "floxed" genes in the hematopoietic lineage in addition to the endothelium [56]. Both myeloid and platelet lineages contribute to *S. aureus* induced liver damage [47]. To test if myeloid and platelet specific *Ndst1* inactivation blocks liver damage in *S. aureus* sepsis, *Ndst1* was inactivated selectively in myeloid cells and platelets using a combination of *LysMCre* and *PF4Cre*, respectively (*Ndst1$^{f/f}$LysM/PF4Cre*). *Ndst1$^{f/f}$LysM/PF4Cre+* mice had the same levels of liver CFU and damage markers as *Ndst1$^{f/f}$LysM/PF4Cre-* mice 24 hr post-infection (Figure 4.1J-L), indicative that reducing endothelial HS sulfation drives the hepatoprotective phenotype.

4.4.2 Undersulfation of heparan sulfate reduces neutrophil trafficking to the liver during *S. aureus* sepsis

Neutrophilic infiltration is required for the hepatic damage induced by *S. aureus* sepsis. Neutrophils bind to HA deposited in the sinusoidal glycocalyx to sequester neutrophils to the inflamed liver vasculature early after infection, whereupon they promote inflammation and vascular coagulation [14,18]. Further, depletion of neutrophils completely abolishes *S. aureus* induced hepatotoxicity [14]. Although it was shown that endothelial HS regulates neutrophil trafficking in the peripheral vasculature, the role of endothelial HS in neutrophil trafficking to the liver or any major organ has not been explored. To test if altering endothelial HS causes a leukocyte trafficking deficiency, a flow cytometry method was developed to count the number of neutrophils and monocytes that traffic to the liver early after *S. aureus* infection (Figure 4.2A). A dramatic increase in liver neutrophil infiltration into the liver occurs in *Ndst1$^{f/f}$Tie2Cre-* mice 6 hr post-infection. However, the extent of infiltration in the livers of *Ndst1$^{f/f}$Tie2Cre+* mice neutrophils was reduced ~2-fold (Figure 4.2B-C), consistent with trafficking deficiencies observed in the skin of these mice using air pouch models [26]. Monocytes also infiltrated the liver but did differ in the mutant (Figure 4.2D). Circulating neutrophil and monocyte counts also did not differ in mutant and wild-type mice, in both uninfected and infected mice (Figure 4.2E-F), suggesting that the difference in neutrophil counts in the liver were not due to differential blood counts. Immunofluorescent staining of liver sections revealed that *Ndst1$^{f/f}$Tie2Cre-* mice had extensive sinusoidal myeloperoxidase (MPO) (Figure 2G-H), consistent with neutrophils infiltrating the liver and sequestering to the sinusoids during *S. aureus* sepsis [14]. MPO stained cells were not as prominent in *Ndst1$^{f/f}$Tie2Cre+* liver, indicative of fewer infiltrating neutrophils (Figure 2I-J). The reduction

of neutrophil infiltration diminishes liver damage in *S. aureus* sepsis, thus reducing neutrophil trafficking in *Ndst1*-deficient mice likely spares the organ from severe hepatoxicity.

4.4.3 Heparan sulfate mediates neutrophil trafficking in the liver during sterile and non-sterile inflammation

Next, we used intravital microscopy (IVM) to measure the kinetics of neutrophil trafficking. GFP+ *S. aureus* were injected i.v. and were instantly visible and adherent within the liver sinusoids. Bacteria cease to circulate by 20 minutes post-injection (Video 1). The majority of bacteria adhere to resident macrophage KCs [57] and neutrophils, and some neutrophils appear to phagocytose *S. aureus* and continue to traffic through the liver vasculature (Video 2). Altering vascular HS did not affect bacteria-neutrophil colocalization 20 minutes post-infection (Figure 4.3A). *Ndst1$^{f/f}$Tie2Cre-* mice exhibited detectable increases in neutrophil count a few minutes after injection, with neutrophil counts increasing over the first hour of infection (Figure 4.3B-D, Video 3). In contrast, *Ndst1$^{f/f}$Tie2Cre+* mice showed only a marginal increase in neutrophil counts over the first hour after infection (Figure 4.3E-G, Video 3). Rapid neutrophil recruitment occurred within the first 20 minutes of infection and over the next 60 minutes, but *Ndst1$^{f/f}$Tie2Cre+* mice exhibited a neutrophil recruitment rate of ~50% what is observed in *Ndst1$^{f/f}$Tie2Cre-* mice (Figure 4.3H-I), consistent with the defect observed at 6 hr post-infection (Figure 4.2C). *S. aureus* counts slowly declined over time but did not differ in mutant and wild-type animals (Figure 4.3J).

Neutrophil trafficking during sterile liver inflammation is based upon an integrin-dependent mechanism and not on HA [19]. To determine if vascular HS modulates neutrophil trafficking in sterile inflammation, a focal sterile injury was applied to the livers of *Ndst1$^{f/f}$Tie2Cre* mice with a two-photon laser and neutrophils were tracked using IVM. Immediately following sterile injury, neutrophils were attracted to the injury site in *Ndst1$^{f/f}$Tie2Cre-* mice (Figure 4.4A,C,

Video 4), but neutrophil trafficking to the injury site was blunted in *Ndst1$^{f/f}$Tie2Cre+* mice (Figure 4.4B-C, Video 4). Endothelial HS has previously been shown to act as a ligand for L-selectin during neutrophil rolling [26,27]. However, altering endothelial HS did not change trafficking characteristics such as mean speed, speed variance, or track straightness during sterile liver inflammation, suggesting that L-selectin mediated tethering might not be affected in the mutant (Figure 4.4D-F).

4.5 Discussion

In summary, these findings show that HS, a critical component of the vascular glycocalyx, facilitates rapid neutrophil recruitment in both sterile and *S. aureus* induced inflammation in the liver. Thus, we can now extend our earlier studies that showed that altering the structure of HS decreased neutrophil infiltration induced by acute inflammatory challenges. Further studies are needed to understand the mechanism by which HS mediates neutrophil migration in the liver and how this system is coordinated with CD44-HA interactions.

Studies of the glycocalyx during bacterial infection or sepsis have focused on the impact of shedding on individual organ function. In the liver, the vascular glycocalyx and other host factors assist with filtering and clearing circulating bacteria [14,57–59]. KCs bind to and sequester circulating complement-tagged bacteria, and we showed neutrophils exhibit similar filtering behavior (Video 2, Figure S3A). After bacteria are quickly ensnared in the liver, HA, which is abundant in the liver sinusoids at baseline, sequesters neutrophils upon bacterial insult [14,18]. We have shown that endothelial HS also plays a role with rapid neutrophil recruitment upon infection. With both HA and HS, the liver vascular glycocalyx appears “primed” for septic inflammatory insults that suits the function of the organ. Upon bacterial entrapment in the liver, the vascular

glycocalyx promotes an immediate neutrophilic response that promotes removal of the pathogen, or in cases of high bacterial load, leads to a hyper-inflammatory and pathological state.

The mechanism of neutrophil adherence and sequestration in the liver is dependent upon the inflammatory insult, with sterile injury using an integrin-based adhesion mechanism and septic inflammation utilizing an HA-dependent process that involves binding of CD44 on neutrophils to HA produced by the endothelium [14,18,19]. Our work shows that vascular HS is important for attracting neutrophils in both types of inflammation. However, additional studies are needed to understand the mechanism of HS-dependent neutrophil recruitment.

Our previous studies showed that each organ's vascular glycocalyx undergoes unique changes during sepsis that reflect the organ microenvironment [13]. These compositional analyses, and subsequent genetic manipulation, give critical insight into why certain organs are prone to failure in sepsis since the glycocalyx is critical to vascular function [60]. Understanding how the organ-vascular interface changes in sepsis and fuels organ dysfunction could provide critical information on how to support organs prone to failure, thus promoting positive outcomes in sepsis [4]. Future efforts will focus on increasing the molecular and temporal resolution of the vascular glycocalyx in sepsis and how genetically altering critical components impacts sepsis outcome in an organotypic manner.

4.6 Acknowledgements

Chapter 4, in part, is being formulated into a manuscript for publication of the material. GJ Golden, A Gomez Toledo, A Marki, C Morris, RJ Riley, Q Chen, I Cornax, N Varki, D Le, K Ley, V Nizet, and JD Esko. The dissertation author is the primary investigator and author of this material. We would like to thank the study participants and their loved ones. Special thanks to the UCSD Mouse Phenotyping Core, especially Michelle Abueg for hematology and Sandra Bretton

for histology. Thank you to the La Jolla Institute of Immunology Microscopy and Histology Core, in particular Zbigniew Mikulski and Sara McArdle for intravital microscopy insight and Angela Denn for histology. Thank you to the UCSD Microscopy Core, especially Jennifer Santini and Marcy Erb, for their assistance with immunofluorescence. Additional thanks to James Sorrentino for discussing statistical analyses, and to all the Jeffrey Esko and Victor Nizet lab members for their insight into developing this research. The authors declare no competing financial interests. Funding sources include: NHLBI P01 HL131474 to J.D.E., UCSD Microbial Sciences Graduate Research Initiative 1-F17GG and 1-F18GG to G.J.G., and NINDS P30 NS047101 to UCSD Microscopy.

4.7 Figures

Figure 4.1 Endothelial heparan sulfate mediates liver damage during *S. aureus* sepsis. (A) Liver, (B) kidney, and (C) blood CFU from the indicated time points. n ≥7 per group. Boxes indicate min, max, and quartile datapoints. ** indicates $p<0.01$ as determined by a Mann-Whitney U-test due to non-normal distribution of datapoints. (D) Representative liver gross pathology 24 hr post-infection. Pale lesions demark necrotic occlusions. (E) Representative liver pathology at the indicated timepoints post-infection. Red thrombi (red arrow) occlude vessels that form necrotic lesions (yellow arrow) that may contain bacterial colonies (blue arrow). Scale bars = 100 μm. (F) Liver pathology scores 24 hr post-infection. n=7-8 per group. Scores were assigned from 0 = no pathology to 4 = severe pathology. (G) Serum ALT and (H) AST levels across the indicated timepoints. n≥7 per group. Errors bars represent mean +/- SEM. ** indicates $p<0.01$ and *** indicates $p<0.001$ as determined by a 2-way ANOVA with Sidak's multiple comparison test between genotypes. (I) Serum blood urea nitrogen levels across the indicated timepoints post-infection. n=7 per group. Error bars represent mean +/- SEM. (J) Liver CFU from 24 hr post-infection. n =9-12 per group. Boxes indicate min, max, and quartile datapoints. (K) Serum ALT and (L) AST levels from 24 hr post-infection. n=9-12 mice per group. Errors bars represent mean +/- SEM.

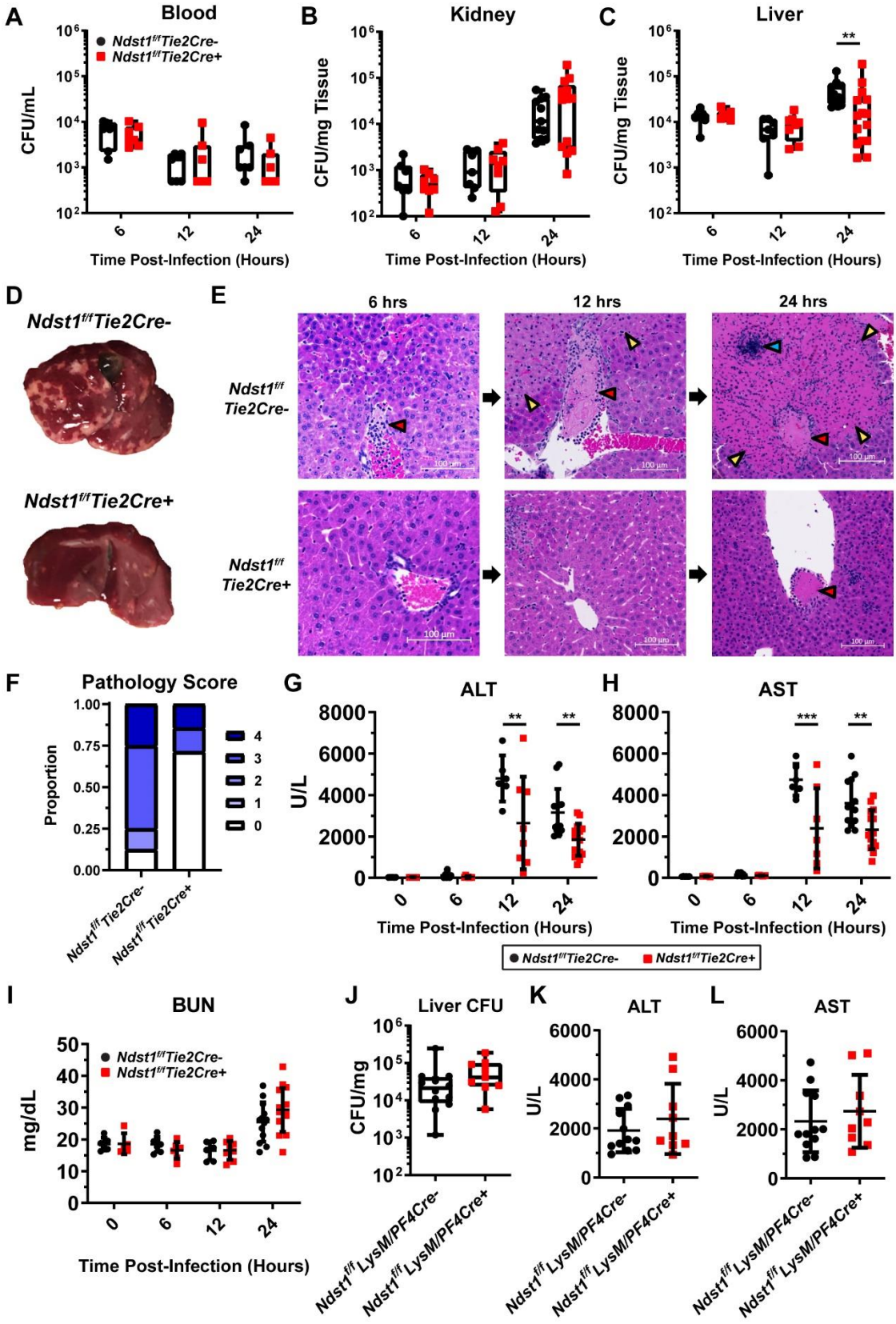
A
Blood
CFU/mL
Ndst1f/fTie2Cre-
Ndst1f/fTie2Cre+
Time Post-Infection (Hours)
B
Kidney
CFU/mg Tissue
Time Post-Infection (Hours)
C
Liver
CFU/mg Tissue
**
Time Post-Infection (Hours)
D
Ndst1f/fTie2Cre-
Ndst1f/fTie2Cre+
E
6 hrs
12 hrs
24 hrs
Ndst1f/f Tie2Cre-
Ndst1f/f Tie2Cre+
100 µm
F
Pathology Score
Proportion
4
3
2
1
0
Ndst1f/fTie2Cre-
Ndst1f/fTie2Cre+
G
ALT
U/L
**
**
Time Post-Infection (Hours)
H
AST
***
**
Time Post-Infection (Hours)
Ndst1f/fTie2Cre-
Ndst1f/fTie2Cre+
I
BUN
mg/dL
Ndst1f/fTie2Cre-
Ndst1f/fTie2Cre+
Time Post-Infection (Hours)
J
Liver CFU
CFU/mg
Ndst1f/f LysM/PF4Cre-
Ndst1f/f LysM/PF4Cre+
K
ALT
U/L
Ndst1f/f LysM/PF4Cre-
Ndst1f/f LysM/PF4Cre+
L
AST
U/L
Ndst1f/f LysM/PF4Cre-
Ndst1f/f LysM/PF4Cre+

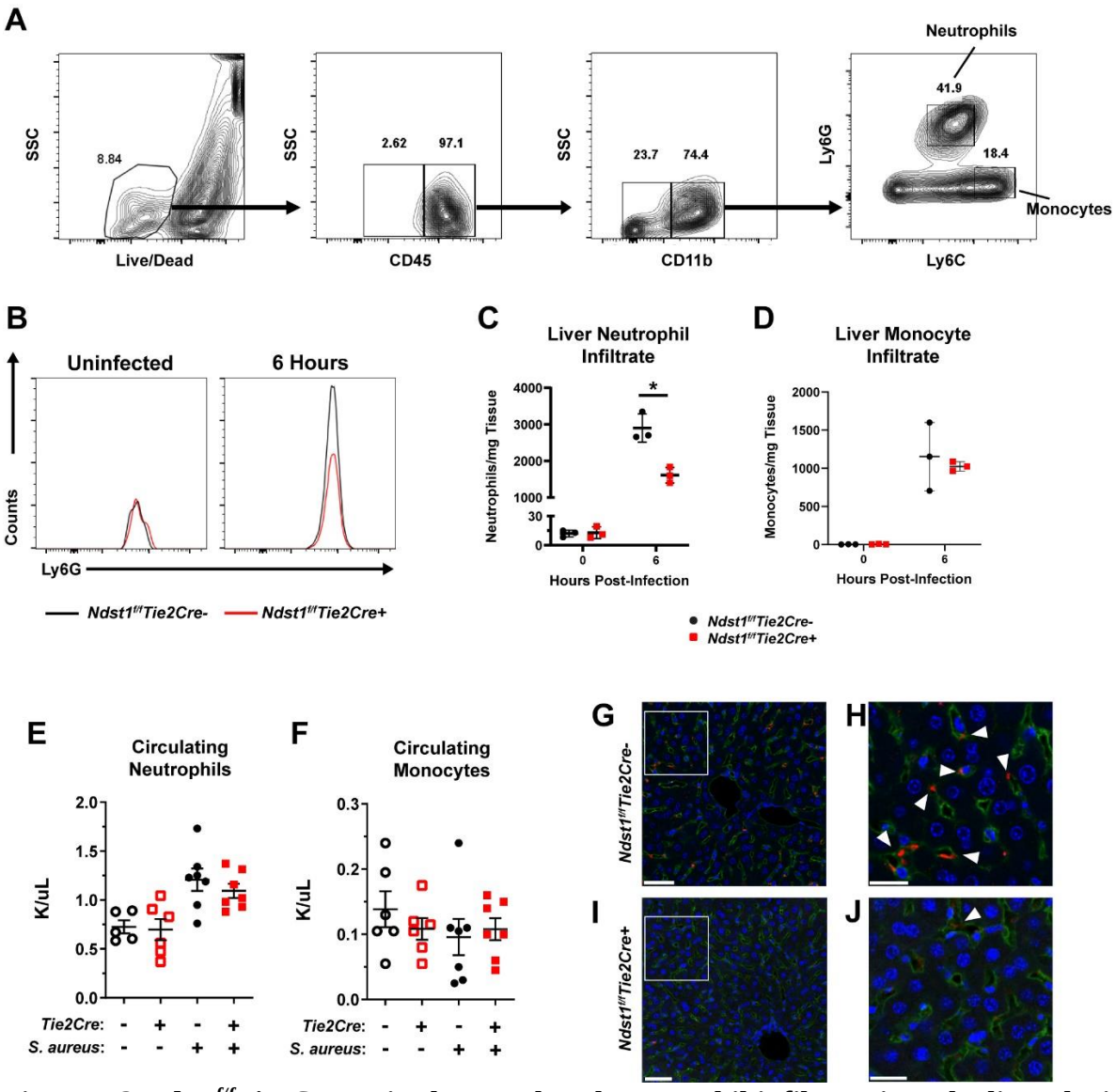

Figure 4.2 *Ndst1$^{f/f}$Tie2Cre+* mice have reduced neutrophil infiltrate into the liver during *S. aureus* sepsis. (A) Representative flow cytometry workflow of CD45^{+}CD11b^{+}Ly6G^{+} neutrophil and CD45^{+}CD11b^{+}Ly6C^{hi} monocyte infiltrate in the liver. (B) Representative flow distributions of neutrophils (Ly6G+) from uninfected and 6 hr post-infection livers. (C) Neutrophil counts per mg liver at indicated timepoints, as determined by flow cytometry. n=3 per genotype, and is representative of 3 independent experiments. * indicates $p<0.05$. (D) Monocyte counts in the liver as counted by flow cytometry at the indicated timepoints. Representative of 3 experiments. (E) Neutrophil and (F) monocyte counts in the blood in healthy or 18 hr post-infection mice. (G-J) Representative immunofluorescent images of liver 6 hr post-infection. Green = CD68 (macrophages and endothelial cells), red = MPO, blue = DAPI. (G) Representative immunofluorescent image of *Ndst1$^{f/f}$Tie2Cre-* liver. (H) Magnified area indicated in G. Arrows indicate sinusoidal MPO. (I) Representative immunofluorescent image of *Ndst1$^{f/f}$Tie2Cre+* liver. (J) Magnified area indicated in I. In C and E scale bars = 100 μm and in D and F scale bars = 25 μm.

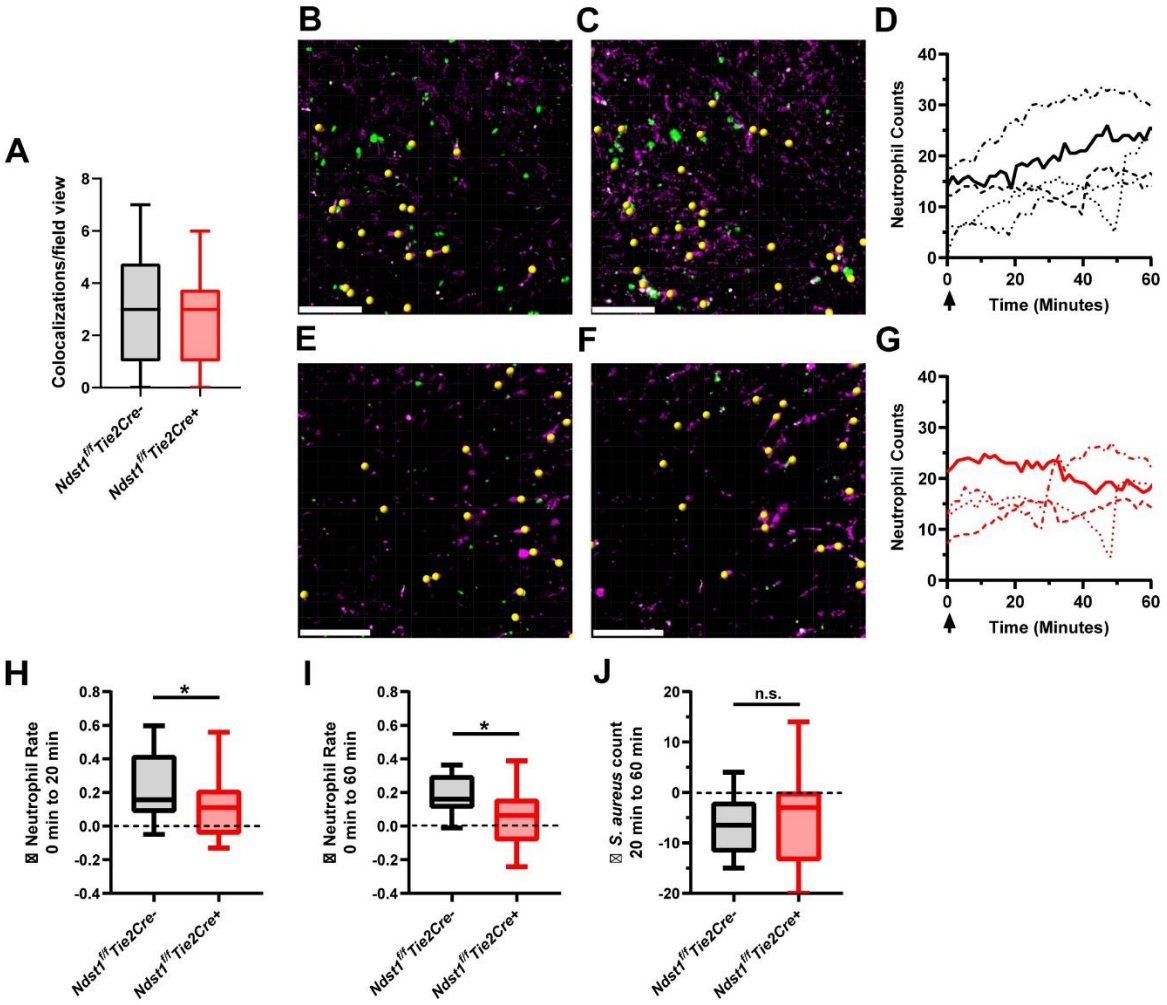

Figure 4.3 Immediate neutrophil trafficking after *S. aureus* infection is reduced in *Ndst1$^{f/f}$Tie2Cre*+ mice. (A) Counts of bacteria-neutrophil colocalization events 20 minutes post infection with *S. aureus*. Each datapoint represents 1 FOV, with n=4 FOV per mouse and n=4-5 mice per genotype. (B) Representative intra-vital image of liver from a *Ndst1$^{f/f}$Tie2Cre*- mouse immediately post-i.v. infection of *S. aureus* (green) and (C) 60 min post-infection. B and C are the same FOV. Neutrophils are demarked by yellow spheres. Ly6G antibody (magenta) strongly labels neutrophils, as well as lightly labeled non-specific staining (magenta that is not marked with a yellow sphere). (D) Liver neutrophil counts over time as tracked by IVM in *Ndst1$^{f/f}$Tie2Cre*- mice. Each line represents counts from 4 FOVs per mouse, with single data points determined by averaging neutrophil counts from the 4 FOVs. Black arrow denotes time of *S. aureus* injection. (E) Representative intra-vital image of liver from a *Ndst1$^{f/f}$Tie2Cre*+ mouse immediately post-infection and (F) 60 min post-infection. All colors and markings are the same as in B and C. (G) Liver neutrophil counts over time as tracked by IVM in *Ndst1$^{f/f}$Tie2Cre*+ mice. Data generated as in C. (H) Rates of neutrophil recruitment for 20 min and (I) 60 min post-infection as determined by IVM. (J) Change in *S. aureus* count from 20 min to 60 min post-infection. For G-I, each datapoint represents 1 FOV, with n=4 FOV per mouse and n=4-5 mice per genotype. Box and whisker plots are min to max with quartiles demarked. * is $p<0.05$.

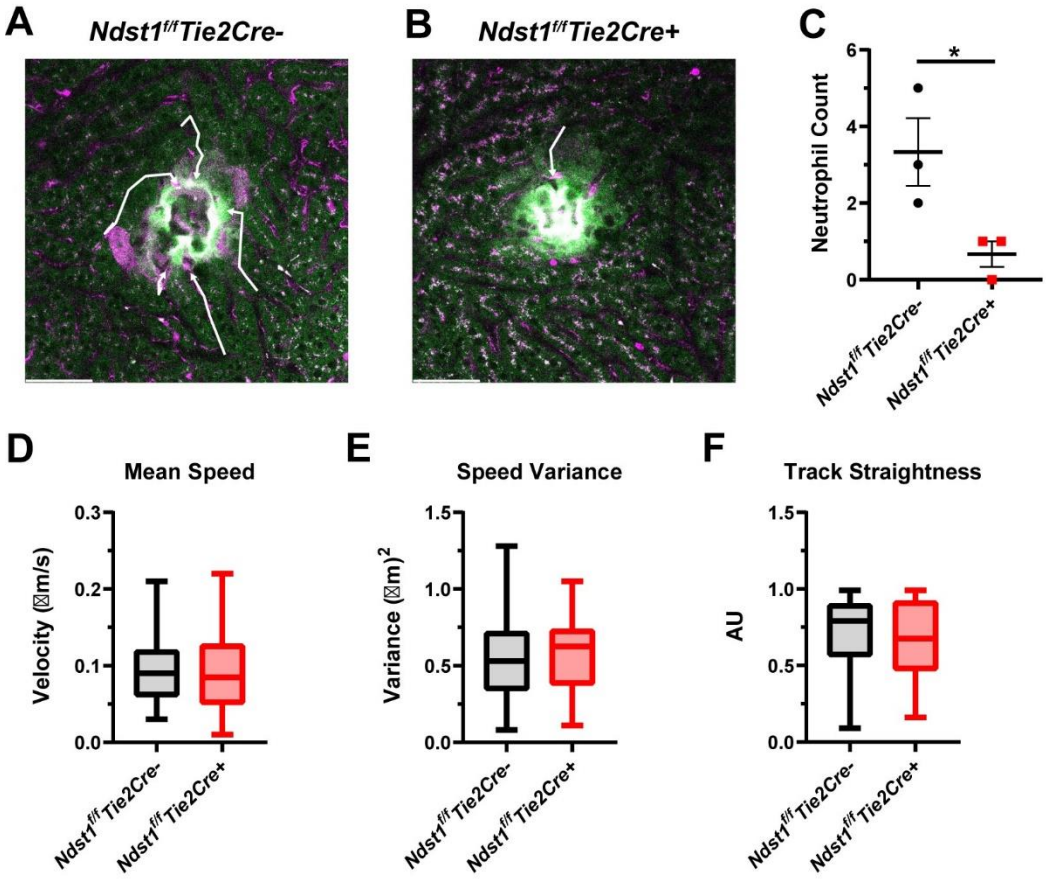

Figure 4.4 Liver infiltration is reduced in *Ndst1$^{f/f}$Tie2Cre+* mice during sterile injury. (A) Representative intravital image of *Ndst1$^{f/f}$Tie2Cre-* and (B) *Ndst1$^{f/f}$Tie2Cre+* livers 20 min after sterile injury. Ly6G+ neutrophils (magenta) that trafficked to the injury are denoted by white arrows. Autofluorescence was used to visualize the injury (green) and surrounding hepatocytes (light green). (C) Number of neutrophils that reach the injury within 20 min of insult. Each point represents 1 FOV in 1 mouse. Each mouse is an independent experiment. * is $p<0.05$. (D) Mean speed, (E) speed variance, and (F) track straightness of neutrophils that reached the sterile wound. For D-F, each data point represents a single neutrophil that reached the wound over a 3 hr timespan with n≥36 with data pooled across 3 mice per genotype. For D-F, box and whisker plots are min to max with quartiles demarked.

4.8 References

1. Singer, M., Deutschman, C. S., Seymour, C. W., Shankar-Hari, M., Annane, D., Bauer, M., Bellomo, R., Bernard, G. R., Chiche, J.-D., Coopersmith, C. M., Hotchkiss, R. S., Levy, M. M., Marshall, J. C., Martin, G. S., Opal, S. M., Rubenfeld, G. D., van der Poll, T., Vincent, J. & Angus, D. C. The Third International Consensus Definitions for Sepsis and Septic Shock (Sepsis-3). *JAMA* **315,** 801–10 (2016).

2. Rossaint, J. & Zarbock, A. Pathogenesis of multiple organ failure in sepsis. *Crit. Rev. Immunol.* **35,** 277–291 (2015).

3. Van Der Poll, T., Van De Veerdonk, F. L., Scicluna, B. P. & Netea, M. G. The immunopathology of sepsis and potential therapeutic targets. *Nat. Rev. Immunol.* **17,** 407–420 (2017).

4. Lelubre, C. & Vincent, J. L. Mechanisms and treatment of organ failure in sepsis. *Nat. Rev. Nephrol.* **14,** 417–427 (2018).

5. Marshall, J. C. Why have clinical trials in sepsis failed? *Trends Mol. Med.* **20,** 195–203 (2014).

6. Reitsma, S., Slaaf, D. W., Vink, H., Van Zandvoort, M. A. M. J. & Oude Egbrink, M. G. A. The endothelial glycocalyx: Composition, functions, and visualization. *Pflugers Arch. Eur. J. Physiol.* **454,** 345–359 (2007).

7. Vink, H. & Duling, B. R. Identification of distinct luminal domains for macromolecules, erythrocytes, and leukocytes within mammalian capillaries. *Circ. Res.* **79,** 581–589 (1996).

8. Sieve, I., Münster-Kühnel, A. K. & Hilfiker-Kleiner, D. Regulation and function of endothelial glycocalyx layer in vascular diseases. *Vascul. Pharmacol.* **100,** 26–33 (2018).

9. Schmidt, E. P., Yang, Y., Janssen, W. J., Gandjeva, A., Perez, M. J., Barthel, L., Zemans, R. L., Bowman, J. C., Koyanagi, D. E., Yunt, Z. X., Smith, L. P., Cheng, S. S., Overdier, K. H., Thompson, K. R., Geraci, M. W., Douglas, I. S., Pearse, D. B. & Tuder, R. M. The pulmonary endothelial glycocalyx regulates neutrophil adhesion and lung injury during experimental sepsis. *Nat Med* **18,** 1217–1223 (2012).

10. Marki, A., Esko, J. D., Pries, A. R. & Ley, K. Role of the endothelial surface layer in neutrophil recruitment. *J. Leukoc. Biol.* **98,** 503–515 (2015).

11. Iba, T. & Levy, J. H. Derangement of the endothelial glycocalyx in sepsis. *J. Thromb. Haemost.* **17,** 283–294 (2019).

12. Yang, Y., Haeger, S. M., Suflita, M. A., Zhang, F., Dailey, K. L., Colbert, J. F., Ford, J. A., Picon, M. A., Stearman, R. S., Lin, L., Liu, X., Han, X., Linhardt, R. J. & Schmidt, E. P. Fibroblast growth factor signaling mediates pulmonary endothelial glycocalyx reconstitution. *Am. J. Respir. Cell Mol. Biol.* **56,** 727–737 (2017).

13. Gómez Toledo, A., Golden, G., Campos, A. R., Cuello, H., Sorrentino, J., Lewis, N., Varki, N., Nizet, V., Smith, J. W. & Esko, J. D. Proteomic atlas of organ vasculopathies triggered by Staphylococcus aureus sepsis. *Nat. Commun.* **10,** (2019).

14. Kolaczkowska, E., Jenne, C. N., Surewaard, B. G. J., Thanabalasuriar, A., Lee, W. Y., Sanz, M. J., Mowen, K., Opdenakker, G. & Kubes, P. Molecular mechanisms of NET formation and degradation revealed by intravital imaging in the liver vasculature. *Nat. Commun.* **6,** 1–13 (2015).

15. Surewaard, B. G. J., Deniset, J. F., Zemp, F. J., Amrein, M., Otto, M., Conly, J., Omri, A., Yates, R. M. & Kubes, P. Identification and treatment of the Staphylococcus aureus reservoir in vivo. *J. Exp. Med.* **213,** 1141–1151 (2016).

16. Zeng, Z., Surewaard, B. G. J., Wong, C. H. Y., Geoghegan, J. A., Jenne, C. N. & Kubes, P. CRIg Functions as a Macrophage Pattern Recognition Receptor to Directly Bind and Capture Blood-Borne Gram-Positive Bacteria. *Cell Host Microbe* **20,** 99–106 (2016).

17. Engelmann, B. & Massberg, S. Thrombosis as an intravascular effector of innate immunity. *Nat. Rev. Immunol.* **13,** 34–45 (2013).

18. Mcdonald, B., Mcavoy, E. F., Lam, F., Gill, V., Motte, C. De, Savani, R. C. & Kubes, P. Interaction of CD44 and hyaluronan is the dominant mechanism for neutrophil sequestration in inflamed liver sinusoids. *J. Exp. Med.* **205,** 915–927 (2008).

19. Mcdonald, B., Pittman, K., Menezes, G. B., Hirota, S. a, Slaba, I., Waterhouse, C. C. M., Beck, P. L., Muruve, D. a & Kubes, P. Intravascular Danger Signals Guide Neutrophils to Sites of Sterile Inflammation. *Science (80-.).* **330,** 362–367 (2011).

20. Fuster, M. M. & Wang, L. Endothelial heparan sulfate in angiogenesis. *Prog. Mol. Biol. Transl. Sci.* **93,** 179–212 (2010).

21. Bishop, J. R., Schuksz, M. & Esko, J. D. Heparan sulphate proteoglycans fine-tune mammalian physiology. *Nature* **446,** 1030–1037 (2007).

22. Kusche-Gullberg, M. & Kjellén, L. Sulfotransferases in glycosaminoglycan biosynthesis. *Curr. Opin. Struct. Biol.* **13,** 605–611 (2003).

23. Esko, J. D. & Lindahl, U. Molecular diversity of heparan sulfate. *J. Clin. Invest.* **108,** 169–173 (2001).

24. Xu, D. & Esko, J. D. Demystifying heparan sulfate-protein interactions. *Annu. Rev. Biochem.* **83,** 129–157 (2014).

25. Tsuboi, K., Hirakawa, J., Seki, E., Imai, Y., Yamaguchi, Y., Fukuda, M. & Kawashima, H. Role of high endothelial venule-expressed heparan sulfate in chemokine presentation and lymphocyte homing. *J Immunol* **191,** 448–455 (2013).

26. Wang, L., Fuster, M., Sriramarao, P. & Esko, J. D. Endothelial heparan sulfate deficiency

impairs L-selectin- and chemokine-mediated neutrophil trafficking during inflammatory responses. *Nat. Immunol.* **6,** 902–10 (2005).

27. Axelsson, J., Xu, D., Kang, B. N., Nussbacher, J. K., Handel, T. M., Ley, K., Sriramarao, P. & Esko, J. D. Inactivation of heparan sulfate 2- O -sulfotransferase accentuates neutrophil infiltration during acute inflammation in mice. *Blood* **120,** 1742–1751 (2012).

28. Massena, S., Christoffersson, G., Hjertström, E., Zcharia, E., Vlodavsky, I., Ausmees, N., Rolny, C., Li, J. P. & Phillipson, M. A chemotactic gradient sequestered on endothelial heparan sulfate induces directional intraluminal crawling of neutrophils. *Blood* **116,** 1924–1931 (2010).

29. Campanella, G. S. V., Grimm, J., Manice, L. A., Colvin, R. A., Medoff, B. D., Wojtkiewicz, G. R., Weissleder, R. & Luster, A. D. Oligomerization of CXCL10 Is Necessary for Endothelial Cell Presentation and In Vivo Activity. *J. Immunol.* **177,** 6991–6998 (2006).

30. Sarris, M., Masson, J. B., Maurin, D., Van Der Aa, L. M., Boudinot, P., Lortat-Jacob, H. & Herbomel, P. Inflammatory Chemokines Direct and Restrict Leukocyte Migration within Live Tissues as Glycan-Bound Gradients. *Curr. Biol.* **22,** 2375–2382 (2012).

31. Middleton, J., Neil, S., Wintle, J., Clark-Lewis, I., Moore, H., Charles, L., Auer, M., Elin, H. & Antal, R. Transcytosis and surface presentation of IL-8 by venular endothelial cells. *Cell* **91,** 385–395 (1997).

32. Weber, M., Hauschild, R., Schwarz, J., Moussion, C., De Vries, I., Legler, D. F., Luther, S. A., Bollenbach, T. & Sixt, M. Interstitial dendritic cell guidance by haptotactic chemokine gradients. *Science (80-.).* **339,** 328–332 (2013).

33. Bao, X., Moseman, E. A., Saito, H., Petryanik, B., Thiriot, A., Hatakeyama, S., Ito, Y., Kawashima, H., Yamaguchi, Y., Lowe, J. B., von Andrian, U. H. & Fukuda, M. Endothelial heparan sulfate controls chemokine presentation in recruitment of lymphocytes and dendritic cells to lymph nodes. *Immunity* **33,** 817–829 (2010).

34. Arnold, K., Xu, Y., Sparkenbaugh, E. M., Li, M., Han, X., Zhang, X., Xia, K., Piegore, M., Zhang, F., Zhang, X., Henderson, M., Pagadala, V., Su, G., Tan, L., Park, P. W., Stravitz, R. T., Key, N. S., Linhardt, R. J., Pawlinski, R., Xu, D. & Liu, J. Design of anti-inflammatory heparan sulfate to protect against acetaminophen-induced acute liver failure. *Sci. Transl. Med.* **12,** 1–12 (2020).

35. Boff, D., Crijns, H., Janssens, R., Vanheule, V., Menezes, G. B., Macari, S., Silva, T. A., Amaral, F. A. & Proost, P. The chemokine fragment CXCL9(74–103) diminishes neutrophil recruitment and joint inflammation in antigen-induced arthritis. *J. Leukoc. Biol.* **104,** 413–422 (2018).

36. Vanheule, V., Boff, D., Mortier, A., Janssens, R., Petri, B., Kolaczkowska, E., Kubes, P., Berghmans, N., Struyf, S., Kungl, A. J., Teixeira, M. M., Amaral, F. A. & Proost, P. CXCL9-derived peptides differentially inhibit neutrophil migration in vivo through

interference with glycosaminoglycan interactions. *Front. Immunol.* **8,** 1–14 (2017).

37. Vanheule, V., Janssens, R., Boff, D., Kitic, N., Berghmans, N., Ronsse, I., Kungl, A. J., Amaral, F. A., Teixeira, M. M., Van Damme, J., Proost, P. & Mortier, A. The positively charged COOH-terminal glycosaminoglycan-binding CXCL9(74-103) peptide inhibits CXCL8-induced neutrophil extravasation and monosodium urate crystal-induced gout in mice. *J. Biol. Chem.* **290,** 21292–21304 (2015).

38. Park, P. W., Pier, G. B., Hinkes, M. T. & Bernfield, M. Exploitation of syndecan-1 shedding by Pseudomonas aeruginosa enhances virulence. *Nature* **411,** 98–102 (2001).

39. Haynes, A., Ruda, F., Oliver, J., Hamood, A. N., Griswold, J. A., Park, P. W. & Rumbaugh, K. P. Syndecan 1 shedding contributes to Pseudomonas aeruginosa sepsis. *Infect. Immun.* **73,** 7914–7921 (2005).

40. Hayashida, K., Chen, Y., Bartlett, A. H. & Pyong, W. P. Syndecan-1 is an in vivo suppressor of gram-positive toxic shock. *J. Biol. Chem.* **283,** 19895–19903 (2008).

41. Hayashida, A., Bartlett, A. H., Foster, T. J. & Park, P. W. Staphylococcus aureus beta-toxin induces lung injury through syndecan-1. *Am. J. Pathol.* **174,** 509–18 (2009).

42. Hippensteel, J. A., Anderson, B. J., Orfila, J. E., McMurtry, S. A., Dietz, R. M., Su, G., Ford, J. A., Oshima, K., Yang, Y., Zhang, F., Han, X., Yu, Y., Liu, J., Linhardt, R. J., Meyer, N. J., Herson, P. S. & Schmidt, E. P. Circulating heparan sulfate fragments mediate septic cognitive dysfunction. *J. Clin. Invest.* (2019). doi:10.1172/JCI124485

43. Schmidt, E. P., Overdier, K. H., Sun, X., Lin, L., Liu, X., Yang, Y., Ammons, L. A., Hiller, T. D., Suflita, M. A., Yu, Y., Chen, Y., Zhang, F., Burlew, C. C., Edelstein, C. L., Douglas, I. S. & Linhardt, R. J. Urinary glycosaminoglycans predict outcomes in septic shock and ARDS. *Am. J. Respir. Crit. Care Med.* **Published,** (2016).

44. Steppan, J., Hofer, S., Funke, B., Brenner, T., Henrich, M., Martin, E., Weitz, J., Hofmann, U. & Weigand, M. A. Sepsis and major abdominal surgery lead to flaking of the endothelial glycocalix. *J. Surg. Res.* **165,** 136–141 (2011).

45. Hultén, K. G., Kaplan, S. L., Gonzalez, B. E., Hammerman, W. A., Lamberth, L. B., Versalovic, J. & Mason, E. O. Three-year surveillance of community onset health care-associated Staphylococcus aureus infections in children. *Pediatr. Infect. Dis. J.* **25,** 349–353 (2006).

46. Pang, Y. Y., Schwartz, J., Thoendel, M., Ackermann, L. W., Horswill Alexander R & Nausef, W. M. agr -Dependent Interactions of Staphylococcus aureus USA300 with Human Polymorphonuclear Neutrophils. *J. Innate Immun.* **2,** 546–559 (2010).

47. Powers, M. E., Becker, R. E. N., Sailer, A., Turner, J. R. & Bubeck Wardenburg, J. Synergistic Action of Staphylococcus aureus α-Toxin on Platelets and Myeloid Lineage Cells Contributes to Lethal Sepsis. *Cell Host Microbe* **17,** 775–787 (2015).

48. Looney, M. R., Thornton, E. E., Sen, D., Lamm, W. J., Glenny, R. W. & Krummel, M. F. Stabilized imaging of immune surveillance in the mouse lung. **8,** (2011).

49. Fuster, M. M., Wang, L., Castagnola, J., Sikora, L., Reddi, K., Lee, P. H. A., Radek, K. A., Schuksz, M., Bishop, J. R., Gallo, R. L., Sriramarao, P. & Esko, J. D. Genetic alteration of endothelial heparan sulfate selectively inhibits tumor angiogenesis. *J. Cell Biol.* **177,** 539–549 (2007).

50. Schaum, N., Karkanias, J., Neff, N. F., May, A. P., Quake, S. R., Wyss-Coray, T., Darmanis, S., Batson, J., Botvinnik, O., Chen, M. B., Chen, S., Green, F., Jones, R. C., Maynard, A., Penland, L., Pisco, A. O., Sit, R. V., Stanley, G. M., Webber, J. T., Zanini, F., Baghel, A. S., Bakerman, I., Bansal, I., Berdnik, D., Bilen, B., Brownfield, D., Cain, C., Cho, M., Cirolia, G., Conley, S. D., Demers, A., Demir, K., de Morree, A., Divita, T., du Bois, H., Dulgeroff, L. B. T., Ebadi, H., Espinoza, F. H., Fish, M., Gan, Q., George, B. M., Gillich, A., Genetiano, G., Gu, X., Gulati, G. S., Hang, Y., Hosseinzadeh, S., Huang, A., Iram, T., Isobe, T., Ives, F., Kao, K. S., Karnam, G., Kershner, A. M., Kiss, B. M., Kong, W., Kumar, M. E., Lam, J. Y., Lee, D. P., Lee, S. E., Li, G., Li, Q., Liu, L., Lo, A., Lu, W. J., Manjunath, A., May, K. L., May, O. L., McKay, M., Metzger, R. J., Mignardi, M., Min, D., Nabhan, A. N., Ng, K. M., Noh, J., Patkar, R., Peng, W. C., Puccinelli, R., Rulifson, E. J., Sikandar, S. S., Sinha, R., Szade, K., Tan, W., Tato, C., Tellez, K., Travaglini, K. J., Tropini, C., Waldburger, L., van Weele, L. J., Wosczyna, M. N., Xiang, J., Xue, S., Youngyunpipatkul, J., Zardeneta, M. E., Zhang, F., Zhou, L., Castro, P., Croote, D., DeRisi, J. L., Kuo, C. S., Lehallier, B., Nguyen, P. K., Tan, S. Y., Wang, B. M., Yousef, H., Beachy, P. A., Chan, C. K. F., Huang, K. C., Weinberg, K., Wu, S. M., Barres, B. A., Clarke, M. F., Kim, S. K., Krasnow, M. A., Nusse, R., Rando, T. A., Sonnenburg, J. & Weissman, I. L. Single-cell transcriptomics of 20 mouse organs creates a Tabula Muris. *Nature* **562,** 367–372 (2018).

51. Ringvall, M., Ledin, J., Holmborn, K., Van Kuppevelt, T., Ellin, F., Eriksson, I., Olofsson, A. M., Kjellén, L. & Forsberg, E. Defective heparan sulfate biosynthesis and neonatal lethality in mice lacking N-deacetylase/N-sulfotransferase-1. *J. Biol. Chem.* **275,** 25926–25930 (2000).

52. Forsberg, E. & Kjellén, L. Heparan sulfate : lessons from knockout mice Find the latest version : Heparan sulfate : lessons from knockout mice. *J. Clin. Invest.* **108,** 175–180 (2001).

53. Grobe, K., Inatani, M., Pallerla, S. R., Castagnola, J., Yamaguchi, Y. & Esko, J. D. Cerebral hypoplasia and craniofacial defects in mice lacking heparan sulfate Ndst1 gene function. *Development* **132,** 3777–3786 (2005).

54. Fuchs, T. A., Brill, A., Duerschmied, D., Schatzberg, D., Monestier, M., Myers, D. D., Wrobleski, S. K., Wakefield, T. W., Hartwig, J. H. & Wagner, D. D. Extracellular DNA traps promote thrombosis. *Proc. Natl. Acad. Sci.* **107,** 15880–15885 (2010).

55. von Brühl, M.-L., Stark, K., Steinhart, A., Chandraratne, S., Konrad, I., Lorenz, M., Khandoga, A., Tirniceriu, A., Coletti, R., Köllnberger, M., Byrne, R. A., Laitinen, I.,

Walch, A., Brill, A., Pfeiler, S., Manukyan, D., Braun, S., Lange, P., Riegger, J., Ware, J., Eckart, A., Haidari, S., Rudelius, M., Schulz, C., Echtler, K., Brinkmann, V., Schwaiger, M., Preissner, K. T., Wagner, D. D., Mackman, N., Engelmann, B. & Massberg, S. Monocytes, neutrophils, and platelets cooperate to initiate and propagate venous thrombosis in mice in vivo. *J. Exp. Med.* **209,** 819–835 (2012).

56. Tang, Y., Harrington, A., Yang, X., Friesel, R. E. & Liaw, L. The contribution of the Tie2+ lineage to primitive and definitive hematopoietic cells. *Genesis* **48,** 563–567 (2010).

57. Surewaard, B. G. J., Thanabalasuriar, A., Zheng, Z., Tkaczyk, C., Cohen, T. S., Bardoel, B. W., Jorch, S. K., Deppermann, C., Bubeck Wardenburg, J., Davis, R. P., Jenne, C. N., Stover, K. C., Sellman, B. R. & Kubes, P. α-Toxin Induces Platelet Aggregation and Liver Injury during Staphylococcus aureus Sepsis. *Cell Host Microbe* **24,** 1–14 (2018).

58. Honda, M. & Kubes, P. Neutrophils and neutrophil extracellular traps in the liver and gastrointestinal system. *Nat. Rev. Gastroenterol. Hepatol.* **15,** 206–221 (2018).

59. Gaertner, F., Ahmad, Z., Rosenberger, G., Fan, S., Nicolai, L., Busch, B., Yavuz, G., Luckner, M., Ishikawa-Ankerhold, H., Hennel, R., Benechet, A., Lorenz, M., Chandraratne, S., Schubert, I., Helmer, S., Striednig, B., Stark, K., Janko, M., Böttcher, R. T., Verschoor, A., Leon, C., Gachet, C., Gudermann, T., Mederos y Schnitzler, M., Pincus, Z., Iannacone, M., Haas, R., Wanner, G., Lauber, K., Sixt, M. & Massberg, S. Migrating Platelets Are Mechano-scavengers that Collect and Bundle Bacteria. *Cell* **171,** 1368-1382.e23 (2017).

60. Uchimido, R., Schmidt, E. P. & Shapiro, N. I. The glycocalyx: a novel diagnostic and therapeutic target in sepsis. *Crit. Care* **23,** 1–12 (2019).

Chapter 5: Endothelial HS Modulates Host Sensitivity to *Staphylococcus aureus*

5.1 Introduction

Chapter 3 highlights how altering HS sulfation in endothelial and myeloid tissues impacts infection and sepsis outcomes. Interestingly, mice with deficient HS sulfation in endothelial and myeloid tissues (*Ndst1$^{f/f}$Tie2Cre+*) were hypersensitive to a lethal *S. aureus* challenge (Figure 3.6A). Chapter 4 contains studies that continued characterization of *S.* aureus sepsis in the *Ndst1$^{f/f}$Tie2Cre* mouse model. In summary, within the first 6 hours of infection, *Ndst1$^{f/f}$Tie2Cre+* mice have deficient trafficking of neutrophils to the liver, the major early-infection reservoir of *S. aureus* [1]. Therefore, there is a reduction in downstream hepatic pathology derived from pro-thrombotic neutrophils. However, it is unclear how liver pathology impacts overall outcome during *S. aureus* sepsis. It is expected that protecting the liver would protect the organism, but in *Ndst1$^{f/f}$Tie2Cre+* mice the inverse is observed. A potential explanation is *S. aureus* sepsis may have different phases, with pathology in early and late infection being driven by different host and pathogen factors. *S. aureus* can shift its virulence factor expression based upon its extracellular environment. *S. aureus* undergoes large, systems-level transcriptomic shifts in response to metabolic nutrient availability [2]. Further, it changes expression of virulence factors as it progresses from commensal colonization to an invasion infection [3]. Theoretically, the abundance of certain virulence factors would increase as infection progressed, as live *S. aureus* disseminates and increases in abundance over time in the mouse model (Figure 4.6A-C). As this occurs, *S. aureus* virulence factors may also increase and reach a toxic threshold. Altering vascular HS may lower this toxic threshold, thus leading to the observed hypersensitivity of *Ndst1$^{f/f}$Tie2Cre+* mice. Additionally, this hypothesis is supported by the observation that no other bacterial sepsis models induced a hypersensitivity phenotype (Figure 3.6), thus indicating a factor unique to *S. aureus* may responsible.

S. aureus produces a litany of toxins to facilitate inflammation and induce host cell injury [4]. α-hemolysin, also known as α-toxin or Hla, is a secreted toxin that was initially shown to cause rabbit red blood cell lysis [5] but has since become appreciated as a major *S. aureus* virulence factor. It is highly relevant to clinical disease, as it is encoded in 99% and expressed by 83% of clinical isolates [6]. Genetic deletion or antibody-mediated neutralization of Hla results in abrogation of *S. aureus* virulence in animal models [7,8]. Hla toxicity is thought to be mediated through a multifaceted interaction with the host cell surface. Monomeric Hla intercalates and oligomerizes in the host plasma membrane to form a heptameric β-barrel pore [9]. Pore formation results in an influx of extracellular Ca^{2+}, which induces secondary host cell signaling such as arachidonic acid metabolism, cellular contractile dysfunction, NLRP3 inflammasome activation, and cytokine release [10,11]. Further, Hla pore formation is required for platelet-neutrophil aggregates, sinusoidal collections of platelet aggregates, disruption of cell-cell junctions, and vascular leak [7,8,12–14]. Hla cytotoxic effects and its interaction with host cells depends upon its cell surface receptor Adam10 [15]. Mice lacking Adam10 are protected from *S. aureus* skin infection and severe pneumonia [12,13]. There is evidence that Adam10 proteolytic activity is increased through its interaction with Hla. Hla treatment of epithelial cells or endothelial cells results in cleavage of E-cadherin and VE-cadherin, respectively, which can be abrogated by inhibition of Adam10 activity [12,13]. Adam10 cleavage of tight junction proteins may be an important aspect of Hla toxicity, as Hla treatment results in Adam10-depednent epithelial and vascular barrier disruption [12,13]. Further, Adam10 clustering at tight junctions is critical for Hla toxicity [16]. However, it is unclear if inducing Adam10 activity is a primary toxic function of Hla or if Adam10 is merely a receptor that allows Hla to induce cell signaling that disrupts cell-cell junctions. Importantly, Adam10 inhibitors prevent Hla from interacting with epithelial cells [12], indicating that Adam10 inhibitors induce conformational

changes that preclude Hla association or that Adam10 proteolytic activity is required for Hla to intercalate into the membrane. Importantly, Hla induces cell death in the presence of Adam10 inhibitor [17]. Further research is needed to understand which host factors control Hla toxicity, whether it's through initial interaction with the host cell, oligomerization of the pore structure, or induction of damaging host cell Adam10 activity and signaling.

Since Hla is a critical virulence factor and *Ndst1$^{f/f}$Tie2Cre+* animals are hypersensitive to *S. aureus* (Figure 3.6A), it was predicted that altering endothelial HS sulfation sensitizes the host to systemic Hla toxicity. *Ndst1$^{f/f}$Tie2Cre+* mice were hypersensitive to recombinant Hla and exhibited striking heart VGC changes with implications in heart damage during *S. aureus* sepsis. Additionally, Hla binds to heparin, a highly sulfated and short-chain species of HS, and HS can inhibit Adam10 activity. HS may play multiple roles in Hla host cell cytotoxicity.

5.2 Materials and methods

5.2.1 Animal model

Ndst1$^{f/f}$Tie2Cre animals were bred as described in Chapter 3 and according to Wang, 2015 [18]. *Ndst1$^{f/f}$LysM/PF4Cre* mice were generated by crossing *Ndst1$^{f/f}$* mice to *PF4Cre* and *LysMCre* mice [19,20]. *Hs2st$^{f/f}$Tie2Cre* mice were generated by crossing *Hs2st$^{f/f}$* mice and *Tie2Cre+* males as described in Axelsson, 2012 [21]. All experiments used age- and sex-matched littermates. Offspring were genotyped by PCR with genomic DNA isolated from tail clip tissue.

5.2.2 *S. aureus* infection and systemic Hla intoxication

S. aureus USA300 TCH1516 infection was carried out as described in Chapters 2-4. *S. aureus* USA300 TCH1516 with a deletion in *hla* (also known as *hly*) was conducted by precise, markerless allelic replacement of USA300 TCH1516 *hla* (Locus tag USA300HOU_1099, NC_010079.1) by PCR-based methods adapting the pKOR1 knock-out strategy as described in a

forthcoming publication [22]. Bacterial CFU during systemic infection was enumerated as described in Chapters 2-4. Two different sources of Hla were used to induce systemic cytotoxicity. Recombinant Hla purified from *E. coli* [15] was diluted from 1 mg/mL PBS+10% glycerol stocks to 35 µg/mL in sterile PBS and injected i.v. via retro-orbital sinuses at 175 µg/kg (~3.5 µg per mouse). Hla purified from *S. aureus* was acquired from Sigma-Aldrich and was ~60% protein by dry weight (Sigma-Aldrich #H9395). Sigma Hla was reconstituted in PBS+10% glycerol, diluted to ~100 µg/mL in sterile PBS and injected i.v. via retro-orbital sinuses at 500 µg/kg (~10 µg per mouse). Morbidity and mortality was observed as described in Chapter 3.

5.2.3 Vascular tagging and all data analysis

S. aureus sepsis was induced in *Ndst1$^{f/f}$Tie2Cre* animals as described in Chapter 2-4. Infected animals were perfused and harvested at 24 hours post infection. Five animals were included in each genotype per timepoint, for a total of 20 labeled mice. Vascular tagging, mass spectrometry, and label free quantification were carried out as described in Chapter 2. Significantly enriched or de-enriched proteins across all samples were determined by ANOVA with FDR truncation after 250 permutations. Of the significantly enriched or de-enriched proteins, a Student's two-tailed T-test between infected *Ndst1$^{f/f}$Tie2Cre*- and *Ndst1$^{f/f}$Tie2Cre*+ samples was used to distinguish proteins significantly enriched or de-enriched during sepsis.

5.2.4 Heparin column

50 µg of recombinant Hla was applied to a 1-mL HiTrap heparin-Sepharose column (GE Healthcare) in PBS. Protein was eluted with 50 mM HEPES buffer and a NaCl gradient from 150 mM to 1 M.

5.2.5 Protein modeling

Crystal structures for heptameric Hla [9] and monomeric Hla [23] were visualized using Pymol. Heparin 4-mers were modeled onto Hla structures using ClusPro [24].

5.2.6 Adam10 activity assay

Recombinant Adam10 from the AnaSpec Adam10 activity kit (AnaSpec AS-72226) was incubated with 500 µg/mL unfractionated heparin or HS isolated from wild-type CHO cells (TEGA Therapeutics) according to manufacturer's specifications.

5.2.7 Whole Blood Aggregometer

Whole blood aggregation studies were performed on a CHRONO-LOG® Model 700 Whole Blood/Optical Lumi-Aggregometer (Havertown, PA) as per manufacturer's instruction. To isolate anti-coagulated whole blood, 30 µL of Citrate-Dextrose Solution (Sigma) was pre-loaded in a syringe used for cardiac puncture. After cardiac puncture, additional Citrate-Dextrose Solution was added to the isolated blood to create a 1:9 Citrate-Dextrose to blood mixture. Blood from 4 mice per genotype, *Ndst1$^{f/f}$Tie2Cre-* and *Ndst1$^{f/f}$Tie2Cre+*, was pooled. To induce blood aggregation, 5 µg of toxin was added to 200 µL of blood diluted 1:5 in 800 µL saline solution, as stated in the manufacturer's protocol, and measurements were started.

5.3 Results

5.3.1 Reducing HS sulfation in the endothelium sensitizes mice to *S. aureus* sepsis and Hla

Mice with reduced HS sulfation in endothelial and myeloid tissues (*Ndst1$^{f/f}$Tie2Cre+*) are hypersensitive to *S. aureus* sepsis (Figure 5.1A, also shown as Figure 3.6A). However, it was not clear if *Ndst1* inactivation in endothelial or myeloid tissues causes the observed hypersensitivity, as *Tie2Cre* expresses Cre recombinase in both tissue subsets [25]. To test if the phenotype was driven by alterations in endothelial or myeloid HS, *Ndst1$^{f/f}$* mice were crossed with *LysMCre* and *PF4Cre* mice to yield *Ndst1$^{f/f}$LysM/PF4Cre+* mice. *PF4Cre* and *LysMCre* were utilized for their selective

expression in myeloid lineages and megakaryocytes, respectively [19,20]. Both Cre-recombinase lines were used since *Adam10*$^{f/f}$*LysM/PF4Cre+* mice, but not *Adam10*$^{f/f}$*LysM+* or *Adam10*$^{f/f}$*PF4Cre+* mice, were protected from *S. aureus* sepsis [14]. *Ndst1*$^{f/f}$*LysM/PF4Cre+* mice were not protected from *S. aureus* sepsis (Figure 5.1B), indicating that undersulfating endothelial HS results in susceptibility to *S. aureus*. It was predicted that *Ndst1*$^{f/f}$*Tie2Cre+* mice are hypersensitive to *S. aureus* Hla, which is required for rapid *S. aureus* mortality in sepsis models [7]. *Ndst1*$^{f/f}$*Tie2Cre+* mice infected with *S. aureus* lacking Hla (*S. aureus* Δ*hla*) did not exhibit hypersensitivity to Hla (Figure 5.1C). As the mortality rate in *Ndst1*$^{f/f}$*Tie2Cre-* animals was lower in *S. aureus* Δ*hla* infection, slightly higher doses of *S. aureus* Δ*hla* were tested. However, higher dosing resulted in rapid mortality within 24 hours of infection in both *Ndst1*$^{f/f}$*Tie2Cre-* and *Ndst1*$^{f/f}$*Tie2Cre+* animals (data not shown). To test if purified Hla intoxication recapitulates *S. aureus* hypersensitivity, *Ndst1*$^{f/f}$*Tie2Cre+* mice were injected with recombinant Hla. *Ndst1*$^{f/f}$*Tie2Cre+* mice exhibited increased susceptibility to recombinant Hla (Figure 5.1D). Importantly, this phenotype repeated with two different sources of recombinant Hla (Figure 5.1D-E). Hla-induced blood aggregation did not differ between wild-type and *Ndst1*$^{f/f}$*Tie2Cre+* blood (Figure 5.1F), further supporting that endothelial HS dictates hypersensitivity to Hla. While reduction of *N*-sulfation can reduce overall HS sulfation [18], deletion of the HS biosynthesis enzyme *Hs2st* in endothelial cells (*Hs2st*$^{f/f}$*Tie2Cre*) results in a loss of 2-*O*-sulfation and a compensatory increase in *N*- and *O*- sulfation [26]. *Hs2st*$^{f/f}$*Tie2Cre+* mice were slightly protected from Hla cytotoxicity (Figure 5.1G). While this implies that general HS sulfation may impact Hla toxicity, further studies detailing how specific HS sulfation moieties or patterns is needed to understand how HS modulates Hla function.

5.3.2 The heart VGC of *Ndst1*$^{f/f}$*Tie2Cre+* mice has unique features during *S. aureus* sepsis

As highlighted in Chapter 2, changes in the VGC induced by *S. aureus* sepsis can be characterized by tagging vascular proteins with biotin, enriching tagged proteins using streptavidin, and using proteomics to quantify protein abundance. To give further insight into *S. aureus* hypersensitivity in mice with undersulfated endothelial HS, healthy and septic *Ndst1$^{f/f}$Tie2Cre* mice were subjected to VGC tagging and proteomics analysis. In healthy animals, no difference in VGC proteins was detectable (data not shown). During sepsis, liver, kidney, brain, and white adipose tissue did not display major differences in VGC protein composition (data not shown). However, in septic animals the heart VGC showed distinct differences between *Ndst1$^{f/f}$Tie2Cre-* and *Ndst1$^{f/f}$Tie2Cre+* mice. The proteomic signature in the heart of wild-type animals showed changes associated with cardiac damage/recovery and extracellular matrix remodeling (Fig. 5.2A). Gene ontology analysis of heart VGC proteins differentially enriched between septic *Ndst1$^{f/f}$Tie2Cre-* and *Ndst1$^{f/f}$Tie2Cre+* mice showed an enrichment for extracellular matrix proteins and proteoglycans (Figure 5.2B). Heart recovery proteins, such as periostin and clusterin [27,28], increased in wild-type animals during sepsis, but not in *Ndst1$^{f/f}$Tie2Cre+* mice (Fig. 5.2C-D). ECM proteins, including collagen Type VI α6 chain and inter-alpha trypsin inhibitor heavy chain-1 also increased in wild-type animals (Fig. 5.2E-F). These findings are intriguing given that Hla acts on the endothelium and increases vascular permeability [7], implying that undersulfation of vascular HS interferes with a *S. aureus*-induced repair response in the heart vasculature and correlates to hypersensitivity to *S. aureus* sepsis and Hla. Therefore, it's predicted that in *Ndst1$^{f/f}$Tie2Cre+* mice the cardiac endothelium is sensitized to Hla-mediated damage and vascular stress. Importantly, altering HS in the VGC does not impact bacterial loads in the heart, indicative that altering HS does not change bacterial dissemination but changes the host response to equivalent bacterial infection (Figure 5.2G).

5.3.3 Hla binds to heparin

The hypersensitivity of *Ndst1*-deficient mice to Hla suggests Hla might directly interact with HS. To test this possibility, recombinant Hla binding to heparin was measured by affinity chromatography. Heparin is structurally similar to HS, although it is more highly sulfated, enriched in iduronic acid, and more highly-negatively charged. When tissue extracts or plasma are fractionated over heparin-Sepharose, weakly bound proteins can be washed out with low ionic strength buffer, while strongly bound heparin-binding proteins elute at higher ionic strength. As shown in Figure 5.3A, a substantial fraction of Hla bound to heparin and eluted at a 470 mM NaCl, suggesting that Hla binds to heparin at comparable strength to other heparin-binding proteins [29]. The material that elutes in the loading fraction may be denatured Hla. Hla oligomerizes and mutation of His35 decreases oligomerization [15]. Interestingly, this residue lies in a strongly cationic domain of monomeric Hla where it is predicted heparin interacts (Fig. 5.3B). The cationic domain, including His35, forms an interface between monomers in the cap domain of the heptameric pore (Fig. 5.3C). Interaction of heparin and cellular HS at this interface could interfere with Hla oligomerization and decrease Hla toxicity. In this model, decreasing HS sulfation would permit Hla oligomerization, which could explain the hypersensitivity of *Ndst1*$^{f/f}$*Tie2Cre+* mice to Hla.

5.3.4 HS modulates Adam10 activity

Since mice with altered vascular HS are hypersensitive to Hla (Figure 5.1), we hypothesized that reducing sulfation of HS increases Adam10 activity, leading to more potent Adam10 activation by Hla. Incubating recombinant Adam10 with heparin reduced Adam10 activity while HS only slightly decreased activity (Figure 5.4A). These results imply that level of HS sulfation controls Adam10 activity level.

5.4 Discussion

Results from these studies provide novel insights into the participation of endothelial HS in Hla toxicity in the vasculature during *S. aureus* sepsis. Future studies characterizing how HS modulates Hla activity would be crucial to understanding how a clinically relevant *S. aureus* virulence factor promotes host dysfunction. However, it remains unclear how altering endothelial HS alters sensitivity to Hla. Three hypotheses that will be explored in future studies (Figure 5.5A). First, HS disrupts Hla oligomerization and subsequent toxicity, and undersulfated HS has diminished inhibitory activity. Second, lowering HS sulfation increases the activity of Adam10, therefore enhancing Hla activation of Adam10. Third, undersulfated HS enhances Hla induced dysregulation of Ca^{2+} host cell signaling.

The interaction of HS and Hla will be studied by incubation of [^{35}S]HS derived from [^{35}S]O4 labeled endothelial cells, with resolution of the complex by size-exclusion FPLC. If Hla binds to [^{35}S]HS, then the larger complex will cause [^{35}S]HS to elute earlier from the column. According to the model, HS might interfere with oligomerization. Oligomerization of Hla can be induced by incubation of 2-methyl-2,4-pentanediol (MPD), independently of a lipid membrane [30]. It is hypothesized that the addition of heparin or HS should block Hla oligomerization. Binding of Hla to cells will also be measured. To discriminate between binding to cell surface HS and Adam10, the difference in binding before and after treatment of the cells with heparin lyases, which degrade HS, with and without an antibody to Adam10, or after silencing of Adam10 with an siRNA will be measured.

To test if HS modulates Adam10 activity in live cells, its activity will be measured in wild-type and *Ndst1*$^{-/-}$ primary cardiac endothelial cells (PCECs) at baseline and in the presence of Hla using a commercially available Adam10 activity assay. The ratio of inactive pro-Adam10 and

cleaved active Adam10 will be measured via western blotting. To measure cleavage of Adam10 substrates after Hla treatment, cell lysates will be blotted for cleavage of VE-cadherin [7]. To test if HS affects Adam10 activity in human endothelial cells, human umbilical vein endothelial cells (HUVECs) and PCECs will be treated with heparin lyases to remove cell surface HS and treated with Hla, and then Adam10 activity and VE-cadherin cleavage will be assayed. To assure that VE-cadherin cleavage is Adam10 dependent, cells will be incubated with and without the Adam10 inhibitor GI254023X [12]. Lastly, positive results are obtained, direct binding of HS to recombinant Adam10 will be measured by gel filtration using recombinant ectodomain of Adam10 and [^{35}S]HS.

The modulation of Ca^{2+} signaling in Hla-treated host cells with undersulfated HS will be measured through signaling systems downstream of Ca^{2+} flux. Hla intoxication of endothelial cells, which increases cytosolic Ca^{2+} levels, affects critical vascular functions including metabolism of arachidonic acid to thromboxane A2, generation of nitric oxide, and activation of protein kinase C [31–33]. These responses will be measured after Hla addition to *Ndst1*$^{-/-}$ wild-type and endothelial cells, or after treatment of endothelial cells with heparin lyases. Other studies have shown that TRPC Ca^{2+} channels can be affected by cell surface syndecans [34], suggesting the possibility that altering *Ndst1* could affect calcium flux through this channel, which can be measured with a calcium dependent dye.

Further research into the connection between heart VGC responses, HS, and Hla may uncover how altering endothelial HS sensitizes the host to *S. aureus*. The heart VGC profile in mice with undersulfated HS is enriched with ECM and basement membrane proteoglycans, implying that vascular integrity is lost. Potentially, this could lead to acute heart failure and ultimately death. Vascular integrity will be tested using the Miles dye leakage assay [35]. Additionally, acute heart stress of infected animals will be tracked using ELISAs against

circulating troponin and B natriuretic peptide, cardiac markers that are elevated after cardiac damage [36]. Immunohistochemistry of neutrophils and monocytes will be assessed in the heart to discern the location of inflammation that could potentially damage the vasculature. Primary cardiac endothelial cells (PCECs) will be isolated and cultured from *Ndst1$^{f/f}$Tie2Cre-* and *Ndst1$^{f/f}$Tie2Cre+* mice [37]. After Hla intoxication, the permeability of mutant and wild-type PCEC monolayers will be assessed by measuring permeation of fluorescently labeled dextran across cell monolayers grown on a permeable filter substrate. Responses of mutant and wild-type PCECs to Hla will be observed by VE-cadherin cleavage and modification of tight junctions, which are well characterized responses of endothelial cells to Hla [7,38]. VE-cadherin cleavage will be measured through western blots and by immunofluorescence to measure disruption of VE-cadherin clustering at adherens junctions [7,16,39].

5.5 Acknowledgments

Chapter 5, in part, is being formulated into a manuscript for publication of the material. GJ Golden, A Gomez Toledo, C Morris, V Nizet, and JD Esko. The dissertation author is the primary investigator and author of this material. Thank you to Joshua Olson for assistance with culture and mouse sepsis methods. Thank you to Juliane Bubeck-Wardenburg for providing recombinant Hla and Hla $H_{35}L$. Special thanks to Alejandro Gomez Toledo for mass spectrometry analysis and assistance with mouse infections. Thank you to the Sanford Burnham Prebys Proteomics Core for mass spectrometry analysis. Thank you to Claire Morris for assistance with animal husbandry, animal infections, and for working on the Adam10 activity assay. Thank you to Chelsea Painter for assistance with the ion exchange chromatography and Daniel Sandoval for assistance with ion exchange chromatography and protein modeling. These studies were supported by the National

Institute of Health (P01- HL131474) and the UCSD Microbiome Center for Innovation (Microbial Sciences Graduate Research Fellowship Award 1-F17GG and 1-F18GG).

5.6 Figures

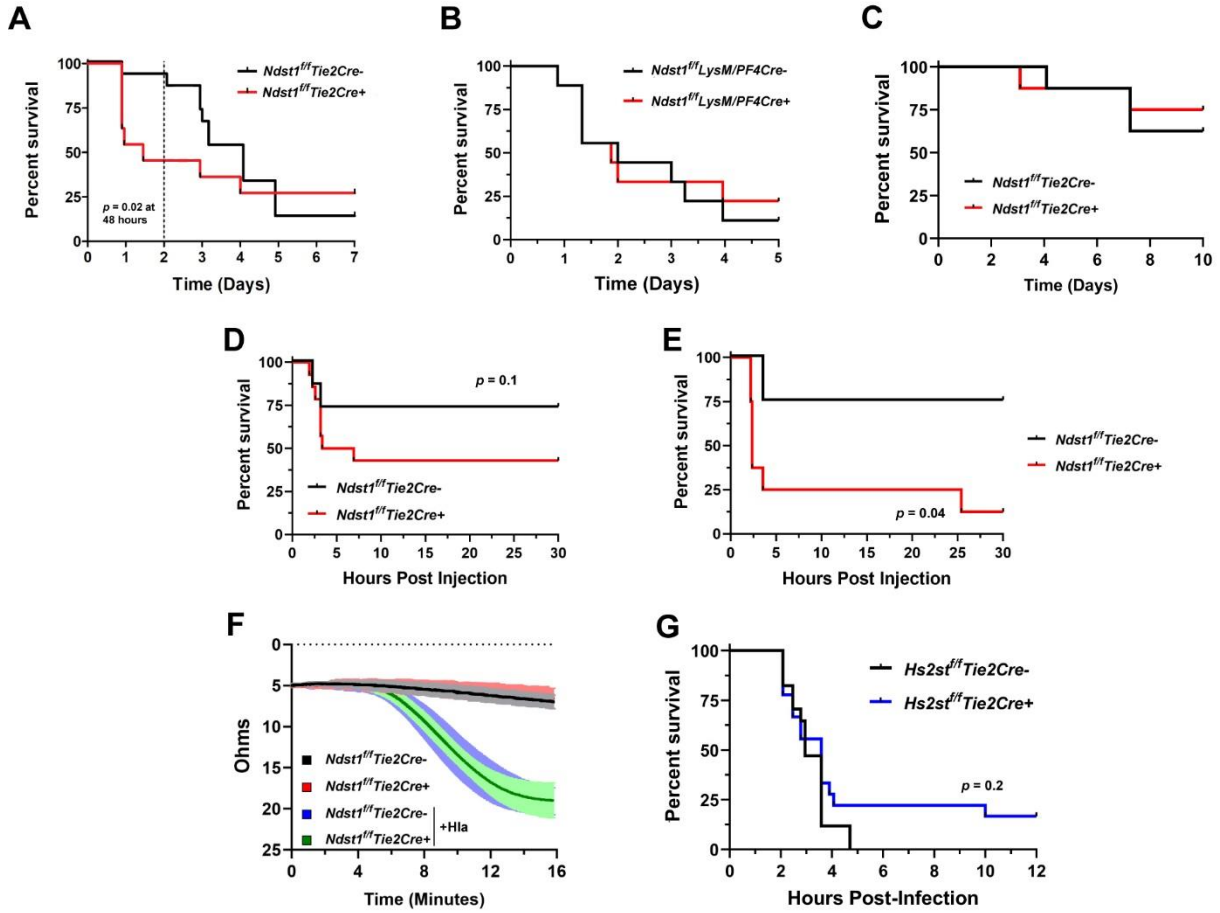

Figure 5.1 *Ndst1$^{f/f}$Tie2Cre+* mice are hypersensitive to *S. aureus* Hla. (A) Survival of *Ndst1$^{f/f}$Tie2Cre* and (B) *Ndst1$^{f/f}$LysM/PF4Cre* mice infected with a lethal dose of *S. aureus*. N ≥10 per group, representative of 3 experiments. (C) Survival of *Ndst1$^{f/f}$Tie2Cre* mice infected with *S. aureus* Δ*hla*. (D) Survival of *Ndst1$^{f/f}$Tie2Cre* mice injected with 175 µg/kg Hla (recombinant) and (E) 500 µg/kg Hla (Sigma-Aldrich). For D, two experiments were combined for an n=14-15 per group, and E is one experiment with n=4 mice for *Ndst1$^{f/f}$Tie2Cre-* group and n=8 mice for the *Ndst1$^{f/f}$Tie2Cre+* group. All *p* values above determined by Log-rank Mantel-Cox test. (F) Aggregometer readings of *Ndst1$^{f/f}$Tie2Cre* blood treated with vehicle or 5 µg/mL recombinant Hla. N=3 technical replicates per group, after pooling blood from 4 animals per genotype. (G) Survival of *Hs2st$^{f/f}$Tie2Cre* mice infected with injected with 175 µg/kg Hla (recombinant). n ≥15 per group, combination of 2 independent experiments.

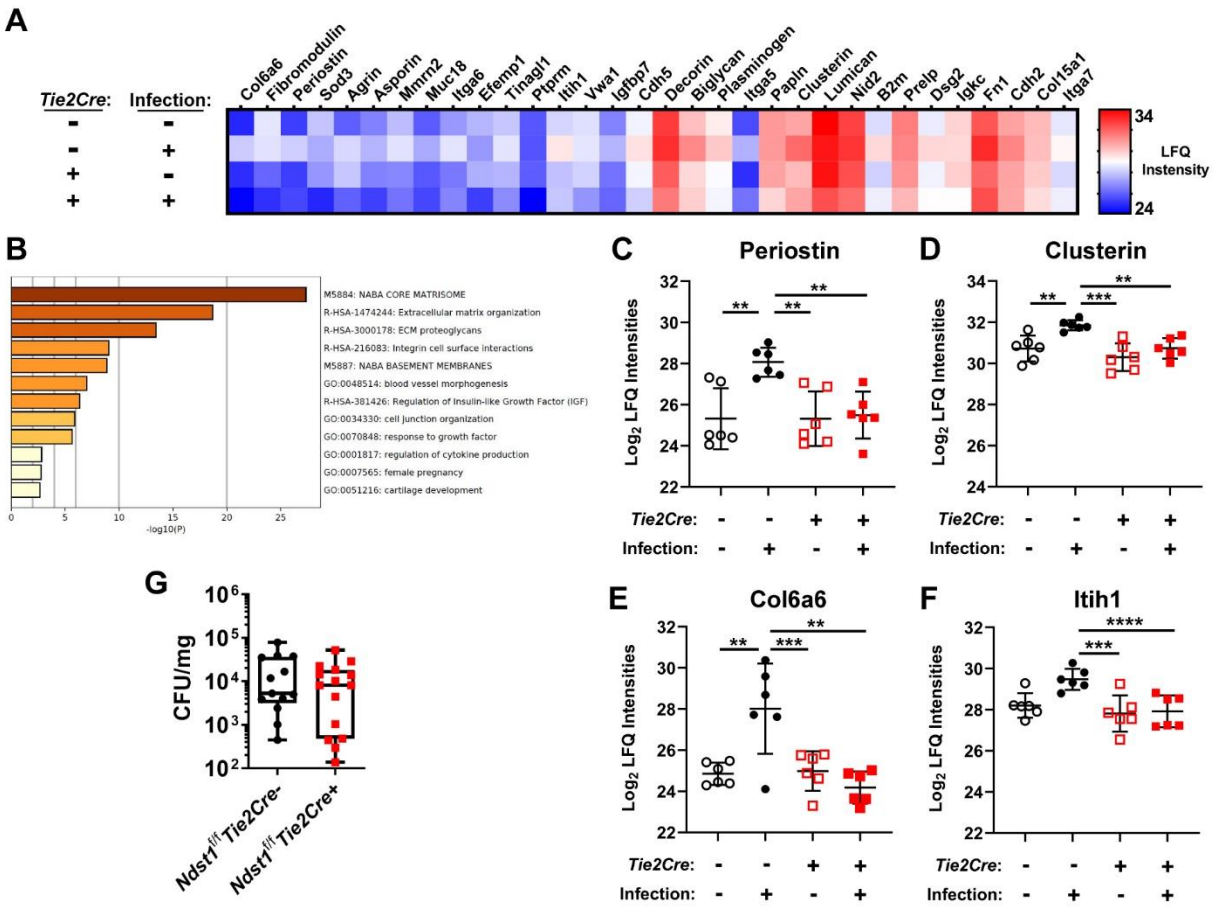

Figure 5.2 The Heart VGC in *Ndst1$^{f/f}$Tie2Cre* mice during *S. aureus* sepsis. (A) Heatmap of label free quantification levels of heart VGC proteins differentially enriched in septic *Ndst1$^{f/f}$Tie2Cre* animals. (B) Gene ontology analysis of the protein list in A. (C) Periostin and (D) Clusterin quantification values, representative of the enrichment of heart stress recovery proteins in the heart VGC of wild-type animals during *S. aureus* sepsis. (E) Col6a6 and (F) Itih1 quantification values, representative of the ECM protein enrichment in the heart VGC of wild-type animals during *S. aureus* sepsis. N=5 mice per group. *p* value determined with one-way ANOVA using Tukey's multiple comparison test. ** is $p<0.01$ and *** is $p<0.001$. (G) CFU in the heart of *Ndst1$^{f/f}$Tie2Cre* mice 24 hours post-infection.

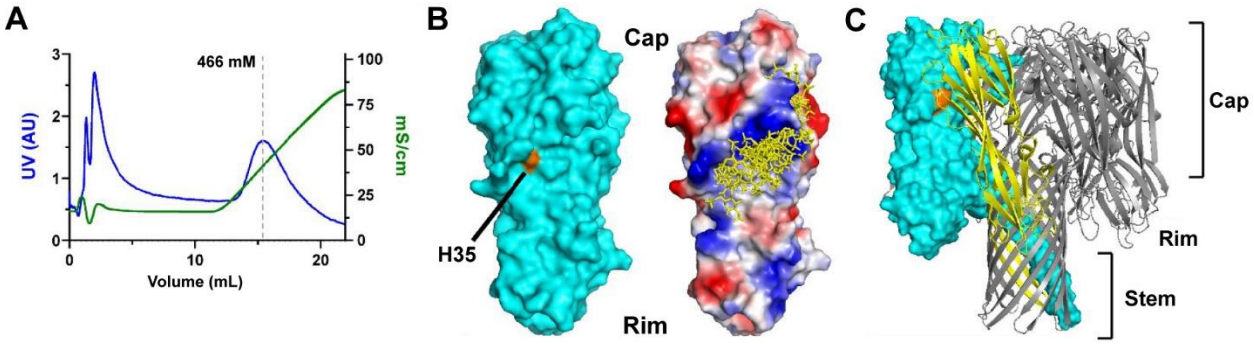

Figure 5.3 Biochemical and structural evidence of Hla interaction with heparin. (A) Ion-exchange chromatography of Hla with a heparin Sepharose column. The blue line is UV absorption across the column as a measure of protein elution. The large protein elution that occurs in early fractions may result from protein aggregation. The green line is conductivity across the column, which is a correlated to salt concentration of the buffer and is used to calculate salt concentration at the maximal elution of Hla off the column (grey dotted line). (B) 3D surface model (cyan) of the monomeric Hla crystal structure with H35 highlighted (orange) juxtaposed with the electrostatic surface model containing the top 10 likeliest heparin (yellow) interaction conformations. For the electrostatic model, blue regions, white regions, and red regions correspond to electropositive, electroneutral, and electronegative domains, respectively. (C) 3D model of the heptamer pore structure of Hla. H35 lies in the interface between two monomers (blue, surface model and yellow, ribbon model).

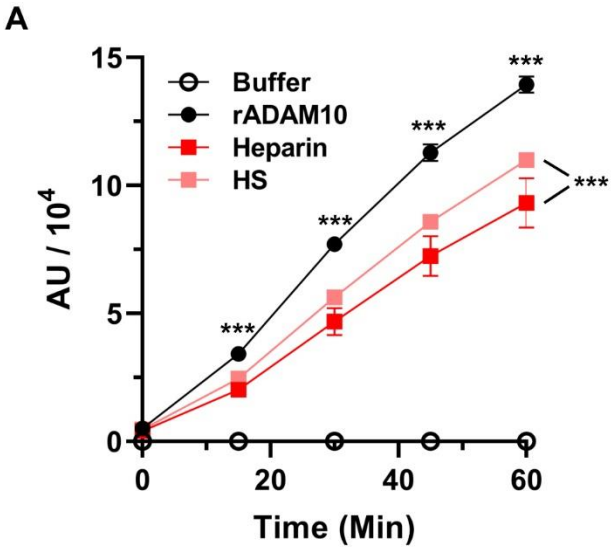

Figure 5.4 Recombinant Adam10 activity is inhibited with HS and heparin. Recombinant Adam10 from the AnaSpec Adam10 activity kit was incubated with 500 µg/mL unfractionated heparin or HS isolated from wild-type CHO cells. The buffer control is the reaction without enzyme addition.

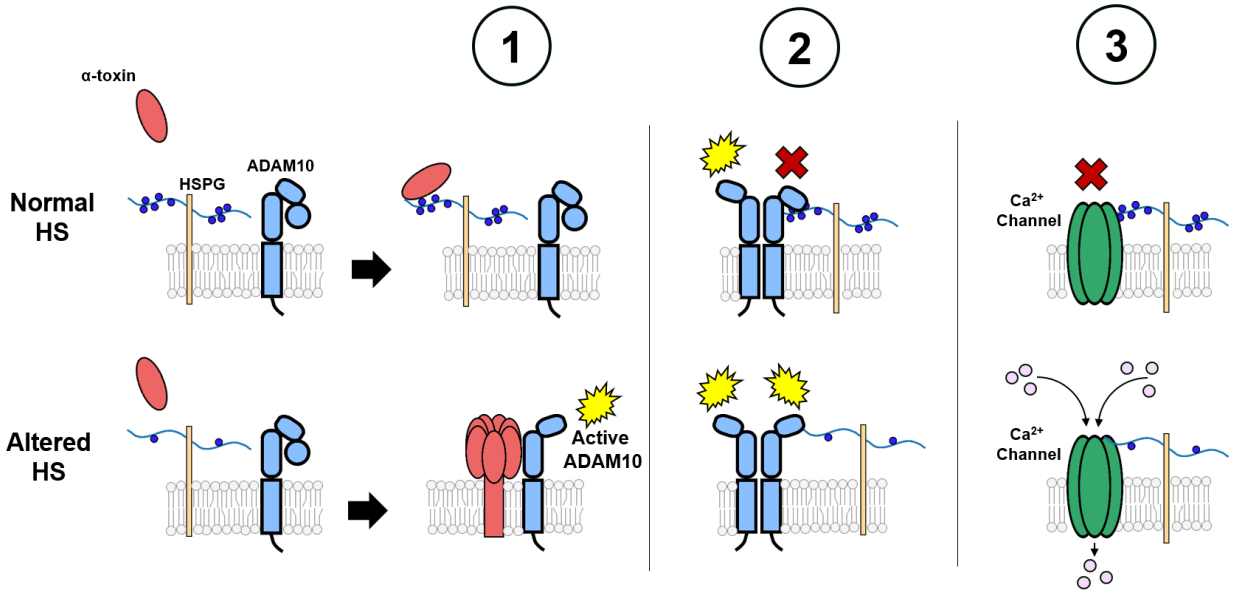

Figure 5.5 Models of HS alteration and impacts on Hla intoxication. Model 1 predicts that HS sulfation inhibits oligomerization of the Hla pore, and reducing HS sulfation allows for pore formation to occur. Model 2 predicts undersulfated HS increases Adam10 activity, thus potentiating Adam10 activation by Hla. Model 3 predicts reducing HS sulfation increases Ca^{2+} signaling during Hla intoxication.

5.7 References

1. Kolaczkowska, E., Jenne, C. N., Surewaard, B. G. J., Thanabalasuriar, A., Lee, W. Y., Sanz, M. J., Mowen, K., Opdenakker, G. & Kubes, P. Molecular mechanisms of NET formation and degradation revealed by intravital imaging in the liver vasculature. *Nat. Commun.* **6,** 1–13 (2015).

2. Poudel, S., Tsunemoto, H., Seif, Y., Sastry, A. V., Szubin, R., Xu, S., Machado, H., Olson, C. A., Anand, A., Pogliano, J., Nizet, V. & Palsson, B. O. Revealing 29 sets of independently modulated genes in Staphylococcus aureus, their regulators, and role in key physiological response. *Proc. Natl. Acad. Sci. U. S. A.* **117,** 17228–17239 (2020).

3. Jenkins, A., An Diep, B., Mai, T. T., Vo, N. H., Warrener, P., Suzich, J., Kendall Stover, C. & Sellman, B. R. Differential expression and roles of Staphylococcus aureus virulence determinants during colonization and disease. *MBio* **6,** 1–10 (2015).

4. Powers, M. E. & Wardenburg, J. B. Igniting the Fire: Staphylococcus aureus Virulence Factors in the Pathogenesis of Sepsis. *PLoS Pathog.* **10,** 10–13 (2014).

5. Cassidy, P. S. & Harshman, S. The Binding of S laphylococcal (B) to Erythrocytes. *J. Biol. Chem.* **248,** 5545–5546 (1973).

6. Tabor, D. E., Yu, L., Mok, H., Tkaczyk, C., Sellman, B. R., Wu, Y., Oganesyan, V., Slidel, T., Jafri, H., McCarthy, M., Bradford, P. & Esser, M. T. Staphylococcus aureus alpha-toxin is conserved among diverse hospital respiratory isolates collected from a global surveillance study and is neutralized by monoclonal antibody MEDI4893. *Antimicrob. Agents Chemother.* **60,** 5312–5321 (2016).

7. Powers, M. E., Kim, H. K., Wang, Y. & Wardenburg, J. B. ADAM10 mediates vascular injury induced by staphylococcus aureus α-hemolysin. *J. Infect. Dis.* **206,** 352–356 (2012).

8. Surewaard, B. G. J., Thanabalasuriar, A., Zheng, Z., Tkaczyk, C., Cohen, T. S., Bardoel, B. W., Jorch, S. K., Deppermann, C., Bubeck Wardenburg, J., Davis, R. P., Jenne, C. N., Stover, K. C., Sellman, B. R. & Kubes, P. α-Toxin Induces Platelet Aggregation and Liver Injury during Staphylococcus aureus Sepsis. *Cell Host Microbe* **24,** 1–14 (2018).

9. Song, L., Hobaugh, M. R., Shustak, C., Cheley, S., Bayley, H. & Gouaux, J. E. Structure of Staphylococcal a-Hemolysin , a Heptameric Transmembrane Pore. *Science (80-.).* **274,** 1859–1866 (1996).

10. Bhakdi, S. & Tranum-Jensen, J. Alpha-toxin of Staphylococcus aureus. *Microbiol. Rev.* **55,** 733–751 (1991).

11. Gao, X., Ting, J. P., Wardenburg, J. B., Duncan, J. A., Allen, I. C., McElvania-TeKippe, E., Gris, D. & Craven, R. R. Staphylococcus aureus α-Hemolysin Activates the NLRP3-Inflammasome in Human and Mouse Monocytic Cells. *PLoS One* **4,** e7446 (2009).

12. Inoshima, I., Inoshima, N., Wilke, G. A., Powers, M. E., Frank, K. M., Wang, Y. &

Wardenburg, J. B. A Staphylococcus aureus pore-forming toxin subverts the activity of ADAM10 to cause lethal infection in mice. *Nat. Med.* **17,** 1310–1314 (2011).

13. Inoshima, N., Wang, Y. & Wardenburg, J. B. Genetic requirement for ADAM10 in severe staphylococcus aureus skin infection. *J. Invest. Dermatol.* **132,** 1513–1516 (2012).

14. Powers, M. E., Becker, R. E. N., Sailer, A., Turner, J. R. & Bubeck Wardenburg, J. Synergistic Action of Staphylococcus aureus α-Toxin on Platelets and Myeloid Lineage Cells Contributes to Lethal Sepsis. *Cell Host Microbe* **17,** 775–787 (2015).

15. Wilke, G. A. & Wardenburg, J. B. Role of a disintegrin and metalloprotease 10 in Staphylococcus aureus α-hemolysin-mediated cellular injury. *Proc. Natl. Acad. Sci.* **107,** 13473–13478 (2010).

16. Shah, J., Rouaud, F., Guerrera, D., Vasileva, E., Popov, L. M., Kelley, W. L., Rubinstein, E., Carette, J. E., Amieva, M. R. & Citi, S. A Dock-and-Lock Mechanism Clusters ADAM10 at Cell-Cell Junctions to Promote α-Toxin Cytotoxicity. *Cell Rep.* **25,** 2132-2147.e7 (2018).

17. Ezekwe, E. A. D., Weng, C. & Duncan, J. A. ADAM10 cell surface expression but not activity is critical for staphylococcus aureus a-hemolysin-mediated activation of the nlrp3 inflammasome in human monocytes. *Toxins (Basel).* **8,** 1–14 (2016).

18. Wang, L., Fuster, M., Sriramarao, P. & Esko, J. D. Endothelial heparan sulfate deficiency impairs L-selectin- and chemokine-mediated neutrophil trafficking during inflammatory responses. *Nat. Immunol.* **6,** 902–10 (2005).

19. Tiedt, R., Schomber, T., Hao-Shen, H. & Skoda, R. C. Pf4-Cre transgenic mice allow the generation of lineage-restricted gene knockouts for studying megakaryocyte and platelet function in vivo. *Blood* **109,** 1503–1506 (2007).

20. Clausen, B. E., Burkhardt, C., Reith, W., Renkawitz, R. & Förster, I. Conditional gene targeting in macrophages and granulocytes using LysMcre mice. *Transgenic Res.* **8,** 265–277 (1999).

21. Axelsson, J., Xu, D., Kang, B. N., Nussbacher, J. K., Handel, T. M., Ley, K., Sriramarao, P. & Esko, J. D. Inactivation of heparan sulfate 2- O -sulfotransferase accentuates neutrophil infiltration during acute inflammation in mice. *Blood* **120,** 1742–1751 (2012).

22. Sun, J., Uchiyama, S., Olson, J., Morodomi, Y., Cornax, I., Ando, N., Kohno, Y., Kyaw, M., Aguilar, B., Haste, N., Kanaji, S., Kanaji, T., Rose, W., Sakoulas, G., Marth, J. & Nizet, V. Repurposed Drugs Block Toxin-Driven Platelet Clearance by the Hepatic Ashwell-Morell Receptor to Clear Staphylococcus aureus Bacteremia. *bioRxiv* (2020). doi:10.1101/2020.07.06.190322

23. Sugawara, T., Yamashita, D., Kato, K., Peng, Z., Ueda, J., Kaneko, J., Kamio, Y., Tanaka, Y. & Yao, M. Structural basis for pore-forming mechanism of staphylococcal α-hemolysin. *Toxicon* **108,** 226–231 (2015).

24. Mottarella, S. E., Beglov, D., Beglova, N., Nugent, M. A., Kozakov, D. & Vajda, S. Docking server for the identification of heparin binding sites on proteins. *J. Chem. Inf. Model.* **54,** 2068–2078 (2014).

25. Tang, Y., Harrington, A., Yang, X., Friesel, R. E. & Liaw, L. The contribution of the Tie2+ lineage to primitive and definitive hematopoietic cells. *Genesis* **48,** 563–567 (2010).

26. Xu, D., Olson, J., Cole, J. N., van Wijk, X. M., Brinkmann, V., Zychlinsky, A., Nizet, V., Esko, J. D. & Chang, Y. C. Heparan sulfate modulates neutrophil and endothelial function in antibacterial innate immunity. *Infect. Immun.* **83,** 3648–3656 (2015).

27. Turkieh, A., Fertin, M., Bouvet, M., Mulder, P., Drobecq, H., Lemesle, G., Lamblin, N., De Groote, P., Porouchani, S., Chwastyniak, M., Beseme, O., Amouyel, P., Mouquet, F., Balligand, J. L., Richard, V., Bauters, C. & Pinet, F. Expression and Implication of Clusterin in Left Ventricular Remodeling After Myocardial Infarction. *Circ. Hear. Fail.* **11,** 1–13 (2018).

28. Shimazaki, M., Nakamura, K., Kii, I., Kashima, T., Amizuka, N., Li, M., Saito, M., Fukuda, K., Nishiyama, T., Kitajima, S., Saga, Y., Fukayama, M., Sata, M. & Kudo, A. Periostin is essential for cardiac healingafter acute myocardial infarction. *J. Exp. Med.* **205,** 295–303 (2008).

29. Xu, D. & Esko, J. D. Demystifying heparan sulfate-protein interactions. *Annu. Rev. Biochem.* **83,** 129–157 (2014).

30. Tanaka, Y., Hirano, N., Kaneko, J., Kamio, Y., Yao, M. & Tanaka, I. 2-Methyl-2,4-pentanediol induces spontaneous assembly of staphylococcal α-hemolysin into heptameric pore structure. *Protein Sci.* **20,** 448–456 (2011).

31. Filippini, A., D'Amore, A. & D'Alessio, A. Calcium mobilization in endothelial cell functions. *Int. J. Mol. Sci.* **20,** 1–13 (2019).

32. Eichstaedt, S., Gäbler, K., Below, S., Müller, C., Kohler, C., Engelmann, S., Hildebrandt, P., Völker, U., Hecker, M. & Hildebrandt, J. P. Effects of Staphylococcus aureus-hemolysin A on calcium signalling in immortalized human airway epithelial cells. *Cell Calcium* **45,** 165–176 (2009).

33. Suttorp, N., Seeger, W., Dewein, E., Bhakdi, S. & Roka, L. Staphylococcal alpha-toxin-induced PGI2 production in endothelial cells: role of calcium. *Am. J. Physiol.* **248,** (1985).

34. Gopal, S., Søgaard, P., Multhaupt, H. A. B., Pataki, C., Okina, E., Xian, X., Pedersen, M. E., Stevens, T., Griesbeck, O., Park, P. W., Pocock, R. & Couchman, J. R. Transmembrane proteoglycans control stretch-activated channels to set cytosolic calcium levels. *J. Cell Biol.* **210,** 1199–1211 (2015).

35. Radu, M. & Chernoff, J. An in vivo assay to test blood vessel permeability. *J. Vis. Exp.* 2–5 (2013). doi:10.3791/50062

36. Hoffman, M., Kyriazis, I. D., Lucchese, A. M., de Lucia, C., Piedepalumbo, M., Bauer, M., Schulze, P. C., Bonios, M. J., Koch, W. J. & Drosatos, K. Myocardial Strain and Cardiac Output are Preferable Measurements for Cardiac Dysfunction and Can Predict Mortality in Septic Mice. *J. Am. Heart Assoc.* **8,** 1–20 (2019).

37. Luo, S., Truong, A. H. & Makino, A. Isolation of mouse coronary endothelial cells. *J. Vis. Exp.* **2016,** 2–6 (2016).

38. Becker, K. A., Fahsel, B., Kemper, H., Mayeres, J., Li, C., Wilker, B., Keitsch, S., Seitz, A. & Fraunholz, M. Staphylococcus aureus Alpha-Toxin Disrupts Endothelial-Cell Tight Junctions via Acid Sphingomyelinase and Ceramide. *Infect. Immun.* **86,** 1–12 (2018).

39. Shah, J., Bagnoli, F., Guerrera, D., Citi, S., Starkl, P. M., Carette, J. E., Merakou, C., Lumb, J. H., Popov, L. M., Cooper, R. L., Bouley, D. M., Galli, S. J., Kiyonari, H., Takeichi, M., Meng, W., Marceau, C. D. & Amieva, M. R. The adherens junctions control susceptibility to Staphylococcus aureus α-toxin. *Proc. Natl. Acad. Sci.* **112,** 14337–14342 (2015).

Chapter 6: Closing Remarks

6.1 Conclusions and implications

Although sepsis is a widely studied disease that kills an estimated 11 million people worldwide each year [1], the mechanisms that contribute to the hallmark systemic vascular dysregulation in sepsis are largely misunderstood. Extensive VGC remodeling that occurs during sepsis has been correlated to poor outcomes and vascular dysfunction [2]. However, few studies have focused on the actual changes that occur *in vivo* in the VGC. Most studies thus far have used indirect measures of VGC remodeling such as shed proteoglycans or GAGs in circulation [2]. However, the source of these markers is not known,l as they could come from the parenchyma. Therefore, a detailed analysis of the VGC composition *in vivo* would be highly useful to characterizing VGC remodeling that occurs in sepsis. The studies detailed in Chapter 2 are the first *in vivo* comprehensive analysis of the VGC not only during sepsis but also during baseline conditions. During baseline conditions, the VGC is populated with ECM proteins and cell-cell junction proteins. During sepsis, the VGC drastically changes with acute phase markers, degranulation proteins, and ECM remodeling. Importantly, the studies highlighted in Chapter 2 provide an organotypic analysis of VGC remodeling. Vascular dysfunction followed by organ failure causes mortality in sepsis [3], and characterizing VGC remodeling in each organ is a major step in uncovering changes in the organ-vascular interface that may dictate sepsis outcome.

The studies in Chapter 2 open several avenues of further experimentation. First, direct VGC component analysis provides a list of excellent candidates for VGC markers in circulation during sepsis. Use of these markers to characterize vascular health and recovery in an organotypic manner would be highly valuable clinically. Additionally, use of these markers as theragnostic tools to measure vascular responses to therapy would be highly useful to stabilizing sepsis patients. Several of the potential markers detailed in Chapter 2 were not known to be involved in VGC remodeling

in sepsis and need further characterization. The surprising enrichment of PRG4 and HA remodeling factors in the liver VGC during *S. aureus* sepsis highlight previously uncharacterized host responses that may have impacts on sepsis pathology in that organ. Importantly, other organs have distinctive VGC components that are enriched during sepsis that would be interesting to pursue. One drawback of the studies in Chapter 2 is the use of only one pathogen. Inducing sepsis with another pathogen may reveal unique pathogen-specific VGC remodeling that gives insights into differences in sepsis responses. Additionally, the studies in Chapter 2 analyzed one timepoint, the acute pro-inflammatory phase, in the septic response. Studying very early sepsis responses would be highly valuable in understanding sepsis onset in the vasculature, or looking at the VGC of sepsis survivors may give insight into why patients have lingering sequalae after sepsis [4]. Last, the studies in Chapter 2 use proteomics to study VGC composition, which excludes characterization of the glycan components of the VGC. Further characterization of changes in VGC glycans during sepsis, either though glycomics or glycoproteomics, would be valuable avenues to further characterize VGC remodeling in sepsis.

Most sepsis studies focusing on individual VGC components have utilized non-targeted abrogation of a component of interest. Global inactivation of a specific VGC protein, or treatment with exogenous enzymes, are common strategies. Although these studies are valuable, they do not specifically target the VGC or individual components. The studies described in Chapter 3 are the first analysis of how manipulating a VGC component in a tissue-specific manner impacts sepsis and infection across multiple pathogens. Reducing sulfation of VGC HS results in differential outcomes depending upon the pathogen, implying that the role VGC HS plays in sepsis is pathogen-specific. Additionally, these results show that the host factors that participate in sepsis onset do not play the same role in every case of sepsis. Rather, sepsis onset may stratify depending

upon the pathogen. Further studies using targeted VGC modulation strategies may demonstrate pathogen-specific responses depending on certain VGC components.

Further analysis of the *S. aureus* sepsis model in *Ndst1$^{f/f}$Tie2Cre* mice showed that reducing HS sulfation in the VGC reduced liver damage by mitigating neutrophil trafficking during infection. Previously, endothelial HS has been shown to mediate neutrophil trafficking by engaging L-selectin and sequestering chemokine gradients [5–7]. However, these studies were mostly conducted in endothelial monolayers or using air-pouch infiltrate methods. Chapter 4 demonstrates for the first time that endothelial HS also controls neutrophil recruitment to a major internal organ. Importantly, HS is the only VGC component that has been described to mediate neutrophil trafficking in the liver during both sterile and non-sterile inflammation, which were previously described to use integrin- and HA-dependent processes, respectively [8–10]. Utilizing HS-based strategies to mitigate neutrophil trafficking may protect the liver during injury. A synthesized HS octadecasaccharide has been utilized to reduce inflammation and neutrophil trafficking to livers during acetaminophen-induced acute liver failure [11]. I.V. injection of the heparin-binding domain of CXCL9 binds the lumenal surface of the endothelium and blunts neutrophil adherence to the lumenal wall [12], although this has not been tested in the liver. These therapeutic strategies may be valuable during sepsis. Liver dysfunction or failure occurs in 4 – 45.9% of patients with a mortality rate of 54.3-61% [13], highlighting the critical role of this organ in sepsis tolerance. The studies highlighted in Chapter 4 suggest that HS, synthesized HS, or HS-binding therapeutics could protect the liver from damaging inflammation during sepsis.

S. aureus is well known for its pro-inflammatory and invasive infections [14], many of which are driven by pro-inflammatory virulence factors such as Hla [15,16]. There have been no studies indicating glycosylation plays a role in Hla toxicity besides a haploid screen showing inactivation

of some *N*-glycosylation biosynthesis machinery reduces Hla toxicity [17]. Studies in Chapter 5 are the first *in vivo* evidence that a glycan plays a role in Hla toxicity. Importantly, this is the first time specific *in vivo* manipulation of a VGC component resulted in Hla hypersensitivity. Knocking out *Adam10* in megakaryocytes and myeloid cells was shown to block Hla toxicity in sepsis [18], and Hla was shown to disrupt the endothelial barrier [19]. However, neither of these studies used targeted alteration of endothelial Adam10 or any other VGC component *in vivo*. Chapter 5 shows that cell surface endothelial factors beyond Adam10 are involved in systemic Hla toxicity. How endothelial HS is involved in Hla toxicity has yet to be determined. Potential experiments highlighted in Chapter 5 aim to distinguish between the role of HS in Hla oligomerization, Adam10 activity, and calcium signaling. By teasing out HS involvement in Hla, targeted therapies can be developed that inhibit Hla toxicity. Importantly, higher sulfation levels in HS are more protective during Hla toxicity, hinting that adding competitive sulfated HS would be a potential therapeutic option. Any non-antibiotic therapeutics that reduce inflammation induced by aggressive *S. aureus* infection would be valuable, especially in an era with increasing antibiotic resistance [20] and the threat of community acquired methicillin resistant *S. aureus* [14].

At 24 hours post-infection with *S. aureus*, the heart VGC composition in *Ndst1*$^{f/f}$*Tie2Cre-* mice showed an increase in proteins associated with heart recovery and extracellular matrix, while *Ndst1*$^{f/f}$*Tie2Cre+* mice did not exhibit increases in these proteins. Interestingly, no other organ showed differences in the VGC between genotypes during infection, showing for the first time that altering the VGC impacts remodeling during sepsis in an organotypic fashion. These studies also denote a potential relationship between the heart and Hla that was previously unknown. Hla treatment of endothelial cells induces arachidonic acid metabolism and prostacyclin generation, which acts as potent vasodilator [21]. The heart VGC may reflect a response in which

Ndst1$^{f/f}$Tie2Cre+ animals are undergoing vasodilation and vascular stress. Future studies may be able to tie the VGC, vascular stress, and heart failure as a mechanism of why Hla can be toxic systemically. Heart failure is a common disease, and further study into how the heart VGC impacts heart health and recovery from injury would be highly valuable for studying heart failure.

As interest increases in how VGC remodeling impacts sepsis outcome, more targeted analysis and manipulation of the VGC, such as in the studies highlighted in Chapters 2-5, are increasingly needed to unwrap how individual VGC components are involved in sepsis responses. In short, it is now possible to use "omics" level analysis to find lead VGC components of interest, and then pursue said components with tissue-specific deletion or manipulation of the component. The glycocalyx is often thought of as too complex to study in a mechanistic way. Indeed, the original "cuticle layer" descriptions and images of the earthworm VGC by Hama visualize how complicated the structure is [22]. However, the work described in this thesis follows an "omics to component" framework that may allow scientists to finally unravel the composition and function of the vascular "cuticle layer" in infection and sepsis.

6.2 References

1. Rudd, K. E., Johnson, S. C., Agesa, K. M., Shackelford, K. A., Tsoi, D., Kievlan, D. R., Colombara, D. V, Kissoon, N., Finfer, S., Fleischmann-struzek, C., Ikuta, K. S., Machado, F. R., Reinhart, K. K., Rowan, K., Seymour, C. W., Watson, R. S., West, T. E., Marinho, F., Hay, S. I., Lozano, R., Lopez, A. D., Angus, D. C., Murray, C. J. L. & Naghavi, M. Global, regional, and national sepsis incidence and mortality, 1990 – 2017: analysis for the Global Burden of Disease study. *Lancet* **6736,** 1–12 (2020).

2. Uchimido, R., Schmidt, E. P. & Shapiro, N. I. The glycocalyx: a novel diagnostic and therapeutic target in sepsis. *Crit. Care* **23,** 1–12 (2019).

3. Singer, M., Deutschman, C. S., Seymour, C. W., Shankar-Hari, M., Annane, D., Bauer, M., Bellomo, R., Bernard, G. R., Chiche, J.-D., Coopersmith, C. M., Hotchkiss, R. S., Levy, M. M., Marshall, J. C., Martin, G. S., Opal, S. M., Rubenfeld, G. D., van der Poll, T., Vincent, J. & Angus, D. C. The Third International Consensus Definitions for Sepsis and Septic Shock (Sepsis-3). *JAMA* **315,** 801–10 (2016).

4. Mostel, Z., Perl, A., Marck, M., Mehdi, S. F., Lowell, B., Bathija, S., Santosh, R., Pavlov, V. A., Chavan, S. S. & Roth, J. Post-sepsis syndrome- An evolving entity that afflicts survivors of sepsis. *Mol. Med.* **26,** 1–14 (2020).

5. Wang, L., Fuster, M., Sriramarao, P. & Esko, J. D. Endothelial heparan sulfate deficiency impairs L-selectin- and chemokine-mediated neutrophil trafficking during inflammatory responses. *Nat. Immunol.* **6,** 902–10 (2005).

6. Axelsson, J., Xu, D., Kang, B. N., Nussbacher, J. K., Handel, T. M., Ley, K., Sriramarao, P. & Esko, J. D. Inactivation of heparan sulfate 2- O -sulfotransferase accentuates neutrophil infiltration during acute inflammation in mice. *Blood* **120,** 1742–1751 (2012).

7. Massena, S., Christoffersson, G., Hjertström, E., Zcharia, E., Vlodavsky, I., Ausmees, N., Rolny, C., Li, J. P. & Phillipson, M. A chemotactic gradient sequestered on endothelial heparan sulfate induces directional intraluminal crawling of neutrophils. *Blood* **116,** 1924–1931 (2010).

8. Mcdonald, B., Mcavoy, E. F., Lam, F., Gill, V., Motte, C. De, Savani, R. C. & Kubes, P. Interaction of CD44 and hyaluronan is the dominant mechanism for neutrophil sequestration in inflamed liver sinusoids. *J. Exp. Med.* **205,** 915–927 (2008).

9. Mcdonald, B., Pittman, K., Menezes, G. B., Hirota, S. a, Slaba, I., Waterhouse, C. C. M., Beck, P. L., Muruve, D. a & Kubes, P. Intravascular Danger Signals Guide Neutrophils to Sites of Sterile Inflammation. *Science (80-.).* **330,** 362–367 (2011).

10. Kolaczkowska, E., Jenne, C. N., Surewaard, B. G. J., Thanabalasuriar, A., Lee, W. Y., Sanz, M. J., Mowen, K., Opdenakker, G. & Kubes, P. Molecular mechanisms of NET formation and degradation revealed by intravital imaging in the liver vasculature. *Nat. Commun.* **6,** 1–13 (2015).

11. Arnold, K., Xu, Y., Sparkenbaugh, E. M., Li, M., Han, X., Zhang, X., Xia, K., Piegore, M., Zhang, F., Zhang, X., Henderson, M., Pagadala, V., Su, G., Tan, L., Park, P. W., Stravitz, R. T., Key, N. S., Linhardt, R. J., Pawlinski, R., Xu, D. & Liu, J. Design of anti-inflammatory heparan sulfate to protect against acetaminophen-induced acute liver failure. *Sci. Transl. Med.* **12,** 1–12 (2020).

12. Vanheule, V., Boff, D., Mortier, A., Janssens, R., Petri, B., Kolaczkowska, E., Kubes, P., Berghmans, N., Struyf, S., Kungl, A. J., Teixeira, M. M., Amaral, F. A. & Proost, P. CXCL9-derived peptides differentially inhibit neutrophil migration in vivo through interference with glycosaminoglycan interactions. *Front. Immunol.* **8,** 1–14 (2017).

13. Yan, Jun; Li, Song; Li, S. The role of the liver in sepsis. *Int. Rev. Immunol.* **33,** 498–510 (2014).

14. Tong, S. Y. C., Davis, J. S., Eichenberger, E., Holland, T. L. & Fowler, V. G. Staphylococcus aureus infections: Epidemiology, pathophysiology, clinical manifestations, and management. *Clin. Microbiol. Rev.* **28,** 603–661 (2015).

15. Powers, M. E. & Wardenburg, J. B. Igniting the Fire: Staphylococcus aureus Virulence Factors in the Pathogenesis of Sepsis. *PLoS Pathog.* **10,** 10–13 (2014).

16. Inoshima, I., Inoshima, N., Wilke, G. A., Powers, M. E., Frank, K. M., Wang, Y. & Wardenburg, J. B. A Staphylococcus aureus pore-forming toxin subverts the activity of ADAM10 to cause lethal infection in mice. *Nat. Med.* **17,** 1310–1314 (2011).

17. Shah, J., Bagnoli, F., Guerrera, D., Citi, S., Starkl, P. M., Carette, J. E., Merakou, C., Lumb, J. H., Popov, L. M., Cooper, R. L., Bouley, D. M., Galli, S. J., Kiyonari, H., Takeichi, M., Meng, W., Marceau, C. D. & Amieva, M. R. The adherens junctions control susceptibility to Staphylococcus aureus α-toxin. *Proc. Natl. Acad. Sci.* **112,** 14337–14342 (2015).

18. Powers, M. E., Becker, R. E. N., Sailer, A., Turner, J. R. & Bubeck Wardenburg, J. Synergistic Action of Staphylococcus aureus α-Toxin on Platelets and Myeloid Lineage Cells Contributes to Lethal Sepsis. *Cell Host Microbe* **17,** 775–787 (2015).

19. Inoshima, N., Wang, Y. & Wardenburg, J. B. Genetic requirement for ADAM10 in severe staphylococcus aureus skin infection. *J. Invest. Dermatol.* **132,** 1513–1516 (2012).

20. Dadgostar, P. Antimicrobial resistance: implications and costs. *Infect. Drug Resist.* **12,** 3903–3910 (2019).

21. Suttorp, N., Seeger, W., Dewein, E., Bhakdi, S. & Roka, L. Staphylococcal alpha-toxin-induced PGI2 production in endothelial cells: role of calcium. *Am. J. Physiol.* **248,** (1985).

22. Hama, K. The fine structure of some blood vessels of the earthworm, Eisenia foetida. *J. Biophys. Biochem. Cytol.* **7,** 717–724 (1960).